

#436

Earth Sc

SAGE

xfer to LARC

METEOROLOGICAL, EPHEM, RAD DATA ARCH 79-013A-01A

777c

ESAC-00044

BETA AEROSOL NO. DEN ARCH TAPE 79-013A-01B

(deleted)

Table of Contents

1. Introduction
2. Errata/Change Log
3. LINKS TO RELEVANT INFORMATION IN THE ONLINE NSSDC INFORMATION SYSTEM
4. Catalog Materials
 - a. Associated Documents
 - b. Core Catalog Materials

1. INTRODUCTION:

The documentation for this data set was originally on paper, kept in NSSDC's Data Set Catalogs (DSCs). The paper documentation in the Data Set Catalogs have been made into digital images, and then collected into a single PDF file for each Data Set Catalog. The inventory information in these DSCs is current as of July 1, 2004. This inventory information is now no longer maintained in the DSCs, but is now managed in the inventory part of the NSSDC information system. The information existing in the DSCs is now not needed for locating the data files, but we did not remove that inventory information.

The offline tape datasets have now been migrated from the original magnetic tape to Archival Information Packages (AIP's).

A prior restoration may have been done on data sets, if a requestor of this data set has questions; they should send an inquiry to the request office to see if additional information exists.

2. ERRATA/CHANGE LOG:

NOTE: Changes are made in a text box, and will show up that way when displayed on screen with a PDF reader.

When printing, special settings may be required to make the text box appear on the printed output.

Version	Date	Person	Page	Description of Change
01				
02				

3 LINKS TO RELEVANT INFORMATION IN THE ONLINE NSSDC INFORMATION SYSTEM:

<http://nssdc.gsfc.nasa.gov/nmc/>

[NOTE: This link will take you to the main page of the NSSDC Master Catalog. There you will be able to perform searches to find additional information]

4. CATALOG MATERIALS:

- a. Associated Documents To find associated documents you will need to know the document ID number and then click here.
<http://nssdcftp.gsfc.nasa.gov/miscellaneous/documents/>

- b. Core Catalog Materials

SAGE

METEOROLOGICAL, EPHEM, RAW DATA ARCH

79-013A-01A ESAC-00044

This data set has been restored. There was originally 233 Binary 9-Track, 1600 BPI tapes. There are 20 restored tapes. The DR and DS tapes are 9-track, 6250 BPI. The tapes were created on a CDC computer. The DR and DS numbers along with the corresponding D numbers and the time spans are as follows:

DR#	DS#	D#	FILES	TIME SPAN
DR00140	DS00140	D42920	1-117	03/05/79 - 03/08/79
		D42921	118-211	03/09/79 - 03/12/79
		D42922	212-292	03/13/79 - 03/16/79
		D42923	293-410	03/17/79 - 03/20/79
		D42924	411-518	03/25/79 - 03/28/79
DR00141	DS00141	D42926	1-119	04/01/79 - 04/04/79
		D42927	120-240	04/05/79 - 04/08/79
		D42928	241-351	04/09/79 - 04/12/79
		D42929	352-470	04/13/79 - 04/16/79
DR00142	DS00142	D42930	1-119	04/17/79 - 04/20/79
		D42931	120-238	04/21/79 - 04/24/79
		D42932	239-357	04/25/79 - 04/28/79
		D42934	358-430	05/24/79 - 05/29/79
DR00143	DS00143	D42935	1-89	05/29/79 - 05/31/79
		D42936	90-208	06/01/79 - 06/04/79
		D42937	209-326	06/05/79 - 06/08/79
		D42938	327-408	06/09/79 - 06/13/79
		D42939	409-442	06/19/79 - 06/28/79
		D42940	443-480	07/01/79 - 07/04/79
DR00144	DS00144	D42941	1-36	07/15/79 - 07/18/79
		D42942	37-82	07/19/79 - 07/22/79
		D42943	83-119	07/23/79 - 07/25/79
		D42944	120-155	08/02/79 - 08/06/79
		D42945	156-208	08/06/79 - 08/09/79
		D42946	209-265	08/10/79 - 08/13/79
		D42947	266-319	08/15/79 - 08/17/79
		D42948	320-352	08/18/79 - 08/21/79
		D42949	353-408	08/22/79 - 08/25/79
		D42950	409-468	08/26/79 - 08/29/79
		D42951	469-488	08/30/79 - 08/31/79
		D42952	489-523	09/13/79 - 09/17/79
		D42953	524-566	09/18/79 - 09/26/79
		D42954	567-615	09/27/79 - 09/30/79
		D42955	616-671	10/01/79 - 10/04/79
		D42956	672-713	10/05/79 - 10/08/79
		D42957	714-752	10/09/79 - 10/12/79
D42958	753-781	10/13/79 - 10/16/79		

* F351-354 were O block's
tape was recreated w/ those files
New file 351 is missing record(s) at the beginning.

DR#	DS#	D#	FILES	TIME SPAN
DR00145	DS00145	D42959	1-38	10/17/79 - 10/20/79
		D42960	39-77	10/21/79 - 10/25/79
		D42961	78-103	10/26/79 - 10/29/79
DR00146	DS00146	D42962	1-59	11/21/79 - 11/24/79
		D42963	60-119	11/25/79 - 11/28/79
		D42964	120-149	11/29/79 - 11/30/79
		D42965	150-201	12/05/79 - 12/08/79
		D42966	202-259	12/09/79 - 12/12/79
		D42967	260-318	12/13/79 - 12/16/79
		D42968	319-376	12/17/79 - 12/20/79
		D46070	377-473	02/21/79 - 02/24/79
		D46071	474-586	02/25/79 - 02/28/79
		D46072	587-703	03/01/79 - 03/04/79
		DR00147	DS00147	D46073
D46074	116-199			03/29/79 - 03/31/79
D46075	200-258			04/29/79 - 04/30/79
D46076	259-377			05/01/79 - 05/04/79
D46077	378-494			05/05/79 - 05/08/79
DR00148	DS00148	D46078	1-119	05/09/79 - 05/12/79
		D46084	120-232	05/13/79 - 05/16/79
		D46080	233-278	05/16/79 - 05/17/79
		D46081	279-360	06/09/79 - 06/13/79
		D46082	361-375	06/29/79 - 06/30/79
DR00149	DS00149	D46083	1-30	07/05/79 - 07/09/79
		D46079	31-36	07/10/79 - 07/14/79
		D46085	37-88	09/01/79 - 09/04/79
		D46086	89-146	09/05/79 - 09/08/79
		D46087	147-198	09/09/79 - 09/12/79
		D46088	199-224	10/30/79 - 10/31/79
		D46089	225-246	11/01/79 - 11/04/79
		D46090	247-273	11/05/79 - 11/20/79
		D46091	274-330	12/01/79 - 12/04/79
		D46092	331-389	12/21/79 - 12/24/79
		D46093	390-438	12/25/79 - 12/28/79
		D46094	439-480	12/29/79 - 12/31/79
		D46641	481-531	01/01/80 - 01/04/80
		D46642	532-586	01/05/80 - 01/08/80
		D46643	587-639	01/09/80 - 01/12/80
		D46644	640-655	01/13/80 - 01/14/80
		D46645	656-677	01/27/80 - 01/28/80
D46646	678-722	01/29/80 - 01/31/80		
DR00150	DS00150	D46647	1-60	02/01/80 - 02/04/80
		D46648	61-119	02/05/80 - 02/08/80
		D46649	120-178	02/09/80 - 02/12/80
		D46650	179-237	02/13/80 - 02/16/80
		D46651	238-296	02/17/80 - 02/20/80
		D46652	297-356	02/21/80 - 02/24/80
		D46653	357-416	02/25/80 - 02/28/80

DR#	DS#	D#	FILES	TIME SPAN		
DR00151	DS00151	D46654	1-14	02/29/80 - 03/01/80		
		D46655	15-72	03/01/80 - 03/04/80		
		D46656	73-132	03/05/80 - 03/08/80		
		D46657	133-185	03/09/80 - 03/13/80		
		D46658	186-244	03/13/80 - 03/16/80		
		D46659	245-303	03/17/80 - 03/20/80		
		D46660	304-347	03/21/80 - 03/24/80		
		D46661	348-348	03/25/80 - 03/25/80		
		D46662	349-387	04/08/80 - 04/10/80		
		D46663	388-446	04/11/80 - 04/14/80		
		D46664	447-505	04/15/80 - 04/18/80		
		D46665	506-565	04/19/80 - 04/22/80		
		D46666	566-625	04/23/80 - 04/26/80		
		D46667	626-663	04/27/80 - 04/29/80		
		D46668	664-707	05/09/80 - 05/12/80		
		D46669	708-767	05/13/80 - 05/16/80		
		DR00152	DS00152	D46670	1-60	05/17/80 - 05/20/80
				D46671	61-120	05/21/80 - 05/24/80
				D46672	121-178	05/25/80 - 05/28/80
D46673	179-223			05/29/80 - 05/31/80		
D46674	224-279			06/01/80 - 06/04/80		
D46675	280-338			06/05/80 - 06/08/80		
D46676	339-398			06/09/80 - 06/12/80		
D46677	399-458			06/13/80 - 06/16/80		
D46678	459-518			06/17/80 - 06/20/80		
D46679	519-577			06/21/80 - 06/24/80		
D46680	578-636			06/25/80 - 06/28/80		
D46681	637-666			06/29/80 - 06/30/80		
D46682	667-727			07/01/80 - 07/04/80		
D46683	728-772			07/05/80 - 07/20/80		
D46684	773-832			07/21/80 - 07/24/80		
D46685	833-892			07/25/80 - 07/28/80		
D46686	893-937			07/29/80 - 07/31/80		
DR00153	DS00153			D46687	1-59	08/01/80 - 08/04/80
				D46688	60-119	08/05/80 - 08/08/80
		D46689	120-179	08/09/80 - 08/12/80		
		D46690	180-239	08/13/80 - 08/16/80		
		D46691	240-299	08/17/80 - 08/20/80		
		D46692	300-359	08/21/80 - 08/24/80		
		D46693	360-419	08/25/80 - 08/28/80		
		D46694	420-464	08/29/80 - 09/01/80		
		D46695	465-523	09/01/80 - 09/04/80		
		D46696	524-583	09/05/80 - 09/08/80		
		D46697	584-642	09/09/80 - 09/12/80		
		D46698	643-695	09/13/80 - 09/16/80		
		DR00154	DS00154	D46699	1-60	09/17/80 - 09/20/80
D46700	61-120			09/21/80 - 09/24/80		
D46701	121-180			09/25/80 - 09/28/80		
D46702	181-209			09/29/80 - 09/30/80		
D46703	210-269			10/01/80 - 10/04/80		
D46704	270-327			10/05/80 - 10/08/80		

DR#	DS#	D#	FILES	TIME SPAN
DR00154 (cont.)		D46705	328-383	10/09/80 - 10/12/80
		D46706	384-442	10/13/80 - 10/17/80
		D46707	443-501	10/17/80 - 10/20/80
		D46708	502-516	10/31/80 - 10/31/80
		D46709	517-576	11/01/80 - 11/04/80
		D46710	577-636	11/05/80 - 11/08/80
		D46711	637-696	11/09/80 - 11/12/80
		D46712	697-756	11/13/80 - 11/16/80
		D46713	757-815	11/17/80 - 11/20/80
DR00155	DS00155	D46714	1-60	11/21/80 - 11/24/80
		D46715	61-120	11/25/80 - 11/28/80
		D46716	121-147	11/29/80 - 11/30/80
		D46717	148-206	12/01/80 - 12/04/80
		D46718	207-265	12/05/80 - 12/08/80
		D46719	266-321	12/09/80 - 12/12/80
		D46720	322-381	12/13/80 - 12/16/80
		D46721	382-438	12/17/80 - 12/20/80
		D46722	439-496	12/21/80 - 12/24/80
		D58566	497-553	01/09/81 - 01/12/81
		D58567	554-613	01/13/81 - 01/16/81
		D58568	614-673	01/17/81 - 01/20/81
		D58569	674-733	01/21/81 - 01/24/81
		D58570	734-793	01/25/81 - 01/28/81
		D58571	794-838	01/29/81 - 01/31/81
		D58572	839-897	02/01/81 - 02/05/81
D58573	898-954	02/05/81 - 02/08/81		
DR00156	DS00156	D58574	1-60	02/09/81 - 02/12/81
		D58575	61-120	02/13/81 - 02/16/81
		D58576	121-180	02/17/81 - 02/20/81
		D58577	181-235	02/21/81 - 02/24/81
		D58578	236-293	02/25/81 - 02/28/81
		D58579	294-349	03/01/81 - 03/04/81
		D58580	350-374	03/05/81 - 03/06/81
		D58581	375-417	03/17/81 - 03/20/81
		D58582	418-477	03/21/81 - 03/24/81
		D58583	478-537	03/25/81 - 03/28/81
		D58584	538-582	03/29/81 - 03/31/81
		D58585	583-642	04/01/81 - 04/04/81
		D58586	643-702	04/05/81 - 04/08/81
		DR00157	DS00157	D58587
D58588	54-113			04/21/81 - 04/24/81
D58589	114-173			04/25/81 - 04/28/81
D58590	174-203			04/29/81 - 04/30/81
D58591	204-263			05/01/81 - 05/04/81
D58592	264-314			05/05/81 - 05/08/81
D58593	315-372			05/09/81 - 05/12/81
D58594	373-430			05/13/81 - 05/16/81
D58595	431-489			05/17/81 - 05/20/81
D58596	490-547			05/21/81 - 05/24/81
D58597	548-605			05/25/81 - 05/28/81
D58598	606-616			05/29/81 - 05/30/81
D58599	617-676			06/05/81 - 06/08/81
D58600	677-735			06/09/81 - 06/12/81
D58601	736-808			06/13/81 - 06/30/81
D58602	809-823			06/30/81 - 06/30/81
D58603	824-883	07/01/81 - 07/04/81		

DR#	DS#	D#	FILES	TIME SPAN
DR00158	DS00158	D58604	1-75	07/05/81 - 07/06/81
		D58605	76-150	07/10/81 - 07/14/81
		D58606	151-205	07/15/81 - 07/18/81
		D58607	206-256	07/19/81 - 07/22/81
		D58608	257-312	07/23/81 - 07/26/81
		D58609	313-372	07/27/81 - 07/30/81
		D58610	373-384	07/31/81 - 07/31/81
		D58611	385-442	08/01/81 - 08/04/81
		D58612	443-492	08/05/81 - 08/09/81
		D58613	493-501	08/09/81 - 08/10/81
		D58614	502-520	08/15/81 - 08/16/81
		D58615	521-580	08/17/81 - 08/20/81
		D58616	581-640	08/21/81 - 08/24/81
		D58617	641-682	08/25/81 - 08/27/81
		D58618	683-697	09/04/81 - 09/04/81
		D58619	698-757	09/05/81 - 09/08/81
		D58620	758-816	09/09/81 - 09/12/81
		D58621	817-876	09/13/81 - 09/16/81
		D58622	877-935	09/17/81 - 09/20/81
		DR00159	DS00159	D58623
D58624	61-120			09/25/81 - 09/28/81
D58625	121-150			09/29/81 - 09/30/81
D58626	151-164			10/01/81 - 10/04/81
D58627	165-167			10/12/81 - 10/12/81
D58628	168-224			10/13/81 - 10/16/81
D58629	225-284			10/17/81 - 10/20/81
D58630	285-343			10/21/81 - 10/24/81
D58631	344-403			10/25/81 - 10/28/81
D58632	404-448			10/29/81 - 10/31/81
D58633	449-505			11/01/81 - 11/04/81
D58634	506-563			11/05/81 - 11/08/81
D58635	564-621			11/09/81 - 11/12/81
D58636	622-680			11/13/81 - 11/16/81
D58637	681-707			11/17/81 - 11/18/81

REQ. AGENT
DAD

RAND #
VO014
175

ACQ. AGENT
RNH

SAGE

⁰
METEROLOGICAL, EPHEM, RAW DATA ARCH

79-013A-01A

This data set catalog consists of 233 data tapes. The tapes are 9 track, 1600 BPI, binary and multi-filed. The tapes were created on a CDC computer. Time spans and number of files are as follows:

<u>D#</u>	<u>FILES</u>	<u>TIME SPAN</u>
D-42920	117	03/05/79 - 03/08/79
D-42921	94	03/09/79 - 03/12/79
D-42922	81	03/13/79 - 03/16/79
D-42923	118	03/17/79 - 03/20/79
D-42924	108	03/25/79 - 03/28/79
D-42926	119	04/01/79 - 04/04/79
D-42927	121	04/05/79 - 04/08/79
D-42928	111	04/09/79 - 04/12/79
D-42929	119	04/13/79 - 04/16/79
D-42930	119	04/17/79 - 04/20/79
D-42931	119	04/21/79 - 04/24/79
D-42932	119	04/25/79 - 04/28/79
D-42934	73	05/24/79 - 05/29/79
D-42935	89	05/29/79 - 05/31/79
D-42936	119	06/01/79 - 06/04/79
D-42937	118	06/05/79 - 06/08/79
D-42938	82	06/09/79 - 06/13/79
D-42939	34	06/19/79 - 06/28/79
D-42940	38	07/01/79 - 07/04/79
D-42941	36	07/15/79 - 07/18/79
D-42942	46	07/19/79 - 07/22/79
D-42943	37	07/23/79 - 07/25/79
D-42944	36	08/02/79 - 08/06/79
D-42945	53	08/06/79 - 08/09/79
D-42946	57	08/10/79 - 08/13/79
D-42947	54	08/15/79 - 08/17/79
D-42948	37	08/18/79 - 08/21/79
D-42949	56	08/22/79 - 08/25/79
D-42950	50	08/26/79 - 08/29/79
D-42951	30	08/30/79 - 08/31/79
D-42952	35	09/13/79 - 09/17/79
D-42953	43	09/18/79 - 09/26/79
D-42954	49	09/27/79 - 09/30/79
D-42955	56	10/01/79 - 10/04/79
D-42956	42	10/05/79 - 10/08/79
D-42957	39	10/09/79 - 10/12/79
D-42958	42	10/13/79 - 10/16/79

*list not in
T/S order*

D-42959	38	10/17/79 - 10/20/79
D-42960	39	10/21/79 - 10/25/79
D-42961	26	10/26/79 - 10/29/79
D-42962	59	11/21/79 - 11/24/79
D-42963	60	11/25/79 - 11/28/79
D-42964	30	11/29/79 - 11/30/79
D-42965	52	12/05/79 - 12/08/79
D-42966	58	12/09/79 - 12/12/79
D-42967	59	12/13/79 - 12/16/79
D-42968	58	12/17/79 - 12/20/79
D-46070	97	02/21/79 - 02/24/79
D-46071	113	02/25/79 - 02/28/79
D-46072	117	03/01/79 - 03/04/79
D-46073	115	03/21/79 - 03/24/79
D-46074	84	03/29/79 - 03/31/79
D-46075	59	04/29/79 - 04/30/79
D-46076	119	05/01/79 - 05/04/79
D-46077	117	05/05/79 - 05/08/79
D-46078	119	05/09/79 - 05/12/79
D-46084	113	05/13/79 - 05/16/79
D-46080	46	05/16/79 - 05/17/79
D-46081	82	06/09/79 - 06/13/79
D-46082	15	06/29/79 - 06/30/79
D-46083	30	07/05/79 - 07/09/79
D-46079	6	07/10/79 - 07/14/79
D-46085	52	09/01/79 - 09/04/79
D-46086	58	09/05/79 - 09/08/79
D-46087	52	09/09/79 - 09/12/79
D-46088	26	10/30/79 - 10/31/79
D-46089	22	11/01/79 - 11/04/79
D-46090	27	11/05/79 - 11/20/79
D-46091	57	12/01/79 - 12/04/79
D-46092	59	12/21/79 - 12/24/79
D-46093	49	12/25/79 - 12/28/79
D-46094	42	12/29/79 - 12/31/79
D-46641	51	01/01/80 - 01/04/80
D-46642	55	01/05/80 - 01/08/80
D-46643	53	01/09/80 - 01/12/80
D-46644	16	01/13/80 - 01/14/80
D-46645	22	01/27/80 - 01/28/80
D-46646	45	01/29/80 - 01/31/80
D-46647	60	02/01/80 - 02/04/80
D-46648	59	02/05/80 - 02/08/80
D-46649	59	02/09/80 - 02/12/80
D-46650	59	02/13/80 - 02/16/80
D-46651	59	02/17/80 - 02/20/80
D-46652	60	02/21/80 - 02/24/80
D-46653	60	02/25/80 - 02/28/80
D-46654	14	02/29/80
D-46655	58	03/01/80 - 03/04/80
D-46656	60	03/05/80 - 03/08/80
D-46657	53	03/09/80 - 03/13/80
D-46658	59	03/13/80 - 03/16/80
D-46659	59	03/17/80 - 03/20/80
D-46660	44	03/21/80 - 03/24/80

D-46661	1	03/25/80
D-46662	39	04/08/80 - 04/10/80
D-46663	59	04/11/80 - 04/14/80
D-46664	59	04/15/80 - 04/18/80
D-46665	60	04/19/80 - 04/22/80
D-46666	60	04/23/80 - 04/26/80
D-46667	38	04/27/80 - 04/29/80
D-46668	44	05/09/80 - 05/12/80
D-46669	60	05/13/80 - 05/16/80
D-46670	60	05/17/80 - 05/20/80
D-46671	60	05/21/80 - 05/24/80
D-46672	58	05/25/80 - 05/28/80
D-46673	45	05/29/80 - 05/31/80
D-46674	56	06/01/80 - 06/04/80
D-46675	59	06/05/80 - 06/08/80
D-46676	60	06/09/80 - 06/12/80
D-46677	60	06/13/80 - 06/16/80
D-46678	60	06/17/80 - 06/20/80
D-46679	59	06/21/80 - 06/24/80
D-46680	59	06/25/80 - 06/28/80
D-46681	30	06/29/80 - 06/30/80
D-46682	61	07/01/80 - 07/04/80
D-46683	45	07/05/80 - 07/20/80
D-46684	60	07/21/80 - 07/24/80
D-46685	60	07/25/80 - 07/28/80
D-46686	45	07/29/80 - 07/31/80
D-46687	59	08/01/80 - 08/04/80
D-46688	60	08/05/80 - 08/08/80
D-46689	60	08/09/80 - 08/12/80
D-46690	60	08/13/80 - 08/16/80
D-46691	60	08/17/80 - 08/20/80
D-46692	60	08/21/80 - 08/24/80
D-46693	60	08/25/80 - 08/28/80
D-46694	45	08/29/80 - 09/01/80
D-46695	59	09/01/80 - 09/04/80
D-46696	60	09/05/80 - 09/08/80
D-46697	59	09/09/80 - 09/12/80
D-46698	53	09/13/80 - 09/16/80
D-46699	60	09/17/80 - 09/20/80
D-46700	60	09/21/80 - 09/24/80
D-46701	60	09/25/80 - 09/28/80
D-46702	29	09/29/80 - 09/30/80
D-46703	60	10/01/80 - 10/04/80
D-46704	58	10/05/80 - 10/08/80
D-46705	56	10/09/80 - 10/12/80
D-46706	59	10/13/80 - 10/17/80
D-46707	59	10/17/80 - 10/20/80
D-46708	15	10/31/80
D-46709	60	11/01/80 - 11/04/80
D-46710	60	11/05/80 - 11/08/80
D-46711	60	11/09/80 - 11/12/80
D-46712	60	11/13/80 - 11/16/80
D-46713	59	11/17/80 - 11/20/80
D-46714	60	11/21/80 - 11/24/80
D-46715	60	11/25/80 - 11/28/80
D-46716	27	11/29/80 - 11/30/80

D-46717	59	12/01/80 - 12/04/80
D-46718	59	12/05/80 - 12/08/80
D-46719	56	12/09/80 - 12/12/80
D-46720	60	12/13/80 - 12/16/80
D-46721	57	12/17/80 - 12/20/80
D-46722	58	12/21/80 - 12/24/80
D-58566	57	01/09/81 - 01/12/81
D-58567	60	01/13/81 - 01/16/81
D-58568	60	01/17/80 - 01/20/81
D-58569	60	01/21/81 - 01/24/81
D-58570	60	01/25/81 - 01/28/81
D-58571	45	01/29/81 - 01/31/81
D-58572	59	02/01/81 - 02/05/81
D-58573	57	02/05/81 - 02/08/81
D-58574	60	02/09/81 - 02/12/81
D-58575	60	02/13/81 - 02/16/81
D-58576	60	02/17/81 - 02/20/81
D-58577	55	02/21/81 - 02/24/81
D-58578	58	02/25/81 - 02/28/81
D-58579	56	03/01/81 - 03/04/81
D-58580	25	03/05/81 - 03/06/81
D-58581	43	03/17/81 - 03/20/81
D-58582	60	03/21/81 - 03/24/81
D-58583	60	03/25/81 - 03/28/81
D-58584	45	03/29/81 - 03/31/81
D-58585	60	04/01/81 - 04/04/81
D-58586	60	04/05/81 - 04/08/81
D-58587	53	04/09/81 - 04/12/81
D-58588	60	04/21/81 - 04/24/81
D-58589	60	04/25/81 - 04/28/81
D-58590	30	04/29/81 - 04/30/81
D-58591	60	05/01/81 - 05/04/81
D-58592	51	05/05/81 - 05/08/81
D-58593	58	05/09/81 - 05/12/81
D-58594	58	05/13/81 - 05/16/81
D-58595	59	05/17/81 - 05/20/81
D-58596	58	05/21/81 - 05/24/81
D-58597	58	05/25/81 - 05/28/81
D-58598	11	05/29/81 - 05/30/81
D-58599	60	06/05/81 - 06/08/81
D-58600	59	06/09/81 - 06/12/81
D-58601	73	06/13/81 - 06/30/81
D-58602	15	06/30/81
D-58603	60	07/01/81 - 07/04/81
D-58604	75	07/05/81 - 07/06/81
D-58605	75	07/10/81 - 07/14/81
D-58606	55	07/15/81 - 07/18/81
D-58607	51	07/19/81 - 07/22/81
D-58608	56	07/23/81 - 07/26/81
D-58609	60	07/27/81 - 07/30/81
D-58610	12	07/31/81
D-58611	58	08/01/81 - 08/04/81
D-58612	50	08/05/81 - 08/09/81
D-58613	9	08/09/81 - 08/10/81
D-58614	19	08/15/81 - 08/16/81

D-58615	60	08/17/81 - 08/20/81
D-58616	60	08/21/81 - 08/24/81
D-58617	42	08/25/81 - 08/27/81
D-58618	15	09/04/81 -
D-58619	60	09/05/81 - 09/08/81
D-58620	59	09/09/81 - 09/12/81
D-58621	60	09/13/81 - 09/16/81
D-58622	59	09/17/81 - 09/20/81
D-58623	60	09/21/81 - 09/24/81
D-58624	60	09/25/81 - 09/28/81
D-58625	30	09/29/81 - 09/30/81
D-58626	14	10/01/81 - 10/04/81
D-58627	3	10/12/81
D-58628	57	10/13/81 - 10/16/81
D-58629	60	10/17/81 - 10/20/81
D-58630	59	10/21/81 - 10/24/81
D-58631	60	10/25/81 - 10/28/81
D-58632	45	10/29/81 - 10/31/81
D-58633	57	11/01/81 - 11/04/81
D-58634	58	11/05/81 - 11/08/81
D-58635	58	11/09/81 - 11/12/81
D-58636	59	11/13/81 - 11/16/81
D-58637	27	11/17/81 - 11/18/81

79-013A-01A

B30866-004

SAGE MERDAT

(STRATOSPHERIC AEROSOL AND GAS EXPERIMENT METEOROLOGICAL,
EPHEMERIS, RAW DATA ARCHIVAL TAPE)

USER'S GUIDE

To replace copy mailed
earlier - lost or damaged during
microfilming. See dup copy after
the BANAT User's Guide!

REVISED 24 January 1980

William H. Mitchell

MERDAT TAPE CHARACTERISTICS

AND DATA ORGANIZATION

This data is on 9-track, 1600 CPI, unlabeled magnetic tape in fixed length 616 CDC word (60 BIT) binary records. Each SAGE event is comprised of one record of Meteorological and Ephemeris data (combined) plus ten or more consecutive four second telemetry data records followed by an end-of-file mark. The last event will be followed by two end-of-file marks or end of tape. The number of records and number of events will vary. There will be no padding of missing telemetry data, however, MET and/or EPHEMERIS data dropout will result in zero fill of the appropriate words in record 1 of each file.

MERDAT GROSS FORMAT

EVENT 1 MET and EPHEM. DATA
IRG
EVENT 1 TELEMETRY DATA 1
IRG
⋮
EVENT 1 TELEMETRY DATA N
EOF 1
EVENT 2 MET and EPHEM. DATA
IRG
EVENT 2 TELEMETRY DATA 1
IRG
EVENT 2 TELEMETRY DATA 2
⋮
EOF N-1
EVENT N MET and EPHEM. DATA
IRG
EVENT N MET and EPHEM. DATA 1
IRG
EVENT N MET and EPHEM. DATA 2
IRG
⋮
EOF
EOF

MERDAT MET AND EPHEMERIS

DETAIL DESCRIPTION

The first 616 CDC word record in each file
will contain the following:

MET DATA

CDC WORD #	DESCRIPTION	CDC INTERNAL FORMAT
1	Satellite Code	A9
2	Instrument	A6
3	Year	I4
4	Month	I2
5	Day	I2
6	Hour	I2
7	Minute	I2
8	Second	I2
9	Latitude	A6
10	Longitude	A7
11	Event Type	A7
12	No. Events in Day	I2
13	This Event No. in Day	I2
* 14-32	Temperature Deg K or 9999.	Real
* 33-51	Temp. Error Deg K or 999.	Real
* 52-70	Altitude in Meters or 99999.	Real
* 71-89	Density g/m^3 or 99999.	Real
* 90-108	Density Error ($\frac{Temp. Err}{Temp.}$) or 999.	Real

* The first 13 values correspond to fixed pressure levels in millibars:
1000, 850, 700, 500, 400, 300, 250, 200, 150, 100, 70, 50, 30,
10, 5, 2, 1, 0.4

The 19th value is derived at the variable tropopause pressure.

MERDAT MET AND EPHEMERIS DETAIL
DESCRIPTION (cont.)

EPHEMERIS DATA

CDC

Word # Description (All CDC Floating Point Words)

109		Date of 1st EPH point (YYMMDD.0)									
110		No. days since Jan. 0 of year (DDD.0)									
111		Seconds of Day (SSSSS.S)									
112		Time interval between Eph. points (seconds)									
113	X	<table border="0"> <tr> <td>{</td> <td>Position</td> <td>(DUL)</td> </tr> <tr> <td></td> <td>Vector</td> <td>(DUL)</td> </tr> <tr> <td></td> <td>1</td> <td>(DUL)</td> </tr> </table>	{	Position	(DUL)		Vector	(DUL)		1	(DUL)
{	Position		(DUL)								
	Vector		(DUL)								
	1	(DUL)									
114	Y										
115	Z										
116	VX	<table border="0"> <tr> <td>{</td> <td>Velocity</td> <td>(DUL/DUT)</td> </tr> <tr> <td></td> <td>Vector</td> <td>(DUL/DUT)</td> </tr> <tr> <td></td> <td>1</td> <td>(DUL/DUT)</td> </tr> </table>	{	Velocity	(DUL/DUT)		Vector	(DUL/DUT)		1	(DUL/DUT)
{	Velocity		(DUL/DUT)								
	Vector		(DUL/DUT)								
	1	(DUL/DUT)									
117	VY										
118	VZ										
119-412	49	Additional vector component sets like 113-118									
413		Time of 1st Eph. point in this record (DUT)									
414		Time interval between Eph. points (DUT)									
415		Epoch time (centidays since 0 Hr. Sept. 18, 1957) (DUT)									
416		Greenwich hour angle at epoch time (radians)									
417-615		Repeat of 109-307 for next available Eph. set									
616		Twelve bit one's complement add checksum with end-around carry									

SAGE TELEMETRY DATA

DETAIL DESCRIPTION

Each physical record contains 4 seconds of SAGE data.
(32 minor frames with Goddard Space Flight Center GMT tags
and quality estimate codes.)

Minor Frame Gross Format (1 MF = 1152 BITS)

- A. Telemetry Minor Frame - See GSFC document (included)
Data Reduction Notes for Heat Capacity Mapping Mission
(HCMM) and Stratosphere and Aerosol Gas Experiment (SAGE).
BITS 1-1024
- B. A/D FLAGS BITS 1025-1036 (Figure 1)
- C. DAY BITS 1037-1045
MSEC OF DAY BITS 1046-1072
- D. TELOPS COUNTERS (Figure 2)
- E. TELOPS FLAGS (FIGURE 3)
- F. FILL/EDIT FLAGS (FIGURE 4)
- G. Twelve bit one's complement add checksum with end-around
carry. (Supplied by LaRC in the last word (616) of each
record and not read from the GSFC SAGE Experimenter Tape).

MISC.

- 1.) Events contained on MERDAT have been edited for slow scan quantity only.
- 2.) MET data missing single measurements are filled with 9's.
- 3.) DUL refers to DOD unit of length. 10,000 km = 1 DUL.
- 4.) DUT refers to DOD unit of time 864 sec = 1 centiday = 1 DUT.

F5	F6	F7	F8	F9	F10	F11	F12	SPARE	SPARE	P ₃₅	P ₂₇
----	----	----	----	----	-----	-----	-----	-------	-------	-----------------	-----------------

GLOSSARY

F5 = BIT SLIPPAGE	F10 = LOS FLAG
F6 = INPUT DATA TERMINATION	F11 = "QUICK-LOOK" DATA
F7 = BIT ERRORS IN FS.V	F12 = SPARE
F8 = FRAME SYNC NOT RECOGNIZED	P ₃₅ = PARITY ON 35 BITS OF TIME
F9 = AOS FLAG.	P ₂₇ = PARITY ON 27 BITS MSEC

Figure 1 | Analog-to-Digital Flags

Figure 2 | TELOPS Counters

ITEM DESCRIPTION	STATE	BIT(S) (R TO L)
COUNT OF INPUT FRAMES	0-262,143	1-12
FRAME COUNT ERROR	0-31	19-23
SPARE	0	24
UNCORRECTED TELEMETRY MODE WORD (ONLY IF MODE WORD CORRECTED)	0-255	25-32

Figure 3 TELOPS Precredit Flags

BIT NUMBER (L TO R)	DESCRIPTION
1	DECODING FRAME SUSPECT
2	PARTIAL FRAME (PADDED)
3	MODE ERROR
4	MODIFIED FRAME
5	FRAME IMMEDIATELY AFTER DATA GAP
6	FRAME COUNT ERROR
7	SPARE
8	POSITIVE S/C ERROR
9	NEGATIVE S/C ERROR
10	POSITIVE UTC ERROR
11	NEGATIVE UTC ERROR
12	FRAME COUNT JUMP
13	SPARE
14	POSITIVE S/C JUMP
15	NEGATIVE S/C JUMP
16	POSITIVE UTC JUMP
17	NEGATIVE UTC JUMP
18	ILLEGAL UTC FROM G/STA
19	QUESTIONABLE FRAME COUNTER
20	SUBCOM II ERROR (SYNC)
21	SUBCOM III ERROR (COUNTER)
22	VERIFIED MODE CHANGE
23	FRACTION START
24	FRACTION END
25	DATA POINT OUTSIDE OF FRACTIONS
26	QUESTIONABLE S/C CLOCK
27	QUESTIONABLE UTC VALUE
28	SPARE
29-32	COUNT FRAME SYNC BIT ERRORS BY P.E.

Figure 4 Edit Flag Identification (AEM-B)

DESCRIPTION	STATUS	BIT (R TO L)
FRAME COUNTER VERIFIED	0	1
FRAME COUNTER CORRECTION	1	
SPACECRAFT CLOCK VERIFIED	0	2
SPACECRAFT CLOCK CORRECTION	1	
COMMAND CLOCK VERIFIED	0	3
COMMAND CLOCK CORRECTION	1	
COMMAND CLOCK STABLE	0	4
COMMAND CLOCK RESET	1	
COMMAND REPLICAS VERIFIED	0	5
COMMAND REPLICAS ERROR	1	
SPACECRAFT ID VERIFIED	0	6
SPACECRAFT ID CORRECTION	1	
PCM FORMAT VERIFIED	0	7
PCM FORMAT CORRECTION	1	
PCM FORMAT CONTINUOUS	0	8
PCM FORMAT CHANGE	1	
UTC ACCEPTABLE	0	9
UTC QUESTIONABLE	1	
UTC INTERPOLATED	0	10
UTC EXTRAPOLATED	1	
CONTINUOUS GROUND TIME	0	11
GROUND TIME DISCONTINUITY	1	
DATA CONTINUOUS	0	12
LOSS OF FRAME SYNC	1	
TELEMETRY DATA PRESENT	0	13
FILL DATA PRESENT	1	
DATA QUALITY GOOD	0	14
SUSPECT DATA	1	
SEGMENT INCOMPLETE	0	15
SEGMENT TERMINATION	1	
COMMAND CLOCK VERIFIED	0	16
COMMAND CLOCK UNVERIFIED	1	

B30864-0016

**Inversion of stratospheric
aerosol and gaseous
constituents from spacecraft
solar extinction data in the
0.38–1.0- μ m wavelength region**

W. P. Chu and M. P. McCormick

*a reprint from Applied Optics
volume 18, number 9, May 1, 1979*

Inversion of stratospheric aerosol and gaseous constituents from spacecraft solar extinction data in the 0.38–1.0- μm wavelength region

W. P. Chu and M. P. McCormick

Inversion techniques for the retrieval of stratospheric aerosol, ozone, neutral density, and nitrogen dioxide vertical profiles from numerically simulated spacecraft solar extinction measurements have been analyzed. The analysis is applied toward the space flight mission of the Stratospheric Aerosol and Gas Experiment (SAGE), which will be flown on the Applications Explorer Mission B (AEM-B) spacecraft. The instrument has four radiometric channels located at selected intervals in the 0.38–1.0- μm wavelength range. The expected retrieval accuracies are determined from inverting simulated data with various experimental errors included. The results from this analysis assuming a horizontally homogeneous atmosphere indicate that aerosol, ozone, and neutral density vertical profiles can be retrieved to an accuracy better than 10% with about 1-km vertical resolution over most of the stratosphere. The results also show that nitrogen dioxide can be inverted to an accuracy of about 25% in the 25–38-km altitude range. In addition, the effects of horizontally inhomogeneous distributions of aerosol and ozone on the retrieval accuracies are analyzed based on a simple inhomogeneous model of the atmosphere and found that there is only a small perturbation on the inversion accuracies.

Introduction

The minor constituents in the upper atmosphere, such as aerosols and ozone, have received great attention in recent years because of concerns over their roles in affecting the global environment with subsequent alteration of activities in the biosphere. With mankind's increasing activities in both the stratosphere and troposphere, and naturally occurring events such as volcanic eruptions, large changes in stratospheric aerosol and/or ozone loading could be induced directly or indirectly through various photochemical reactions. A realistic assessment of this problem is still not possible due to the lack of information on the distribution, chemistry, and dynamics of most of the constituents in our atmosphere. Global monitoring of ozone has been carried out by different instruments on-board spacecrafts since the early part of this decade. Monitoring of stratospheric aerosols will begin with the Nimbus-G satellite in 1978 using data from Stratospheric Aerosol Measurement II (SAM II), which will cover the near-polar high-latitude region of the globe.¹ Another mission, the Stratospheric Aerosol and Gas Experiment

(SAGE), will begin global monitoring of stratospheric aerosols and ozone with the Application Explorer Mission-B (AEM-B) satellite in 1979.¹

In this paper we shall discuss a possible data retrieval technique for SAGE. The SAGE instrument has four radiometric channels centered at 1.0- μm , 0.6- μm , 0.45 μm , and 0.385- μm wavelength. The 1.0- μm channel is sensitive primarily to aerosol scattering. The 0.6- μm channel is located at the peak of the ozone Chappius absorption band for providing an ozone measurement. The 0.45- μm and 0.385- μm channels will provide information on nitrogen dioxide and aerosol short wavelength scattering properties. The experimental approach is solar occultation as viewed from an orbiting spacecraft. Each radiometric channel has a field of view (FOV) of 0.5-min of arc, which will provide atmospheric vertical resolution of approximately half km altitude. The radiometer will track the solar disk during each sunrise and sunset event in order to produce atmospheric extinction profiles at the four wavelengths down to cloud top vertical altitudes or approximately below 10 km.

The accuracy of the inference of aerosol and other gaseous constituent vertical distributions from the SAGE four channel radiometric data depends to a large extent on the accuracy of the measurement by the instrument. The understanding of the measurement errors will dictate the proper inversion method to be used with the experimental data. In this paper, we will

The authors are with NASA Langley Research Center, Hampton, Virginia 23665.

Received 16 June 1978.

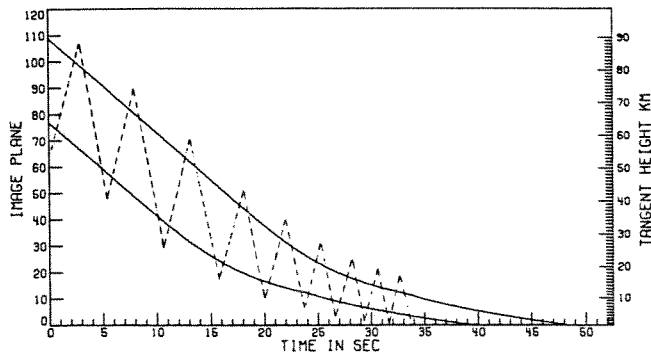


Fig. 1. Data acquisition mode for solar extinction experiment during a sunset event. The solid lines denote top and bottom of solar disk. The zig-zag dashed line shows the data taking sequence.

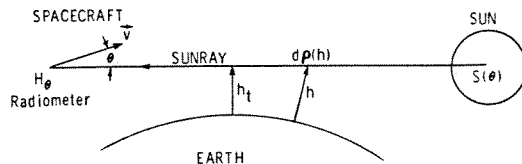


Fig. 2. Experimental geometry for solar extinction measurement.

describe a data reduction procedure for minimization of experimental errors based on a detailed simulation of the measurement sequence. An efficient and accurate inversion method will then be used for the retrieval of all the constituent vertical profiles.

The effects of horizontally inhomogeneous distributions of the constituent vertical profiles are also investigated based on available data of their global distributions. A simple horizontally inhomogeneous model of stratospheric aerosol and ozone will be used to estimate this perturbation on the retrieval accuracies.

Description of the Experiment

The data acquisition mode for the SAGE radiometer is illustrated in Fig. 1. The two solid lines denote, respectively, the image position of the top and bottom of the solar disk during a sunset event as viewed from the spacecraft platform. The gradual shrinking of the vertical sun shape image is due to atmospheric refraction. A ray trace technique based on Snell's law has been used to compute this effect.² The left vertical ordinate denotes relative angle measured from the spacecraft coordinate system in min of arc, while the right vertical ordinate denotes the corresponding vertical tangent altitude. The horizontal abscissa denotes event time in seconds corresponding to a sunset event in which the sun-satellite vector lies in the spacecraft's orbital plane. During a typical data taking sequence, the radiometer vertically scans the solar disk up and down with respect to earth's horizon. This is represented by the dashed line in the figure. The nominal scan rate will be 15 min of arc/sec. For a spacecraft sunrise event, the data taking mode is similar with the time sequence reversed. The radiometric data from each channel will be sampled at a rate of 64 samples/sec and will be digitized to 12 bits.

Simulation of Experimental Data

In order to determine the inversion accuracy for the SAGE solar extinction experiment, a detailed understanding of the various experimental errors and their effects on the retrieval of atmospheric constituent profiles will be required. This type of analysis can serve the purpose of guiding the design of the experiment and assessing the success of the experimental approach. There are two types of experimental errors associated with the SAGE measurement. The first type of error is the usual random noise associated with each measurement. The second type is the so-called pointing error, which is uniquely associated with solar extinction measurements. This error arises from the uncertainty in assigning to each measurement the viewing direction of the instrument with respect to both the atmosphere and the solar position and is caused by several different factors such as inaccurate spacecraft ephemeris data, errors in scanning and tracking of the instrument, and spacecraft drift due to residual angular momentum. To appreciate the magnitude of this error, let us assume the spacecraft ephemeris data are off by 1 sec. With the sun's vertical motion of about 3-km/sec as viewed from the spacecraft platform, this will correspond to an altitude offset error of 3 km.

The simulation of the experiment is based on the experimental geometry as illustrated in Fig. 2. The atmosphere is assumed to be spherically symmetric. The effects due to a horizontally inhomogeneous atmosphere will be considered in a later section. The radiometer is situated on the circularly orbiting satellite with velocity V . Each instantaneous view angle θ measured from V will define a unique tangent altitude h_t for the sun ray. In the inertial frame fixed on the spacecraft with the sun approximately at infinity, the instantaneous irradiance H_λ measured by the instrument at centered wavelength λ and time t is given as

$$H_\lambda(t) = \int_{\Delta\lambda} \int_{\Delta\Omega} F_\lambda(\theta, \phi) S_\lambda(\theta, \phi, t) T_\lambda(\theta) d\Omega d\lambda, \quad (1)$$

where $F_\lambda(\theta, \phi)$ is the radiometer's field of view function, ϕ is the azimuthal angle, Ω is the solid angle, $T_\lambda(\theta)$ is the transmission of the atmosphere as a function of view angle θ , and $S_\lambda(\theta, \phi, t)$ is the extraterrestrial solar radiance profile for wavelength λ . In order to account for atmospheric refraction effects on the solar radiance distribution as described in Fig. 1, an atmospheric refracted solar radiance distribution has to be used in Eq. (1).

Using the Bouguer law, the transmission function $T_\lambda(\theta)$, with the change of variable from θ to h_t , is given by

$$T_\lambda(h_t) = \text{Exp} - [\int \beta_\lambda(h) d\rho_\lambda(h)], \quad (2)$$

where $\beta_\lambda(h)$ is the total extinction coefficient of the atmosphere vs altitude h for wavelength λ , and $\rho_\lambda(h)$ is the sun ray optical pathlength. The integral is evaluated from the spacecraft position through the atmosphere at h_t to the sun. For SAGE with spectral channels located within the spectral range of 0.38–1.0

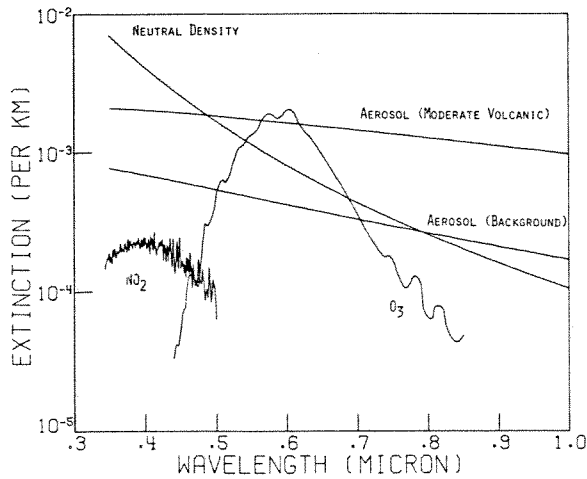


Fig. 3. Extinction contributions from Rayleigh, aerosol, O₃, and NO₂ vs wavelength from 0.35 μm to 1.0 μm at an altitude of 18 km.

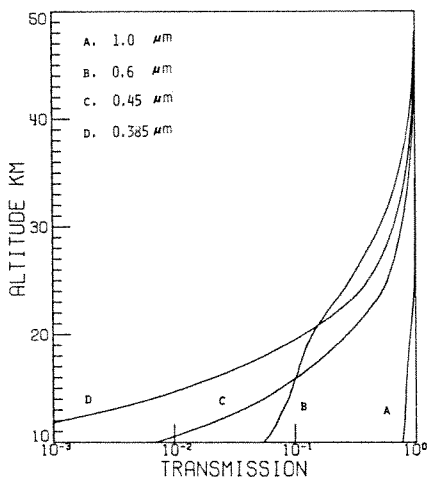


Fig. 4. Atmospheric transmission vs tangent altitude at the four wavelengths for solar extinction geometry.

μm, the total extinction coefficient β_λ at each altitude is composed of contributions from

$$\beta_\lambda = \beta_{ND}(\lambda) + \beta_{O_3}(\lambda) + \beta_{NO_2}(\lambda) + \beta_a(\lambda), \quad (3)$$

where $\beta_{ND}(\lambda)$ is the extinction coefficient at λ for neutral atmospheric density (Rayleigh scattering); $\beta_{O_3}(\lambda)$, $\beta_{NO_2}(\lambda)$, and $\beta_a(\lambda)$ are, respectively, ozone, nitrogen dioxide, and aerosol extinction coefficients at wavelength λ . The Rayleigh scattering term is described by the well-known inverse fourth power law dependence on wavelength. For the gaseous constituents, ozone and nitrogen dioxide, the extinction coefficient is equal to the product of number density and the absorption cross section at the specific wavelength. The aerosol extinction coefficient is a function of aerosol size distribution, shape, and index of refraction. For homogeneous spherical aerosol particles, the extinction coefficient is given by the following equation³:

$$\beta_a(\lambda) = \int_0^\infty \sigma(n, r, \lambda) N(r) dr, \quad (4)$$

where $N(r)$ is the size distribution function for aerosol

particles, $\sigma(n, r, \lambda)$ is the extinction cross section at λ for particle with index of refraction n and radius r . The extinction cross section $\sigma(n, r, \lambda)$ can be computed from Mie theory for homogeneous spherical particles.⁴ Figure 3 shows extinction contributions from each atmospheric constituent vs wavelength at an altitude of 18 km. The ozone number density is assumed to be $4 \times 10^{12}/\text{cm}^3$, NO₂ number density is assumed to be $3 \times 10^9/\text{cm}^3$. Two aerosol extinction models are shown in the figure corresponding to a background model and a moderate volcanic model. Both aerosol models are computed from Rosen's log normal size distribution with refractive index of 1.43 corresponding to composition of 75% H₂SO₄ and 25% H₂O.⁵ The background model assumes a modal radius r_g of 0.0725 μm and a spread σ_g of 1.86, while the moderate volcanic model assumes a modal radius r_g of 0.097 μm and a spread σ_g of 2.02. The total aerosol number density in both models is assumed to be 10/cm³.

Before proceeding to the simulation of the experimental data, different models of the atmosphere have to be constructed. We computed the atmospheric transmission profiles at the four SAGE wavelengths by dividing the atmosphere into homogeneous spherical shells of 0.15-km thickness. The optical pathlength through each layer is computed from the ray trace method properly taking atmospheric refraction into account. Different sets of aerosol, ozone, and nitrogen dioxide vertical profiles are then used to construct transmission vs tangent altitude profiles at the four wavelengths. Figure 4 illustrates typical computational results showing atmospheric transmission vs tangent altitude profiles at the four wavelengths. The vertical distribution for each constituent used in computing these transmission profiles is shown in Fig. 5 in terms of extinction profiles at a given wavelength. The neu-

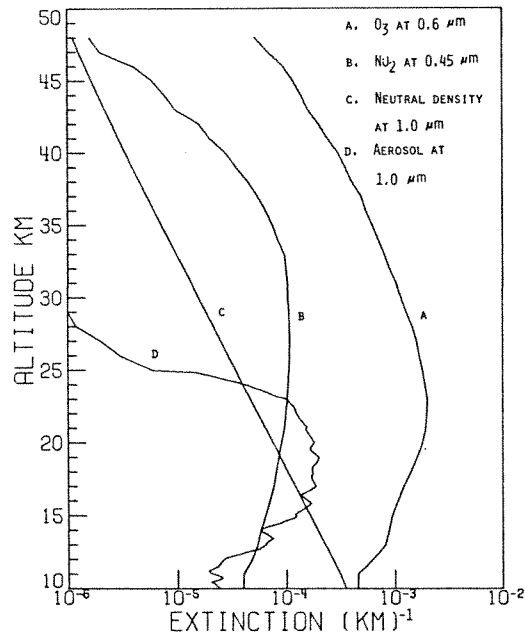


Fig. 5. Vertical extinction profiles for Rayleigh, aerosol, O₃, and NO₂.

tral density and the ozone extinction profiles are computed from the 1976 Standard Atmosphere.⁶ The nitrogen dioxide extinction profile is computed from Concorde measurements,⁷ and the aerosol vertical profile is computed from a typical dustsonde measurement in the 1972 period.⁸ The optical model for the aerosol used in the calculation is the same as illustrated in Fig. 3 for the background aerosol model.

The actual simulation of the experimental data is derived based on Eq. (1) together with the experimental sequence as illustrated in Fig. 1. We have assumed that the spectral bandpass for each radiometric channel is sufficiently narrow so that a single wavelength representation for each channel can be justified. Since the field of view of the instrument, which is 0.5 min of arc, is much smaller than the angular extent of the solar disk, we made the approximation of replacing $F_\lambda(\theta, \phi)$ in Eq. (1) with the line spread function of the instrument to calculate the measured irradiance. The line spread function is determined from instrument specification for the SAGE experiment.¹ Pointing errors associated with the instrument in the form of scan rate fluctuations are then incorporated into the simulation. Moreover, for each measured irradiance, random noise with a fixed maximum magnitude representative of the worst case instrument errors is added. Each simulated measurement is then quantized to 12 bits. Figure 6 shows a typical simulated data set for the 1.0- μm channel during a sunset event. The simulation begins when the suntop is situated at a 92-km tangent altitude. The solar limb darkening profiles used in all the simulations have been tabulated by Allen.⁹

Reduction of Measured Data to Transmission Profiles of the Atmosphere

The reduction of measured data from the SAGE four radiometric channels, such as those illustrated in Fig. 6, is accomplished through the following procedure. First, each measured irradiance is related to view angle with respect to the earth's atmosphere in terms of tangent altitude and with respect to the solar disk in terms of position on the limb darkening curve. This relationship in principle can be established through a calculation with the spacecraft and solar ephemeris data. Accurate determination of this relationship for all measured data during a complete sunrise or sunset event, however, will be difficult due to the atmospheric refraction effects and the pointing uncertainty of the instrument. We have developed, therefore, an iterative method to establish this relationship through a fitting of the measured sun shapes to the computed sun shapes. In this method, the function $\Phi(h_r)$, which is the sum of squares of the time differences between the measured sun edge crossing time and the computed sun edge crossing time with reference altitude h_r , is minimized.

$$\Phi(h_r) = \sum_{i=1}^n [\Delta t_i^{(m)} - \Delta t_i^{(c)}(h_r) - 2\delta t]^2, \quad (5)$$

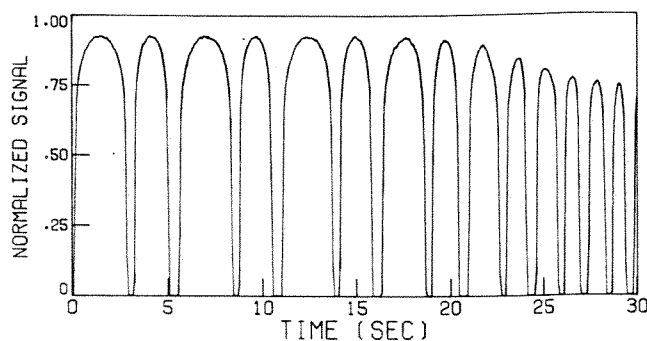


Fig. 6. Simulated experimental data for solar extinction measurement at 1.0- μm wavelength.

where $\Delta t_i^{(m)}$ is the measured sun edge crossing time for the i th scan, $\Delta t_i^{(c)}(h_r)$ is the computed sun edge crossing time for the i th scan with reference altitude h_r , and δt is the sun edge spreading time which is determined by the amount of edge smear produced by the imaging optics and by the intensity threshold level selected for the definition of sun edge. The iterative process begins by making an initial guess of the reference altitude $h_r^{(0)}$ to compute the function $\Phi(h_r)$. The following equation is then used for the update of h_r :

$$h_r^{(k+1)} = h_r^{(k)} + c \sum_i [\Delta t_i^{(m)} - \Delta t_i^{(c)}(h_r) - 2\delta t], \quad (6)$$

where the superscript k is the iteration number, and c is a positive scaling constant to control the speed of convergence of the iteration. The absolute magnitude of c is proportional to the scan rate and is determined by trial and error. The iteration stops when a minimum of the function $\Phi(h_r)$ has been located. The iterative procedure described above has been applied to simulated experimental data with a range of pointing error, and the iteration always converges to within 0.2 km of the true reference altitude in about ten iterations.

The second step in the data reduction procedure is to utilize the self-calibrating property of this type of measurement by making the first few high-altitude scans of the solar disk where the atmospheric extinction is assumed to be zero as the extraterrestrial solar limb darkening profiles. Atmospheric transmittance values for each subsequent measured irradiance are then determined by forming the ratio with the calibrated limb profile at the proper solar limb position. This generates a large number of transmittance values for each wavelength at different tangent altitudes. In order to facilitate the inversion and to minimize the random noise effect, the transmission data are grouped into predetermined altitude steps. The arithmetic mean of the transmittance values within each altitude step is then taken as the representative average transmittance for the particular layer. In this study, we have divided the atmosphere into 80 homogeneous layers from 10 km to 50 km with thickness of 0.5 km. The improvement in the signal-to-noise level based on this averaging process

can be demonstrated with simulated events as illustrated in Fig. 7 where the sunset event of Fig. 6 is used. Instrumental errors of 0.5% random noise on each measurement and 0.5-min of arc/sec scan rate error were introduced into the simulation sequence. These simulated irradiance data are then reduced by first establishing a best fit reference altitude from the sun shape measurements. Subsequently, all irradiance data are normalized to the first scan limb profile to determine the atmospheric transmittance values. Figure 7(A) shows the percentage error associated with the reduced transmittance from each measurement as a function of tangent altitude for the 1.0- μm wavelength channel. Figure 7(B) shows the percentage error associated with the mean transmittance values after averaging the reduced transmittance values within each 0.5-km altitude step. Generally, a significant improvement of signal-to-noise level can be achieved through this simple reduction process.

Inversion of Transmission Profile to Extinction Profile for each Constituent

The inversion of the mean transmittance profiles at the four wavelengths to extinction profile for each constituent is based on inverting the integral equation as described by Eq. (2). Rewriting Eq. (2) in terms of optical thickness $\tau_\lambda(h_t)$, where $\tau_\lambda(h_t) = \ln[1/T_\lambda(h_t)]$, we have

$$\tau_\lambda(h_t) = \int \beta_\lambda(h) d\rho_\lambda(h). \quad (7)$$

The integral can be approximated with a sum over N discrete atmospheric layers with each layer having an averaged extinction coefficient $\beta_j(\lambda)$. Equation (7) can then be replaced by a system of linear equations

$$\tau_i(\lambda) = \sum_{j=i}^N \beta_j(\lambda) \rho_{ij} \quad \text{for } i = 1, 2, \dots, m, \quad (8)$$

where ρ_{ij} is the sunray's pathlength in the j th layer with its tangent height at the i th layer, and $\beta_j(\lambda)$ is the averaged atmospheric extinction coefficient for the j th layer at wavelength λ . $\beta_j(\lambda)$ can be separated into contributions from each constituent as described by Eq. (3). Combining Eqs. (8) and (3), we have

$$\tau_i(\lambda) = \sum_{j=i}^N \rho_{ij} [\beta_{\text{ND}}(\lambda) + \beta_{\text{O}_3}(\lambda) + \beta_{\text{NO}_2}(\lambda) + \beta_a(\lambda)]_j \quad (9)$$

for $i = 1, 2, \dots, m$.

Equation (9) describes four coupled systems of linear equations corresponding to the 1.0 μm , 0.6- μm , 0.45- μm , and 0.385- μm SAGE wavelength measurements. Due to the constraint on the number of wavelength measurements available from the instrument, it is only possible to retrieve a maximum of four independent sets of vertical constituent profiles. It is well known that nitrogen dioxide distribution in the atmosphere peaks at 30 km, while aerosol peaks at 15–20 km with negligible contribution above 25 km. To make full use of the spatial separation of aerosol and NO_2 vertical distri-

butions in the atmosphere, we are inverting the NO_2 vertical profile above 25 km while inverting a two-parameter model for the aerosol layer below 25 km.

There are two approaches for the inversion of multiwavelength transmittance profiles into extinction profiles for each contributing constituent. The first approach is based on two successive steps of inversion.¹⁰ In the first step, Eq. (8) is inverted independently at each wavelength channel to give total extinction coefficients vs tangent altitude profiles. Then in the second step, the inverted total extinction coefficients for all wavelength channels are used at each altitude to invert the contribution from each constituent. The inversion stops when the complete altitude range has been covered. There are inherent difficulties associated with this type of inversion approach. First, the input to the second inversion step is by itself an inverted quantity. Estimating the uncertainty associated with this input for the second inversion process would be difficult, and either an overestimation or underestimation on this uncertainty is undesirable and will affect the final inversion results. Second, this approach does not provide enough flexibility to incorporate a vertical smoothing constraint on the retrieved constituent profiles.

The second approach is a direct one-step inversion from the multiwavelength transmittance profiles to

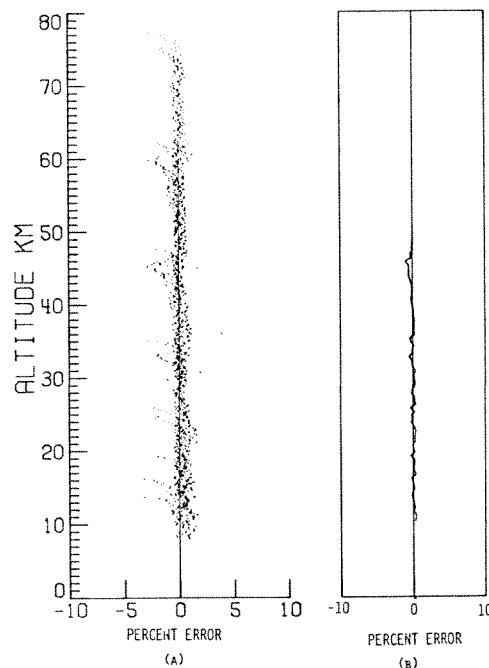


Fig. 7. (a) Percent error of transmittance value associated with each simulated data point for the solar extinction measurement. (b) Percent error of mean transmittance values obtained from averaging data points over 0.5-km altitude steps.

each constituent vertical profile. We have developed this inversion approach based on the consideration that each wavelength channel is most sensitive selectively to an individual constituent. Figure 8 illustrates this point by showing the ratio profiles of $\beta_a/\beta_{\text{total}}$ at 1.0 μm , $\beta_{\text{O}_3}/\beta_{\text{total}}$ at 0.6 μm , $\beta_{\text{ND}}/\beta_{\text{total}}$ at 0.385 μm , $\beta_a/\beta_{\text{total}}$ at 0.45 μm , and $\beta_{\text{NO}_2}/\beta_{\text{total}}$ at 0.45 μm . The atmospheric model used in Fig. 8 is the same as illustrated in Fig. 5. It is obvious that the contributions by aerosol, ozone, and neutral density are heavily weighted at the 1.0- μm , 0.6- μm , and 0.385- μm wavelengths, respectively, with a variable contribution from nitrogen dioxide and aerosol at the 0.45- μm wavelength. This consideration leads us to formulate an iterative approach in which each constituent is inverted at the wavelength channel which is most sensitive to its contribution. A set of initial-guess constituent profiles is first selected. The inversion process begins, for example, at the 1.0- μm wavelength channel by computing the initial aerosol optical thickness $\tau_{ai}^{(0)}$ at 1.0 μm :

$$\tau_{ai}^{(0)} = \tau_i^m - \sum_{j=i}^N \rho_{ij} [\beta_{\text{ND}}^{(0)} + \beta_{\text{O}_3}^{(0)} + \beta_{\text{NO}_2}^{(0)}]_j, \quad (10)$$

where τ_i^m is the measured total optical depth at 1.0 μm , $\beta_{\text{ND}}^{(0)}$, $\beta_{\text{O}_3}^{(0)}$, and $\beta_{\text{NO}_2}^{(0)}$ are, respectively, the initial-guess profile for neutral density, ozone, and NO_2 . The first update of the aerosol extinction profile $\beta_a^{(1)}$ at 1.0 μm is then inverted from the following equation:

$$\tau_{ai}^{(0)} = \sum_{j=i}^N \rho_{ij} \beta_{aj}. \quad (11)$$

In this study, Eq. (11) is inverted with Twomey's modification of Chahine's nonlinear relaxation method.¹¹ The iterative equation in this case

$$\beta_{aj}^{(1)} = \beta_{aj}^{(0)} \left\{ \left[1 + \left[\frac{\tau_{ai}^{(0)}}{\sum_{j=i}^N \rho_{ij} \beta_{aj}^{(0)}} - 1 \right] \frac{\rho_{ij}}{\rho_{ii}} \right] \right\}, \quad (12)$$

where $\beta_{aj}^{(0)}$ is the initial-guess profile for aerosol extinction at 1.0 μm . The absolute value sign in Eq. (12) is to insure a positive solution. Each $\tau_{ai}^{(0)}$ value is used to update the aerosol extinction $\beta_{aj}^{(0)}$ at the j -level connected by the matrix element ρ_{ij} . The matrix ρ_{ij} is sharply peaked at the diagonal and slowly decreasing toward the off-diagonal elements. It is found that by truncating the weighting factor ρ_{ij}/ρ_{ii} to levels close to the diagonal insures the stability of the inversion. This will at the same time provide sufficient smoothing on the retrieved vertical profile. In this work, the weighting factor ρ_{ij}/ρ_{ii} is truncated at 4 km above the diagonal element. After the first updated aerosol profile has been obtained, the inversion process proceeds on to the 0.6- μm wavelength. An updated ozone profile can be calculated with Eq. (12) using the first updated aerosol profile together with the initial profiles for other constituents. The process is continued at 0.45 μm and then at the 0.385- μm wavelength. A complete set of updated constituent profiles is obtained in this manner. The inversion process then repeats itself starting at the 1.0- μm wavelength. This iterative cycle

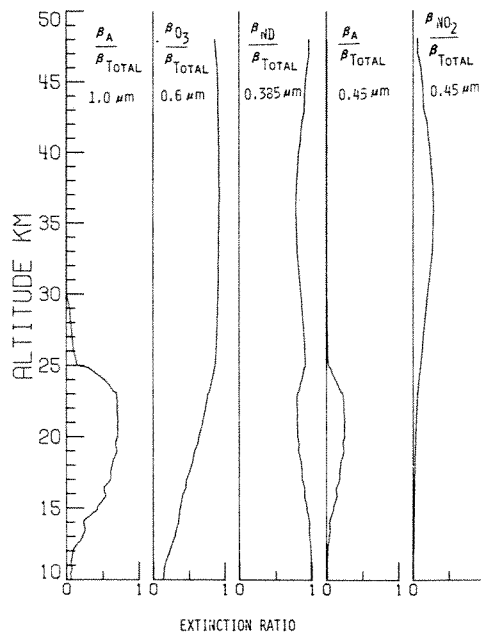


Fig. 8. Vertical profiles of extinction ratio at the four wavelengths

will continue until a certain convergence criterion has been met. We have used a convergence criterion based on the absolute value of the residual between the computed transmittance value and the measurement at each atmospheric level to be less than or equal to the standard deviation associated with the mean transmittance value deduced from the radiometric data. After the convergence criterion is satisfied for all the atmospheric levels in each wavelength channel, the iteration stops. It is found that the inverted solutions show no dependence on the initial-guess profiles, however, the speed of convergence does depend on how closely the shape of the initial guesses and the actual profiles correspond.

Inversion Results for a Horizontally Homogeneous Atmosphere

The data reduction scheme and the inversion approach described above have been applied to simulated experimental data assuming various amounts of experimental error. Figure 9 shows a set of typical inversion results for each constituent extinction profile. The input profiles which are identical to those shown in Fig. 5 are denoted by solid lines. The background aerosol model illustrated in Fig. 3 has been assumed. Experimental errors consisting of a random noise of 0.5% and scan rate error of 0.5 min of arc/sec have been included in the simulation process. These error levels correspond to twice the worst-case expected performance of the SAGE instrument. Ten independent simulations, reductions, and inversions have been performed on the same input profiles. The bars represent one standard deviation in the inverted mean profiles for the ten simulations. In the inversion calculations, a

linear relationship between aerosol extinction coefficient and wavelength has been assumed. This assumption is not strictly correct, but the errors introduced in the retrieval of ozone and neutral density profiles are sufficiently small due to the small aerosol contributions in the 0.6- μm and the 0.385- μm wavelength regions. The inversion results indicated that a vertical ozone extinction profile at 0.6 μm can be retrieved to an accuracy of about 10% between 12 km and 42 km with better accuracy at the peak of the profile. The neutral density vertical profile can be retrieved to a few percent accuracy from 10 km to approximately 40 km. Aerosol vertical extinction profiles at 1.0 μm and 0.45 μm can be retrieved to about 10% accuracy between 13 km and 24 km, extending over the full altitude range of the stratospheric aerosol layer. Nitrogen dioxide vertical extinction profile at 0.45 μm can be retrieved to an accuracy of about 25% between 25 km and 38 km. The vertical resolution achievable is approximately 1 km. The accuracy of retrieving O_3 , NO_2 , and ND above 40 km can be improved by increasing the altitude interval over which the data are averaged with, of course, a concomitant loss of vertical resolution. Simulations and inversions have also been performed on different sets of input profiles. For input ozone profiles showing fine-scale vertical structures, the inversion results show similar retrieval accuracy over the altitude range from 12 km to 42 km. For different input aerosol profiles ranging from moderate volcanic profiles with a corresponding aerosol optical model to background-level profiles showing extinction peaks at various altitudes between 14 km and 22 km corresponding to profiles observed at different latitude regions on the globe, the

inversion results at 1.0 μm and 0.45 μm generally show about 10% accuracy over the full altitude range of the aerosol layer. For nitrogen dioxide input profiles showing a high level of concentration such as those reported by Brewer,¹² a small bias error within the altitude range from 10 km to 20 km could be introduced in the retrieved ozone profile and aerosol profile at 0.45 μm . This bias error arises from neglecting the nitrogen dioxide contribution within this altitude region and, therefore, can be minimized by including a mean NO_2 profile at this region in the inversion.

Effects of Horizontally Inhomogeneous Aerosol and Ozone Distributions

The assumption of spherically symmetric geometry in our modeling of the atmospheric parameters for the solar extinction measurements is only an approximation. Vertical distributions of atmospheric variables over different latitudes or longitudes on the globe generally show variations due to atmospheric dynamical and chemical effects. Since the inversion method discussed here implicitly assumed a spherically symmetric atmosphere, effects due to horizontally inhomogeneous distributions of the atmospheric constituents can be considered as a source of error for the inversion process. In this section, the data retrieval method that was discussed previously will be applied to a simple horizontally inhomogeneous atmospheric model in order to assess this type of perturbation on the retrieval accuracies.

The four atmospheric constituents—neutral density, aerosol, ozone, and nitrogen dioxide—all show certain degrees of horizontal inhomogeneity. Variations of

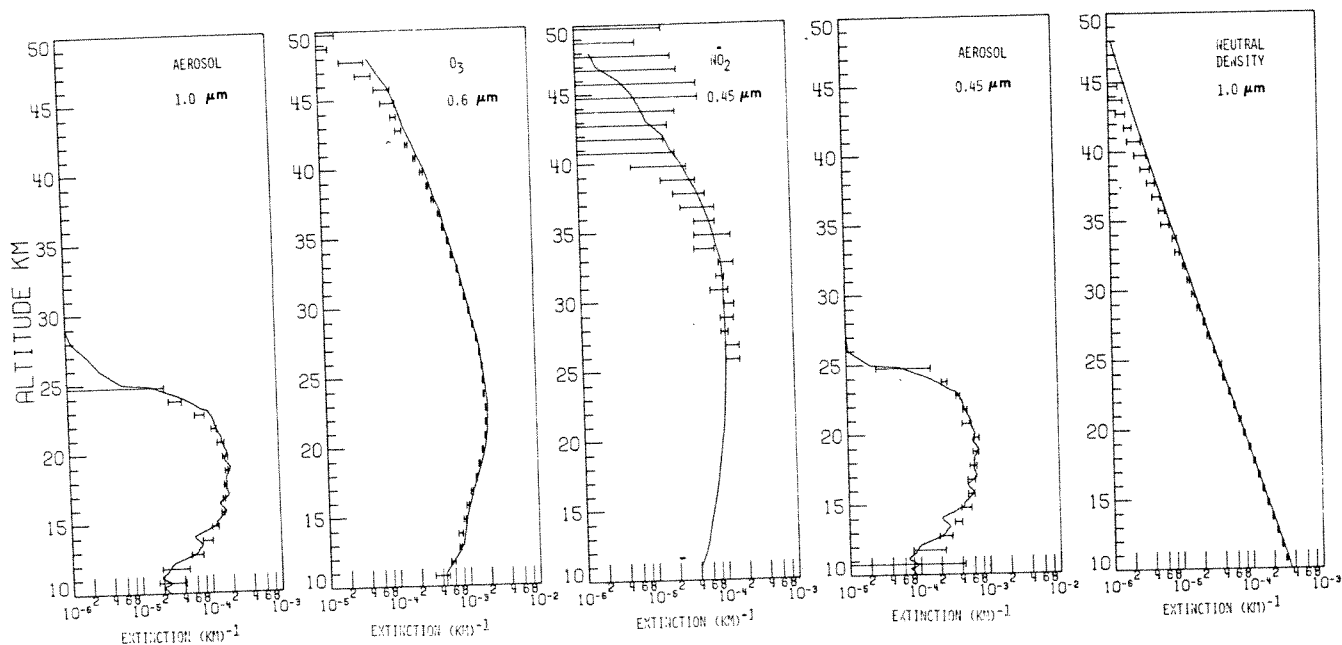


Fig. 9. Inversion results from the four wavelength solar extinction data. Error bars denote one standard deviation from the mean of ten independent simulations and inversions.

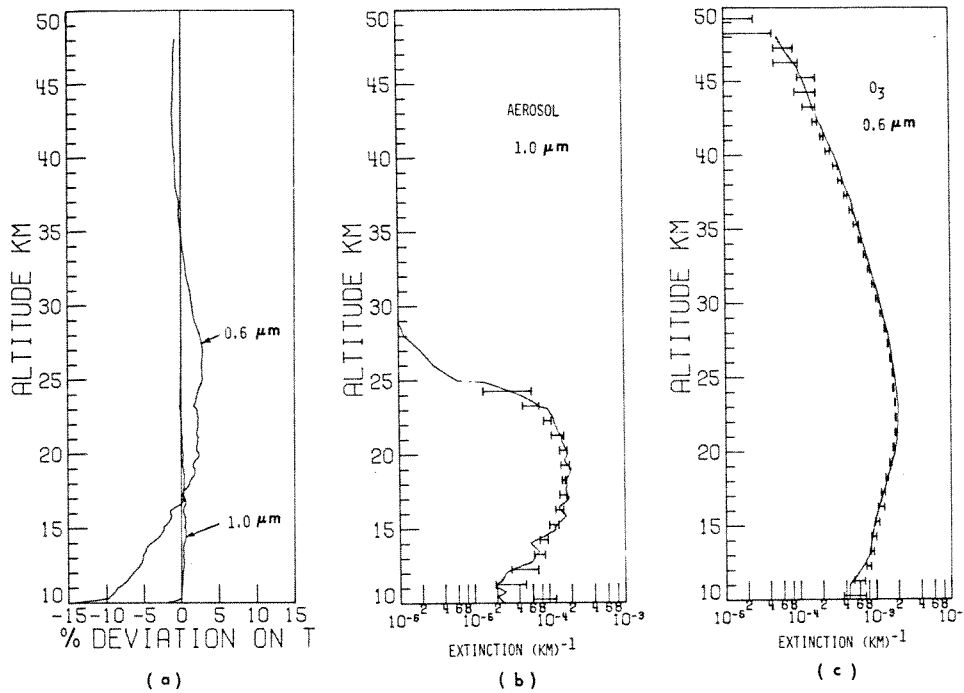


Fig. 10. (a) Percent deviations of transmission profiles for the inhomogeneous atmospheric model to the homogeneous model for 1.0- μm and 0.6- μm wavelengths. (b), (c) Inversion results from the inhomogeneous atmospheric model for aerosol extinction at 1.0 μm and ozone extinction at 0.6 μm .

atmospheric vertical density profiles are generally small over the approximate 300-km horizontal pathlength for SAGE. Aerosol spatial distributions can be more variable, especially during the period of initial volcanic injection and dispersion. Lidar measurements of stratospheric aerosol vertical profiles have shown that during the first 3 months after a large volcanic eruption whose effluents penetrate the stratosphere, that large variations in aerosol vertical distribution were consistently observed. Subsequently, a quasi-steady-state distribution is reached showing a rather smooth vertical profile which persists for a long period of time.¹³ Lidar data have also shown horizontal homogeneity over hundreds of kilometers during these times which are representative of the normal background aerosol. No observational data currently exist on the horizontal distribution of stratospheric aerosol during the initial dispersion phase (first 3 months) after a volcanic injection event. Global aerosol and ozone distribution data at different seasons have been obtained from both balloon and satellite measurements.^{14,15} No observational data currently exist on the global distribution of nitrogen dioxide. Extinction contributions from nitrogen dioxide in the visible spectrum are usually small, however, and the horizontal variation will be neglected in this analysis. In our modeling of the inhomogeneous atmosphere, therefore, we will only consider the horizontally inhomogeneous distributions of aerosol and ozone.

The vertical distribution of aerosol and ozone will be described in terms of mixing ratios profiles $M(h,x)$, where h is the vertical altitude and x is measured along the horizon in earth-center-degree (equivalent to degree latitude or longitude). The mixing ratio profile is considered here because it is this quantity which is

conserved in atmospheric transport processes that do not involve mixing. Moreover, aerosol vertical mixing ratio profiles near polar and equatorial regions have been observed to vary as a simple shift in altitude with respect to tropopause height.¹⁴ We model the horizontal inhomogeneity of aerosol and ozone distributions by assuming that the constant mixing ratio levels are all parallel lines with a horizontal gradient $K = \partial h / \partial x$. To extend this assumption over the entire altitude range of the stratosphere would be a worst case consideration. The horizontal variations of the mixing ratio profile $M(h,x)$ in this case are described by the following equation:

$$M(h,x) = M[h + K(x - x_0), x_0], \quad (13)$$

where x_0 is the horizontal tangent coordinate of the experimental geometry, and $M(h,x_0)$ is the vertical mixing ratio profile at x_0 . Typical values of K deduced from inspection of latitudinal cross-sectional charts for both aerosol and ozone distributions vary from 0.2 km per degree latitude near polar and equatorial regions to a maximum of 1.0 km per degree latitude at midlatitudes near the jet stream region.^{14,15}

In order to analyze the difference between a horizontally inhomogeneous and homogeneous atmospheric model, the atmospheric transmission profiles at different wavelengths for the two models are computed. Figure 10(a) shows the percentage difference between the two calculated transmission profiles at wavelengths of 1.0 μm and 0.6 μm . The vertical profiles for each constituent are the same as those shown in Fig. 5, and they are identical at the horizontal tangent coordinate x_0 for the two models. For the horizontally inhomogeneous model, the aerosol and ozone mixing ratio profiles were computed directly as $\beta_a / \beta_{\text{ND}}$ and $\beta_{\text{O}_3} / \beta_{\text{ND}}$, re-

spectively, with K equal to 1.0 km per degree angle for both profiles. The resultant differences of the two transmission profiles which are equivalent to a "noise" term added in the inversion are either less than or equal to the total instrumental noise level as shown in Fig. 7. By including this level of modeling noise in the simulation, one can conclude that the inversion results should not be perturbed to a large extent. This conclusion is confirmed by the inversion results for aerosol at $1.0 \mu\text{m}$ and ozone at $0.6 \mu\text{m}$ as illustrated in Figs. 10(b) and 10(c), respectively. As for Fig. 9, ten independent simulations, reductions, and inversions have been performed on the horizontally inhomogeneous atmospheric model including the same level of experimental errors as discussed previously. The inverted results denoted by error bars of one standard deviation are shown superimposed on the input profiles (solid lines) at the tangent coordinate. Comparison with Fig. 9 shows that the perturbation on inversion accuracies due to horizontal inhomogeneity is small. Inverted results for neutral density, nitrogen dioxide, and aerosol extinction at $0.45 \mu\text{m}$ are also similar to the results shown in Fig. 9. Additional analysis with K values less than 1.0 km per degree produced proportionally smaller differences.

Effects of a horizontally inhomogeneous atmosphere with aerosol and ozone profiles showing more vertical structure have also been analyzed. Typical results are illustrated in Fig. 11. A moderate volcanic aerosol profile¹⁶ and an ozone profile with additional vertical structure were used as inputs in the simulations with K

equal to 1.0 km per degree. The accuracies of the inversion results are approximately the same as those illustrated in Fig. 9 and 10.

Conclusions

This paper has demonstrated that simulated solar occultation data from the four channel SAGE instrument can be inverted to produce aerosol, ozone, neutral density, and nitrogen dioxide vertical extinction profiles in the stratosphere. A data reduction scheme has been developed to reduce the multiwavelength radiometric data into atmospheric transmittance profiles. An iterative inversion approach is then used to retrieve all the constituent vertical profiles directly from the multiwavelength transmittance profiles with the assumption of a horizontally homogeneous atmosphere. Based on simulations of the experimental events including various instrumental error sources and 1-km height resolution it is found that ozone vertical extinction profiles between 12 km and 42 km can be retrieved to an accuracy of about 10% with much better accuracy at the ozone peak, neutral density profiles can be retrieved to a few percent accuracy up to about 40 km, aerosol extinction profiles at $1.0 \mu\text{m}$ and $0.45 \mu\text{m}$ can be retrieved to about 10% accuracy over the full altitude range of the stratospheric aerosol layer, and nitrogen dioxide extinction profiles at $0.45 \mu\text{m}$ can be retrieved to about 25% accuracy from 25 km to 38 km. Accuracies above 40 km can be improved by vertical smoothing, i.e., averaging over larger height intervals.

The effects of horizontally inhomogeneous distri-

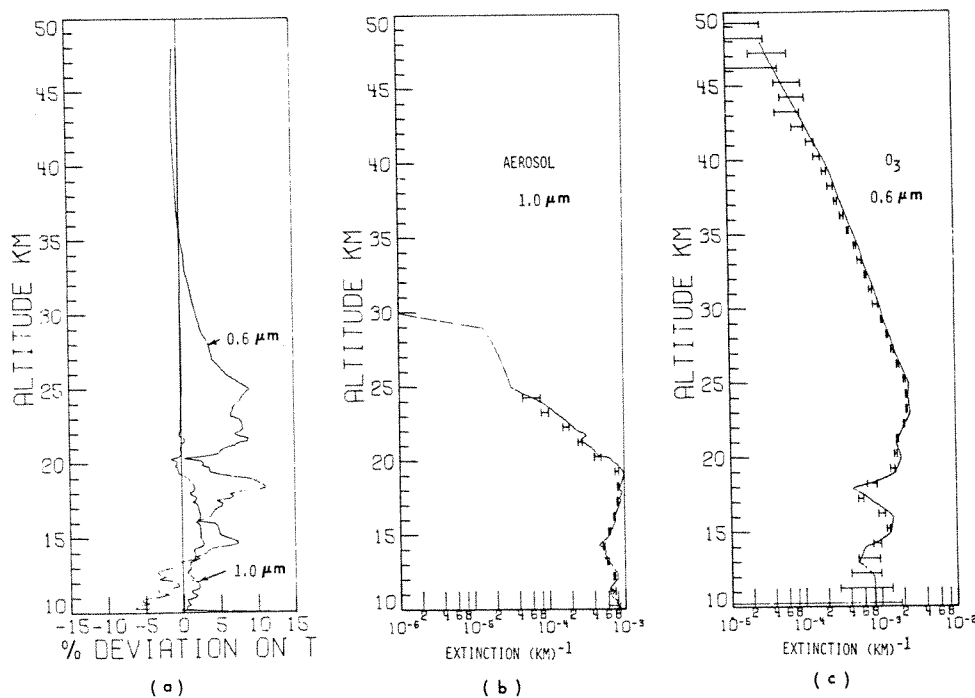


Fig. 11. Same as Fig. 10 with different aerosol and ozone vertical profiles.

butions of aerosol and ozone on the retrieval accuracies have also been analyzed. A simple one parameter model describing the horizontal variations of aerosol and ozone profiles was constructed based on global observational data. Inversion results obtained from the inhomogeneous atmospheric model indicate that the perturbation on the retrieval accuracies is small for a greater than typical amount of horizontal inhomogeneity exhibited in the atmosphere.

The authors thank T. J. Swissler and the SAGE Team comprised of R. A. Craig, D. M. Cunnold, G. W. Grams, B. M. Herman, D. E. Miller, D. G. Murcray, T. J. Pepin, W. G. Planet, and P. B. Russell for their many discussions concerning the development of this inversion technique.

References

1. M. P. McCormick, H. B. Edwards, L. E. Mauldin III, and L. R. McMaster, in "Atmospheric Aerosols: Their Optical Properties and Effects," NASA CP-2004 (1976), p. TUB2.
2. M. V. Klein, *Optics* (Wiley, New York, 1970), p. 31.
3. D. Deirmendjian, *Electromagnetic Scattering on Spherical Polydispersions* (American Elsevier, New York, 1969), Chap. 4.
4. H. C. van de Hulst, *Light Scattering by Small Particles* (Wiley, New York, 1957), Chap. 9.
5. R. G. Pinnick, J. M. Rosen, and D. J. Hofmann, *J. Atmos. Sci.* **33**, 304 (1976).
6. *U. S. Standard Atmosphere* (U.S. GPO, Washington, D.C., 1976).
7. J. C. Fontanella, A. Girard, L. Gramont, and N. Louisnard, *Appl. Opt.* **14**, 825 (1975).
8. G. B. Northam, J. M. Rosen, S. H. Melfi, T. J. Pepin, M. P. McCormick, D. J. Hofmann, and W. H. Fuller, *Appl. Opt.* **13**, 2416 (1974).
9. C. W. Allen, *Astrophysical Quantities* (Athlone, London, 1963), p. 190.
10. W. P. Chu, in *Inversion Methods in Atmospheric Remote Sounding*, A. Deepak, Ed. (Academic, New York, 1977), p. 505.
11. S. Twomey, *J. Comput. Phys.* **18**, 188 (1975).
12. A. W. Brewer, C. T. McElroy, and J. B. Kerr, *Nature* **246**, 129 (1973).
13. M. P. McCormick, T. J. Swissler, W. P. Chu, and W. H. Fuller, *J. Atmos. Sci.* **35**, 1296 (1978).
14. J. M. Rosen, D. T. Hofmann, and J. Laby, *J. Atmos. Sci.* **32**, 1457 (1975).
15. J. London and J. E. Frederick, *J. Geophys. Res.* **82**, 2543 (1977).
16. T. J. Pepin, M. P. McCormick, W. P. Chu, F. Simon, T. J. Swissler, R. R. Adams, K. H. Crumbly, and W. H. Fuller, in *Apollo-Soyuz Test Project, Summary Science Report*, NASA SP-412 (1977), p. 127.

Application Explorer Mission 2 (AEM 2) - Stratospheric Aerosol and Gas Experiment (SAGE)

Dr. M. P. McCormick, Experiment Scientist
Dr. R. A. Craig, deceased
Dr. D. M. Cunnold
Dr. G. W. Grams
Dr. B. M. Herman
Dr. D. E. Miller
Dr. D. G. Murcray
Dr. T. J. Pepin
Dr. W. G. Planet
Dr. P. B. Russell

NASA LaRC
Florida State University
Georgia Institute of Technology
Georgia Institute of Technology
University of Arizona
Met Office, UK
University of Denver
University of Wyoming
NOAA-NESS
SRI International

ABSTRACT:

The objective of the Stratospheric Aerosol and Gas Experiment (SAGE) is to determine the spatial distribution of stratospheric aerosols and ozone on a global scale. Specific objectives are -- (1) to develop a satellite-based remote sensing technique for stratospheric aerosols and ozone, (2) to map aerosol and ozone concentrations on a time scale shorter than major stratospheric changes, (3) to locate stratospheric aerosol and ozone sources and sinks, (4) to monitor circulation and transfer phenomena, (5) to observe hemispheric differences, and (6) to investigate the optical properties of aerosols and assess their effects on global climate. The SAGE instrument consists of a telescope and a spectrometer subassembly which separates and measures the attenuation of solar radiation at four wavelengths (.38, .45, .6, and 1.0 micrometers) during solar occultation. As the spacecraft emerges from the earth's shadow, the sensor scans the earth's atmosphere from the horizon up, and measures the attenuation of solar radiation in different atmospheric height layers. This procedure is repeated during spacecraft sunset. Two vertical scannings are obtained during each orbit, with each scan requiring approximately 1 min of time to cover the atmosphere above the troposphere. The instrument has a field of view of approximately 0.5 arc minutes which results in atmospheric height resolution of less than 1 km.

SUMMARY:

The AEM 2 spacecraft was launched February 18, 1979. Eight months of instrument data have been collected to date and are currently being merged with spacecraft ephemeris and meteorological data for routine data processing. Correlative observations have also been made at several sites and preliminary data analysis indicates excellent comparison with the coincident satellite observations. A complete error analysis of the satellite data is underway as part of the data validation required prior to archival.

During the period April 14-20, 1979, volcano La Soufrière erupted in the Caribbean area. A volcanic plume was observed to penetrate into the stratosphere by an aircraft laser radar while performing ground-truth measurements for SAGE sensor. Immediately after the volcanic eruption, the SAGE sensor was able to map the eruption region in latitude and longitude, and obtain information on the strength and spatial distribution of the injection. These data are currently being analyzed to determine the spreading of the volcanic plume and its influence on stratospheric aerosol loading.

The spacecraft, since June 11, 1979, has experienced a general degradation in the battery resulting in low power capacity. The instrument module continues to work extremely well when adequate power is available for operation but approximately 50% data loss has been experienced.

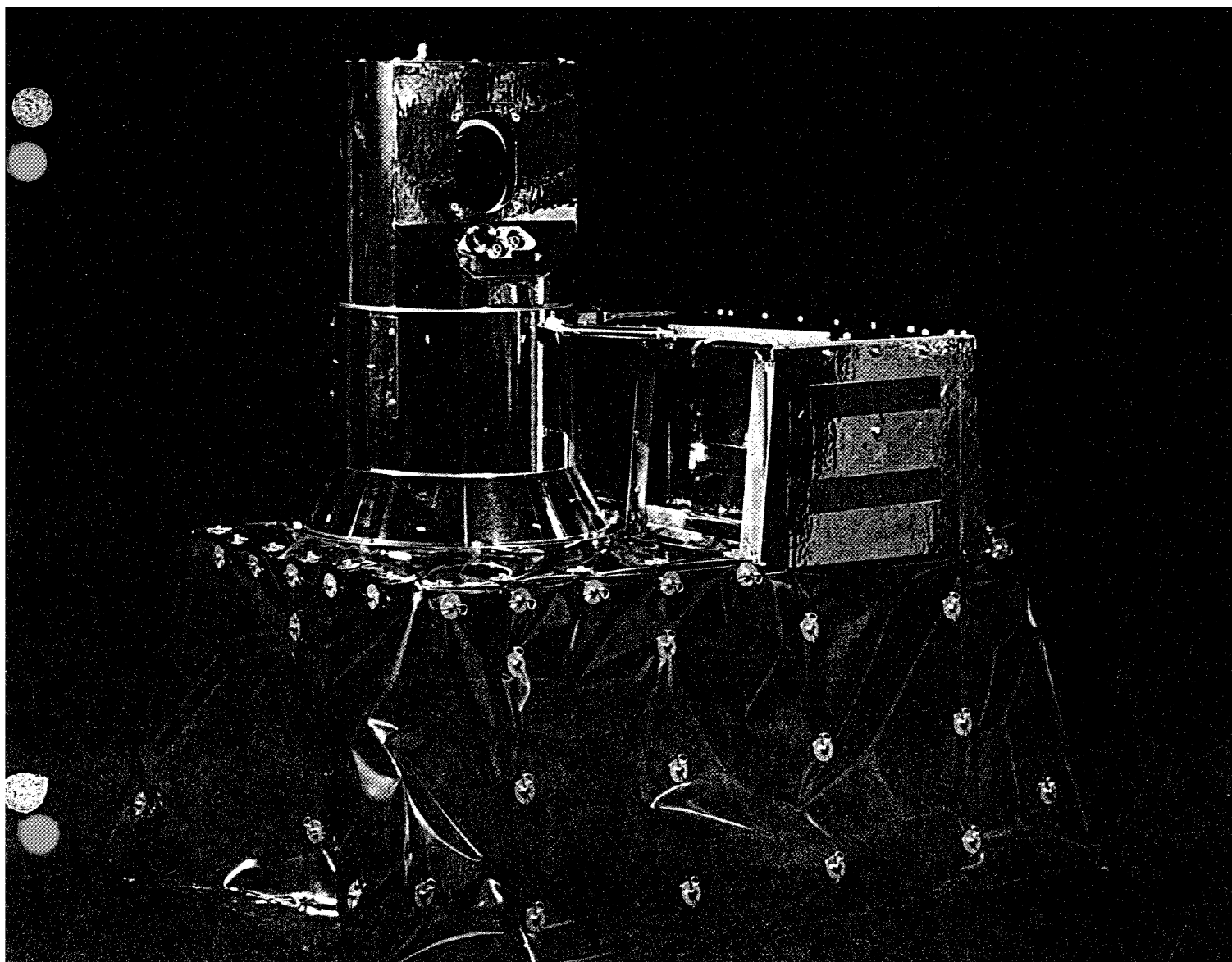
JOURNAL PUBLICATIONS:

1. Chu, W. P. and M. P. McCormick, 1979: Inversion of Stratospheric Aerosol and Gaseous Constituents From Spacecraft Solar Extinction Data in the 0.38-1.0 μm Wavelength Region. Appl. Opt., 18, 1404-1413.
2. McCormick, M. P., P. Hamill, T. J. Pepin, W. P. Chu, T. J. Swissler, and L. R. McMaster, 1979: Satellite Studies of the Stratospheric Aerosol. Bull. Am. Met. Soc., 60.
3. Russell, P. B., Editor 1979: SAGE Ground Truth Plan - Correlative Measurements for the Stratospheric Aerosol and Gas Experiment (SAGE) on the AEM-B Satellite. NASA TM 80076.
4. West, S., 1979: The Best Read Volcano. Science News, 115, 314-318.

Handwritten signature or scribble

Bulletin of the American Meteorological Society

Volume 60 Number 9 September 1979



Cover Photograph: Picture of the flight model of the Stratospheric Aerosol and Gas Experiment (SAGE) presently flying on the Applications Explorer Mission II spacecraft. SAGE, built by the Ball Aerospace Systems Division for the NASA Langley Research Center and launched in February 1979, is a four spectral-channel sensor measuring profiles of stratospheric aerosols and ozone. For more details, see the article by McCormick *et al.*, which begins on page 1038.

Satellite Studies of the Stratospheric Aerosol

M. P. McCormick, Patrick Hamill,¹
T. J. Pepin,² W. P. Chu, T. J. Swissler,¹
and L. R. McMaster
NASA Langley Research Center
Hampton, Va. 23665

Abstract

The potential climatological and environmental importance of the stratospheric aerosol layer has prompted great interest in measuring the properties of this aerosol. In this paper we report on two recently deployed NASA satellite systems (SAM II and SAGE) that are monitoring the stratospheric aerosol. The satellite orbits are such that nearly global coverage is obtained. The instruments mounted in the spacecraft are sun photometers that measure solar intensity at specific wavelengths as it is moderated by atmospheric particulates and gases during each sunrise and sunset encountered by the satellites. The data obtained are "inverted" to yield vertical aerosol and gaseous (primarily ozone) extinction profiles with 1 km vertical resolution. Thus, latitudinal, longitudinal, and temporal variations in the aerosol layer can be evaluated. The satellite systems are being validated by a series of ground truth experiments using airborne and ground lidar, balloon-borne dustsondes, aircraft-mounted impactors, and other correlative sensors. We describe the SAM II and SAGE satellite systems, instrument characteristics, and mode of operation; outline the methodology of the experiments; and describe the ground truth experiments. We present preliminary results from these measurements.

1. Introduction

Nearly 20 years ago Junge *et al.* (1961) carried out a series of measurements on the aerosol content of air in the upper troposphere and lower stratosphere using balloon-borne particle counters. They found that the total number of particles per milligram of air decreases with altitude, but that just above the tropopause there is a substantial increase in the concentration of large particles in a region several kilometers thick. This layer of large particles is called the stratospheric aerosol or, sometimes, the Junge layer. It might be noted, however, that the existence of a stratospheric particulate veil was postulated much earlier. In fact, for centuries scientists have been speculating that the brilliant sunsets commonly observed after volcanic eruptions are due to volcanic dust injected into the stratosphere. But the measurements by Junge and subsequent investigators provided the first quantitative information on the properties of the stratospheric particles. Thus, we now know that the "large" particles

exist in a well-defined layer in the lower stratosphere from slightly above the tropopause to less than 30 km, that they are distributed in size primarily between 0.1 and 1.0 μm diameter in either a unimodal or polymodal size distribution, that they are probably primarily composed of an impure solution of sulfuric acid and water, that they are quite numerous shortly after violent volcanic eruptions, and that the number density slowly decays with an *e*-folding time of about 1 year (McCormick *et al.*, 1978). Excellent reviews of the characteristics of stratospheric aerosols exist in the literature (Junge *et al.*, 1961; Rosen, 1969; Cadle and Grams, 1975; and Toon and Pollack, 1976).

Besides causing colorful twilights, the stratospheric aerosol may both affect weather by being a source of high-altitude cloud condensation nuclei and exert an important influence on climate by modulating the flux of incoming solar radiation and outgoing long wavelength earth radiation (Hansen *et al.*, 1978). For example, it is believed that the eruption of the volcano Tambora in the Dutch East Indies in 1815 (Stommel and Stommel, 1979; Toon and Pollack, 1977) had a significant impact on global weather patterns. In Europe, 1816 was called a "year without a summer" and record low summer temperatures were recorded in New England and elsewhere. The resultant crop damage led to high prices for food and even famines in parts of Britain, France, and Germany.

If we are to expand our knowledge of the stratospheric aerosol, the question arises regarding the best way to measure its properties. In his early work, Junge used impactors and supersaturation chambers carried aloft by balloons, which allowed him to measure total particle number densities. In this country, a group at the University of Wyoming (J. Rosen, D. Hofmann, and T. Pepin) are making stratospheric measurements with balloon-borne optical counters (dustsondes) that allow for differentiation between particles of radius $>0.25 \mu\text{m}$ and particles of radius $>0.15 \mu\text{m}$. Rosen and coworkers have probably made in situ profile measurements of the stratospheric aerosol at more different geographic locations than any other group. The data they have compiled and published are the most comprehensive description of the latitudinal and vertical distribution of the aerosol layer to date. Rosen's work also includes a measurement of the boiling point of the stratospheric particles, showing it to be consistent with that of a 75% sulfuric acid and 25% water solution (Rosen, 1971).

¹Systems and Applied Sciences Corporation, Hampton, Va. 23666.

²University of Wyoming, Laramie, Wyo. 82071.

Another technique for studying the aerosol layer is by analyzing backscattered laser light. Some of the earliest work with this technique was carried out by G. W. Grams, now at Georgia Institute of Technology, and G. Fiocco, now at the University of Rome (Fiocco and Grams, 1966). Presently, a number of investigators are studying the stratospheric aerosol with lidar systems. Among these investigators are P. B. Russell at SRI International, M. P. McCormick's group at the NASA Langley Research Center (LaRC), and non-U.S. groups such as those of M. Hirano in Japan, J. Blamont in France, R. Reiter in Germany, B. R. Clemesha in Brazil, and V. Zuyev in the Soviet Union.

Other methods presently used for measuring the properties of the stratospheric aerosol include the wire impactors flown on a U-2 aircraft by N. Farlow at the NASA Ames Research Center, a quartz crystal microbalance impactor flown by D. C. Woods of NASA LaRC, a polar nephelometer flown by G. W. Grams, and a filter impactor flown by A. Lazrus of the National Center for Atmospheric Research.

All of these techniques (except for the airborne systems) give only a localized picture of the stratospheric aerosol. By patching together the results of a large number of measurements distributed in time and space, one can draw a sketchy picture of the geographic and temporal characteristics of the aerosol layer. However, it is not yet known whether or not the aerosol layer exhibits any systematic longitudinal variations, nor is it known whether or not there is a residual nonvolcanic component to the layer that is maintained by gas and particulate diffusion from the troposphere followed by particle growth in the stratosphere. The size distribution and composition of the particles are still uncertain and the radiative properties of the layer are poorly determined.

The last volcanic eruption to inject a significant amount of matter into the stratosphere was Volcán de Fuego (14.5°N), which exploded in mid-October 1974. Stratospheric particles attributable to this volcano were observed at mid-latitudes (37.1°N) on 26 November 1974 (McCormick *et al.*, 1978). The latitudinal spread of the volcanic veil would have been very interesting to observe since it is an excellent tracer for stratospheric latitudinal diffusion. This information is essential in the development of models to evaluate the spread of volcanic dust and in formulating models to determine the climatic impact of volcanoes. The effects of Fuego on climate have not been well evaluated, but Hansen *et al.* (1978), using a 1-dimensional radiative convective model, showed that Agung, which erupted on Bali in 1963, caused a significant average global tropospheric cooling of a few tenths of a degree. This calculated result agrees well with available data on global temperature fluctuations during the 1963-67 period (Newell and Weare, 1976).

Studies of the spread of a volcanic veil would also shed light on the question as to whether the post-volcanic layer consists of particles injected directly

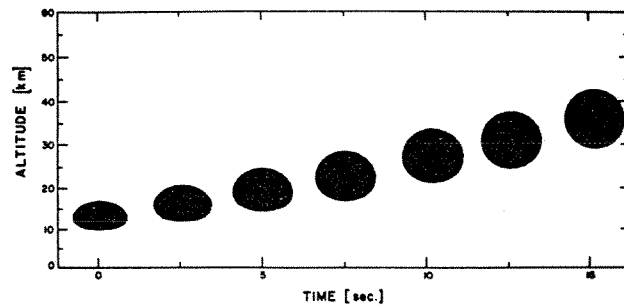


FIG. 1. Sunrise as observed during the Apollo-Soyuz Test Project (Rev. 95, 100°E, 43°S). Note the flattening of the solar disk near the horizon due to refraction.

into the stratosphere or if secondary particle formation and growth is a significant process.

A capability to monitor the aerosol layer in a continuous manner over a wide geographic area has not been available until very recently. In the remainder of this article we describe two new satellite systems that will yield a nearly continuous time coverage of the aerosol layer over most of the surface of the earth.

2. SAM II and SAGE

During the 1975 Apollo-Soyuz Test Project one of the experiments carried on Apollo was the Stratospheric Aerosol Measurement (SAM). The SAM instrument was a lensless single spectral channel sun photometer, which the astronauts pointed at the sun during two satellite sunrises and two satellite sunsets and with which they obtained measurements of the solar intensity in a band centered at 0.83 μm wavelength during these events (Pepin *et al.*, 1977). A series of photographs of the sun rising over the horizon, as observed from Apollo, is shown in Fig. 1, where one notes the interesting optical phenomenon of the apparent flattening of the solar disk due to atmospheric refraction. When the sun's rays reach the satellite they have traversed a portion of the atmosphere and, as described below, the attenuation of the sunlight due to scattering by aerosol particles gives information on the aerosol properties. To interpret these data, however, the effects of refraction must be understood and included in the inversion calculations.

Once the SAM experiment demonstrated the feasibility of the approach, the SAM II and the Stratospheric Aerosol and Gas Experiment (SAGE) programs were developed by NASA with the collaboration of Science Teams drawn from the scientific community.³

³ Science Team for SAM II: M. P. McCormick (leader), NASA-LaRC; G. W. Grams, Georgia Institute of Technology; B. M. Herman, University of Arizona; T. J. Pepin, University of Wyoming; and P. B. Russell, SRI International. Science Team for SAGE: all of the above and, in addition, D. M. Cunnold, Massachusetts Institute of Technology; D. E. Miller, British Meteorological Office; D. G. Murcray, University of Denver; W. G. Planet, National Environmental Satellite Service; and R. A. Craig (deceased), Florida State University.

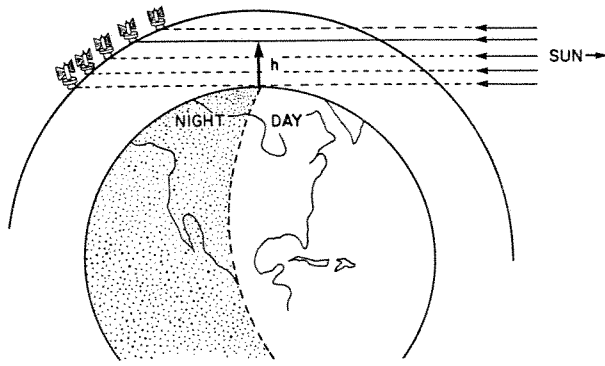


FIG. 2. A sunset as viewed by the Nimbus-7 satellite. The instrument starts to scan the solar disk at a tangent height (h) of about 350 km, and follows it down until the sun disappears. Note that different layers of the atmosphere are successively sampled during the event.

The instruments are, essentially, satellite-mounted sun photometers designed to measure solar intensity profiles during each sunrise and sunset event encountered by the unmanned satellite as it orbits the earth. Since the satellite orbital period is roughly $1\frac{1}{2}$ h, there are approximately 30 sampling opportunities per day (15 sunrises and 15 sunsets) for each instrument. These events occur at different latitudes and longitudes, depending on orbital parameters. Tailoring the satellite orbit for optimal coverage can give a nearly global picture of the stratospheric aerosol. This will be illustrated later for SAM II and SAGE. Longitudinal and latitudinal variations as well as seasonal and short period temporal variations in the layer can then be determined.

Additionally, the data can be utilized to study aerosol sources and sinks in the stratosphere, aerosol transport, aerosol radiative and climatological implications, the effects of sudden warmings, the injection of particulate matter into the stratosphere through the intertropical convergence zone (ITCZ), and, possibly, the development and dispersion of volcanic veils. Furthermore, the experiments will be useful in studies of mesospheric aerosols, noctilucent and nacreous clouds, and thin cirrus clouds near the tropopause. There will also be occasions under cloudless conditions when information on tropospheric aerosols will be obtained.

Figure 2 illustrates the geometrical constraints on the system, showing how the satellite measures solar intensity at different altitudes during a single sunset event. Note that the path of a ray of light from the sun to the satellite successively passes through different air masses, depending on the orbital position of the satellite. The effects of refraction illustrated in Fig. 1 are not shown in Fig. 2. The "tangent height" h is the vertical distance from the surface at the ray tangent. During a typical event, measurements are taken from a tangent height of 350 km, where there is no atmospheric attenuation, to the surface or until the sun is obscured by clouds. The technique, therefore, is

partially self-calibrating since the instrument measures unattenuated sunlight before each sunset and after each sunrise.

SAM II was launched 24 October 1978 on the Nimbus 7 satellite. The payload incorporates several other experiments, including sensors to determine the earth radiation budget; concentrations of various atmospheric trace gases including ozone, H_2O , CH_4 , CO , NO_x , and HNO_3 ; pictures of cloud coverage; and other measurements.

The Stratospheric Aerosol and Gas Experiment (SAGE) was launched 18 February 1979 on a dedicated Applications Explorer Mission (AEM-B) satellite. It is providing measurements of scattering due to aerosols and molecules, as well as absorption due to ozone and nitrogen dioxide. This paper addresses only the aerosol measurements.

An important component of these satellite measuring programs is the associated validation or "ground truth" experiments (Russell *et al.*, 1978; Russell, 1978). These experiments, which are considered in more detail in Section 4, are a concerted study of the stratospheric aerosol utilizing nearly all the techniques presently available. A variety of individual experiments sample the aerosol in the same air mass that is being simultaneously monitored by the satellite. It is felt that these collaborative efforts alone will lead to significant new insights into the properties and nature of the aerosol layer.

3. Satellite and instrument characteristics

As mentioned above, the SAM II instrument is mounted on the Nimbus 7 satellite (Fig. 3). This satellite is in a

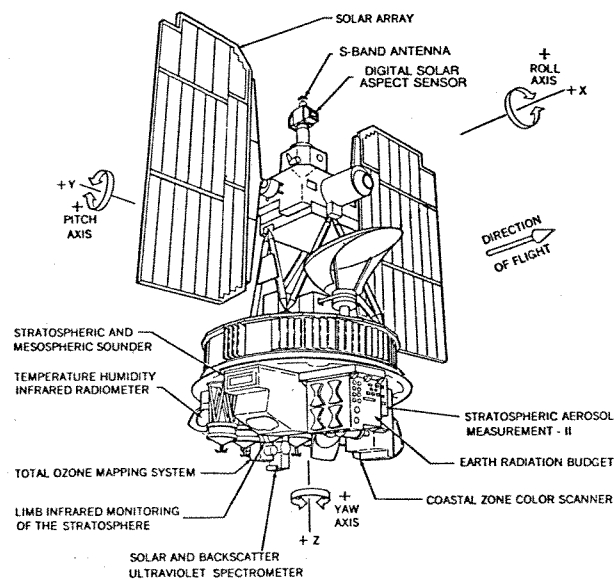


FIG. 3. Nimbus-7 Observatory. The SAM II instrument is mounted on the base of the satellite along with several other atmospheric measurement systems.

TABLE 1. SAM II geographic coverage (Northern Hemisphere, April-June 1979).

Latitude (°N.)	Longitude (°E.)								
	0-40	40-80	80-120	120-160	160-200	200-240	240-280	280-320	320-360
79-77	15*	13	14	14	14	13	14	14	13
77-75	12	15	13	15	13	15	12	14	15
75-73	13	11	13	12	13	11	14	12	12
73-71	10	12	10	11	10	11	10	12	11
71-69	13	11	14	11	13	12	13	12	12
69-67	10	12	9	12	10	11	11	11	11
67-65	15	15	16	15	15	16	15	15	16
65-63	51	52	50	51	50	51	50	52	51

* Number of sunsets or aerosol profiles retrieved between these latitude and longitude bands during the April-June time period.

nearly circular, retrograde orbit with inclination of 99° and orbital altitude of 955 km. The orbit is high-noon sun-synchronous, that is, each equatorial crossing occurs either at 12:00 noon or midnight, local time. The orbital period is 104 min. The satellite encounters sunsets in the polar regions (64°-80°N) of the northern hemisphere and sunrises in the polar regions (64°-80°S) of the Southern Hemisphere. Table 1 illustrates the geographical coverage obtained by SAM II during a typical three-month period.

The SAGE instrument is mounted on a dedicated AEM-B satellite (Fig. 4) with orbit inclined at 55°, an apogee of 660 km, a perigee of 548 km, and period of 96.8 min. This highly precessing orbit provides aerosol profiles distributed around the earth between 79°N and 79°S (depending on the season). Figure 5 gives an idea of the breadth of geographic coverage of the data obtained from SAGE. Indicated in Fig. 5 are the tangent points of the sunrise and sunset events encountered by SAGE during a single month.

The SAM II instrument, a one-spectral channel sun photometer, is illustrated in Fig. 6. The passband, centered at a wavelength of 1 μm, is in a region of the spectrum where absorption by atmospheric gases is negligible. Consequently any attenuation of sunlight is due to scattering by aerosol particles and by molecules (Rayleigh scattering).

In operation, the instrument is activated just before a sunrise or sunset. When the wide field-of-view sun presence sensor indicates a sun intensity of at least 5% relative to the unattenuated sun, the instrument searches for the sun in azimuth. When the sun is nulled to within ±1 arc minute the scan mirror (Fig. 6, right) "fast" scans (3° s⁻¹) in elevation until the sun is acquired. The mirror then "slow" scans vertically across the face of the sun at a rate of 0.25° s⁻¹, reversing itself each time a sun limb crossing occurs. Light from the sun is reflected by the scan mirror to the entrance of a small Cassegrainian telescope. The entrance window of the telescope passes light of wavelength greater than 0.9 μm. A circular aperture placed at the image plane of the telescope serves to define the instrument's instantaneous field of view to be 0.01°, providing an atmospheric vertical resolution on the horizon of approximately 1/2 km altitude. The output

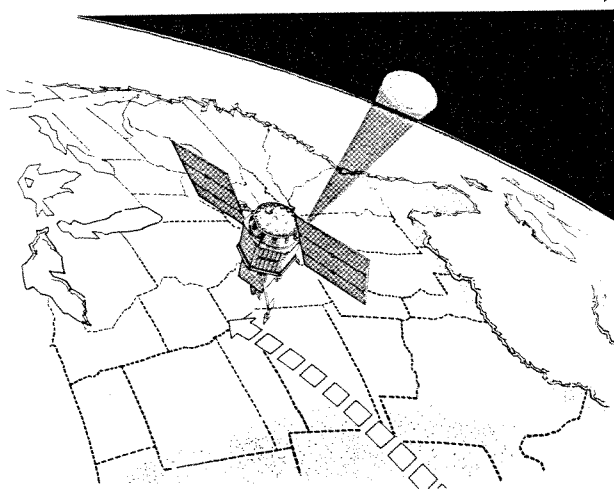


FIG. 4. The Stratospheric Aerosol and Gas Experiment (SAGE) is mounted on a dedicated Applications Explorer Mission Satellite. The orbit of the satellite allows for viewing sunrise and sunset events in the range of latitudes from 79°N to 79°S.

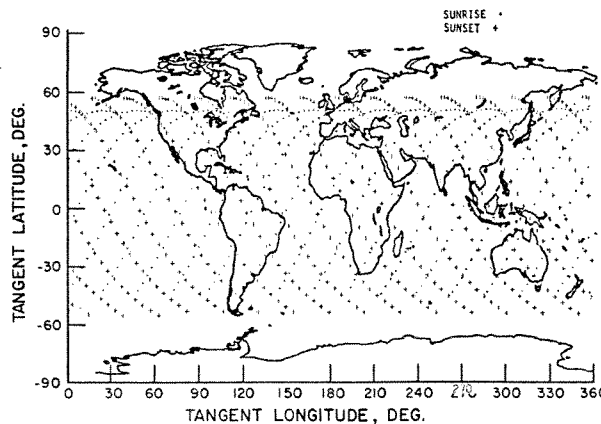


FIG. 5. SAGE sunrise and sunset tangent locations for February 1979. Successive events are shifted slightly in longitude and latitude. The + symbols represent sunsets and the · symbols represent sunrises.

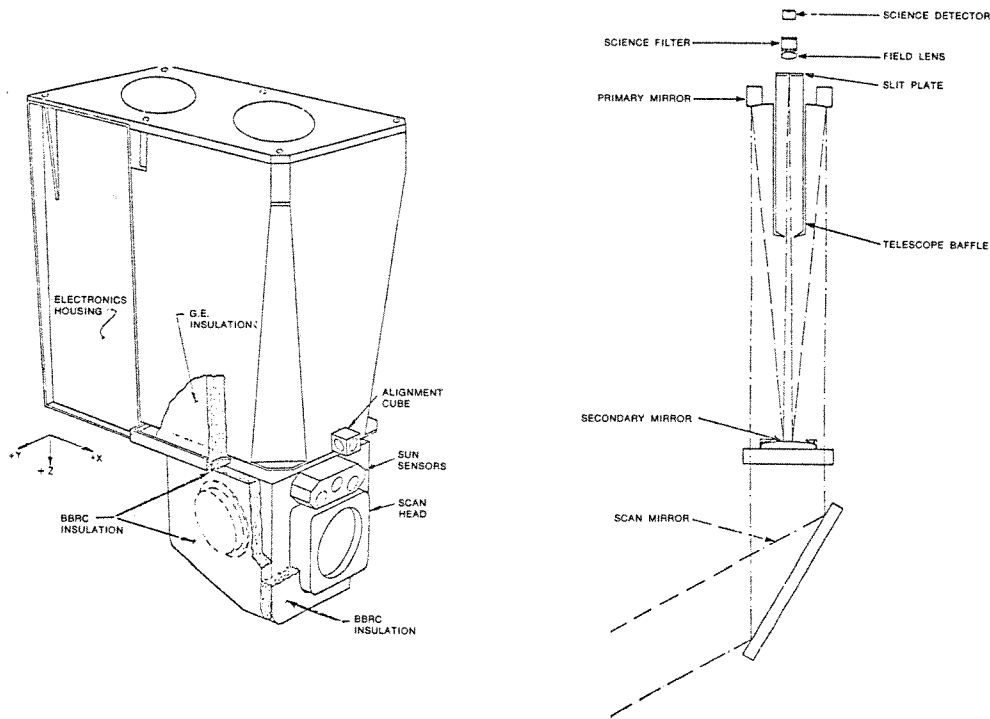


FIG. 6. The SAM II instrument mounted on the interface structure (left). The SAM II optical system (right).

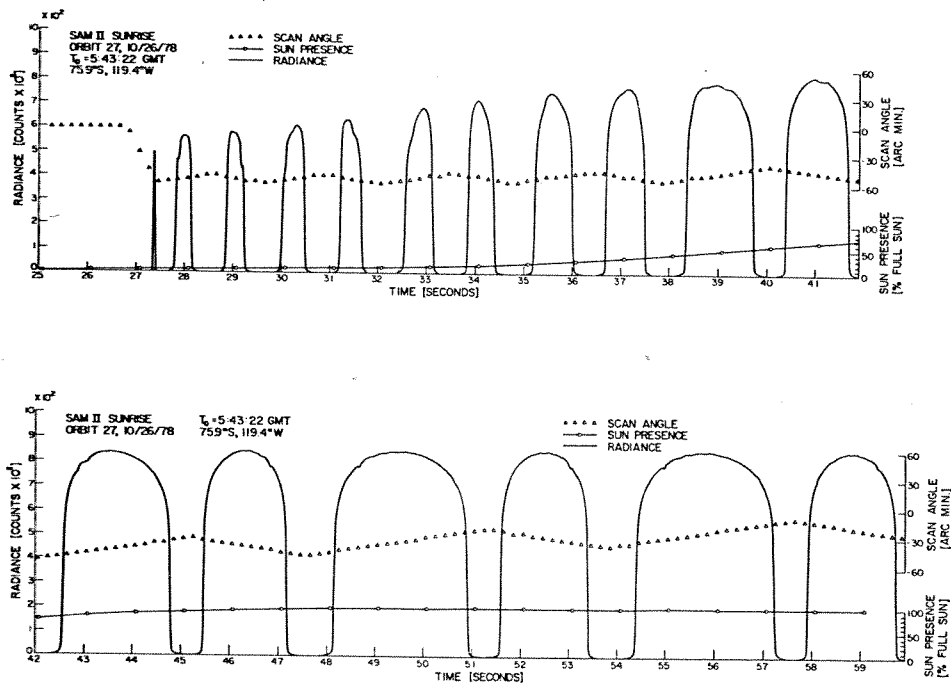


FIG. 7. A SAM II solar sunrise scan taken on 26 October 1978 during the 27th orbit of Nimbus 7. The latitude is 75.9°S. The ordinate (in counts) is directly proportional to the light intensity received by the pin photodiode, and the abscissa (in seconds from beginning of the scan) can be interpreted to give the tangent height, *h*. For description of features see text.

of the telescope is directed through a broadband interference filter that rejects all but the $1 \mu\text{m}$ wavelength ($\pm 0.02 \mu\text{m}$) passband to a photodiode detector. The output of the photodiode is digitized at a rate of 50 samples per second, recorded, and telemetered back to earth where the intensity of received light for each scan across the sun can be reconstructed.

An example of the radiance data is presented in Fig. 7, which shows plots of raw data obtained during a sunrise observed on the 27th SAM II orbit. The scans are alternately upscans and downscans after solar acquisition. Thus, the scan centered at $t = 28 \text{ s}$ is an upscan. The bottom of the sun is encountered at about $t = 27.8 \text{ s}$ corresponding to a tangent height above the earth's surface of about $h = 5 \text{ km}$. The dip in the radiance near the lower edge of the sun is due to a tropospheric cloud layer. This cloud shows up again on the next scan (at $t = 29.2$). The features near the top of the scans between 30 and 33 s are attributable to the stratospheric aerosol layer. At times $t = 39, 41,$ and 43 the dips in the radiance curve may be due to nacreous clouds in the antarctic (the altitude of these features is about 25 km). Finally, it is interesting to note the narrow dip at $t = 46.8 \text{ s}$, which shows up again at $48.7 \text{ s}, 53 \text{ s},$ and 55 s . This repeating feature independent of the earth's atmosphere is a sunspot.

Also given on the same plot are the angle of the scan mirror and the integrated signal from the sun presence sensor. It should be kept in mind that Fig. 7 is a plot of total solar intensity received by the instrument as it scans the sun.

Once the intensity (I) has been determined as a function of tangent height (h), the transmission (T) can be obtained from $T = I/I_0$ where I_0 is the unattenuated intensity (obtained from scans taken at $h \gtrsim 350 \text{ km}$). Then, via inversion techniques described in Chu and McCormick (1979), the transmission profiles are "inverted" to obtain the extinction (attenuation per unit distance) as a function of altitude. Since the contribution due to molecular scattering can, in principle, be calculated, it is possible to determine the extinction caused by aerosol particles. Then, using model results or best estimates for particle size distribution and index of refraction, one can evaluate the aerosol number density as a function of altitude.

The errors associated with calculating the molecular density depend on the temperature and pressure errors in the rawinsonde measurement or the difference between the actual values of these parameters and any model atmosphere that is used. The errors in retrieving the aerosol profile also depend on aerosol loading, i.e., the relative aerosol-to-molecular extinction at a given altitude and instrument uncertainties. Below approximately 25 km the total error in the retrieved aerosol extinction coefficient is typically $\leq 10\%$ in regions where aerosol extinction exceeds molecular extinction by 50%. This means that even under background or nonvolcanic conditions the extinction due to the stratospheric particles can be measured to within 10% accuracy.

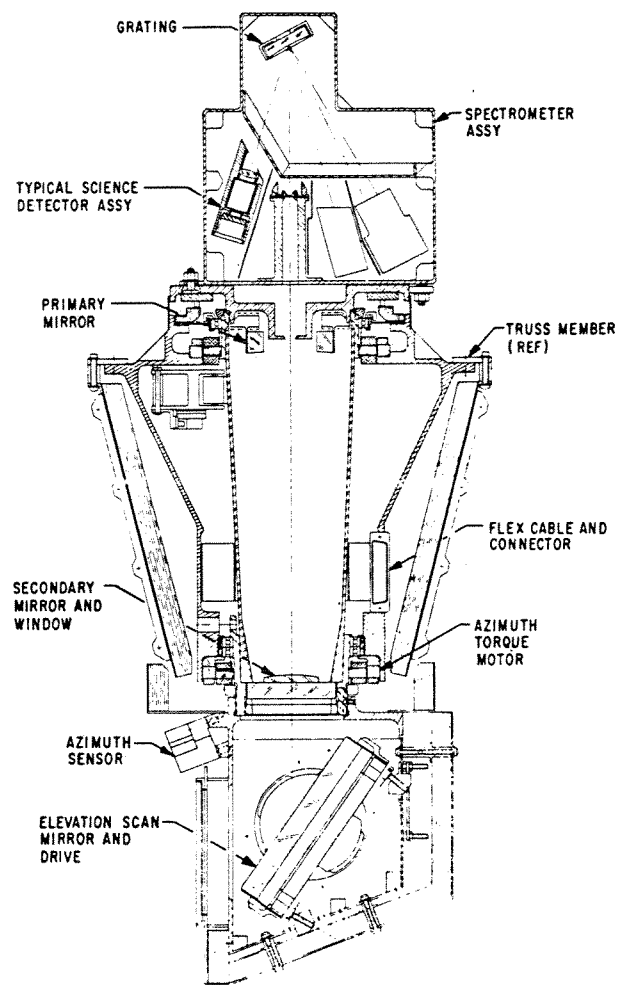


FIG. 8. The SAGE sensor assembly.

SAGE measurements during sunrise and sunset events are very similar to those of SAM II. But, as mentioned above, the SAGE orbit is tailored to complement the SAM II geographical coverage. The SAGE instrument is also somewhat more complex, being a four-channel sun photometer as illustrated in Fig. 8. For SAGE, spectral discrimination is achieved by using a holographic diffraction grating that disperses the different wavelengths in different directions. By placing four sensors at appropriate positions with respect to the grating, it is possible to measure light centered at wavelengths $0.385, 0.45, 0.60,$ and $1.0 \mu\text{m}$. Intensity measurements from these channels can be inverted to obtain profiles of aerosol extinction as well as extinction profiles that can be interpreted to give concentrations of ozone, nitrogen dioxide, and total molecular density. The ozone measurements by SAGE will give accurate, highly spatially resolved ozone profiles from the tropopause to 45 km. Thus, the measurements include the altitude region (35–45 km) where large ozone concentration changes due to the effects of anthropogenic chlorofluoromethane emissions are postulated to take place (Stief *et al.*, 1978). In

addition, the simultaneous measurements of aerosols and ozone will help to determine if aerosol radiative effects influence ozone photochemistry or if there are any other coupled effects, e.g., heterogeneous surface chemistry.

4. The ground truth experiments

The ground truth or validation experiments are an integral part of the SAM II and SAGE projects (Russell *et al.*, 1978; Russell, 1978). These consist of a coordinated set of experiments in which aerosol content and other properties of a given air mass are measured with a variety of different instruments. The results are designed not only to corroborate results of the satellite measurements, but are also intended to independently produce a large body of scientifically significant information. The ground truth experiment sites for SAM II and SAGE are: Sondrestrom, Greenland (November 1978); White Sands, N.Mex. (March 1979); Natal, Brazil (April 1979); Poker Flat, Alaska (July 1979); and Wallops Island (April, June, and October 1979). A practice comparative experiment was carried out at Laramie, Wyo. (September 1978). Other associated experiments will be carried out in Japan, England, Germany, Belgium, France, Australia, and the Soviet Union by participating ground truth experiment teams.

The ground truth experiments are not all the same, and the scientific components will vary. Nevertheless, a good idea of the general type of activities carried out is obtained by considering the Sondrestrom ground truth experiment performed 20–25 November 1978.

Participating in the experiment were personnel from NASA LaRC, NASA Wallops Flight Center, SRI International, Georgia Institute of Technology, NCAR, the University of Wyoming, and NOAA National Weather Service.

The orbit of Nimbus 7 was such that during this period the SAM II instrument made four measurements of the air mass over Greenland. As the satellite passed overhead, the NASA P-3 airborne lidar system studied the aerosol content of the same air mass from below, over the height range from 8–30 km. This required flying the aircraft along the flight paths shown in Fig. 9. At the same time, the NCAR Sabreliner was flying in the stratosphere (tropopause to 15 km), sampling the aerosol with a quartz crystal microbalance impactor and a polar nephelometer. Finally, dustsondes were launched by the University of Wyoming group, measuring concentrations of aerosols in two different size groups over the height range from ground level to 28 km.

All of the experiments were performed without significant problems. The P-3 and Sabreliner flew missions daily from 22–25 November. Dustsondes were launched on 22 and 23 November. In addition, several weather balloons (radiosondes) were launched each day.

Interestingly, during the Natal, Brazil ground truth experiment, there was a large eruption of Soufrière on St. Vincent. The P-3 aircraft studied the volcanic plume

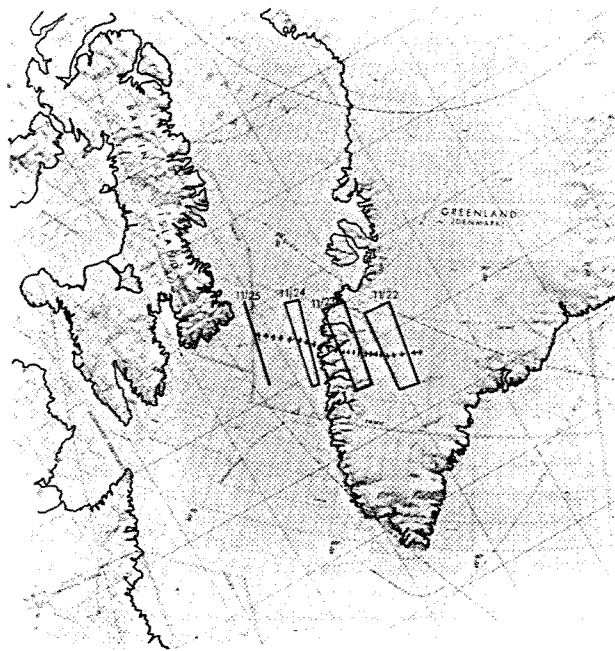


FIG. 9. Flight paths of the P-3 aircraft on 22–25 November 1978 during the SAM II Ground Truth Experiment at Sondrestrom. The dashed lines are projections to the ground of the portion of the atmosphere sampled by the SAM II system during four sunset events. The satellite encountered these events at the same time the airborne lidar on the P-3 was observing the aerosol layer from below. The crosses represent a projection of the SAM II profiles on the surface of the Earth.

with airborne lidar and the quartz crystal microbalance, and SAGE made a number of measurements of the air mass in the general vicinity of the volcano. A more complete description is presented in a recent article in *Science News* (West, 1979).

5. Data

The SAM II and SAGE missions and the associated ground truth experiments will generate a large amount of data that will be processed and made available to the scientific community. The data processing involves merging the data from the satellite sensor with meteorological data to carry out inversions and develop a set of products that include derived aerosol extinction profiles, modeled aerosol number densities, atmospheric molecular extinction coefficients, and total extinction ratios as a function of altitude for each sunrise and sunset event. Additionally, SAGE data will include ozone, nitrogen dioxide, and total molecular concentrations. All of this information will be archived on magnetic tapes and on microfilm.

Display products from the data analysis consist of profiles, cross sections, maps, and time histories. As an example, the SAM II display products are listed in Table 2. SAGE data products will be similar but with the addition of O_3 and NO_2 .

Table 2. SAM II display products.

Title of display products	Frequency	No./Year
Profiles		
Solar irradiance vs time (sunrise/sunset)	Daily	730
Solar irradiance vs altitude		
0-40 km (sunrise/sunset)	Daily	730
40-160 km (sunrise/sunset)	Daily	730
Aerosol coef. of extinction vs altitude		
(0-40 km (sunrise/sunset))	Daily	730
(40-160 km (sunrise/sunset))	Daily	730
Total extinction ratio		
0-40 km (sunrise/sunset)	Daily	730
40-160 km (sunrise/sunset)	Daily	730
6 day avg.—aerosol coef. of ext. vs altitude	1/6 Days	61
Contours		
Long. cross sections of aerosol coef. of ext. vs altitude	1/6 Days	61
Aerosol no. density vs altitude	1/6 Days	61
Total ext. ratio vs altitude	1/6 Days	61
Lat. cross sections aerosol coef. of ext. vs altitude	36/Quarterly	144
Aerosol no. density vs altitude	36/Quarterly	144
Total ext. ratio vs altitude	36/Quarterly	144
Maps		
Aerosol coef. of ext.	14/Quarterly	56
Aerosol no. density	14/Quarterly	56
Total ext. ratio	14/Quarterly	56
Integrated no. density	3/Quarterly	12
Optical depth	3/Quarterly	12
Time histories		
Optical depth from given altitude	15/Quarterly	60
Alt. and peak ext. ratio	2/Quarterly	8

The raw data tapes as well as the products of the data processing, including the ground truth and supporting measurement data, will be archived at the National Space Sciences Data Center at NASA Goddard Space Flight Center, Greenbelt, Md. Additionally, the ozone data products from SAGE will be archived at the World Ozone Data Center, Toronto, Canada. Archiving of the raw radiance has begun. The processed products will be archived beginning in the fall of 1979. Requests for data should be made to the archival center.

6. Preliminary results and conclusions

Preliminary results from SAM II and SAGE indicate that the instruments are performing optimally. Radiance data show stratospheric aerosol concentrations at high latitudes consistent with background levels predicted by models and in agreement with recent lidar observations of the layer (McCormick *et al.*, 1978). Interestingly, a number of measurements actually give aerosol data well down into the lower troposphere, indicating that some information on tropospheric

aerosol content will be obtained. It is also interesting to note that results from the first few SAM II orbits show that the arctic (fall hemisphere) aerosol extends to higher altitudes than does the aerosol layer over the antarctic (spring hemisphere). The data also indicate that the peak aerosol layer over the antarctic gives a greater extinction than the arctic aerosol. This result may be related to a seasonal variation of the aerosol or may indicate a hemispheric difference in the concentration or size distribution of the aerosol particles. It is important to caution the reader that these results are preliminary and based on quick analyses of a small amount of data; we mention them here only to illustrate the kind of information that will be obtained from the satellite projects.

In conclusion, these two satellite systems are expected to give, for the first time, a near-continuous global monitoring of the particulate matter in the upper atmosphere. This information is of fundamental importance in formulating and corroborating radiative models and in evaluating the effects of anthropogenically-produced perturbations of the stratospheric aerosol. Furthermore, as stated earlier, the results obtained should shed light on the questions of aerosol formation and sources and sinks of aerosol particles in the stratosphere, as well as on the properties and characteristics of noctilucent and nacreous clouds.

Future plans for monitoring stratospheric aerosols and gases include the development of SAGE II, which will be flown on a shuttle-launched spacecraft, and of a downward-looking active-probing instrument (shuttle lidar) to map both stratospheric and tropospheric aerosol profiles.

References

- Cadle, R. D., and G. W. Grams, 1975: Stratospheric aerosol particles and their optical properties. *Rev. Geophys. Space Phys.* **13**, 475-501.
- Chu, W. P., and M. P. McCormick, 1979: Inversion of stratospheric aerosol and gaseous constituents from spacecraft solar extinction data in the 0.38-1.0 μm wavelength region. *Appl. Opt.*, **18**, 1404-1413.
- Fiocco, G., and G. Grams, 1966: Observations of the upper atmosphere by optical radar in Alaska and Sweden during the summer 1964. *Tellus*, **18**, 34-38.
- Hansen, J. E., W. C. Wang, and A. A. Lacis, 1978: Mount Agung eruption provides test of a global climatic perturbation. *Science*, **199**, 1065-1067.
- Junge, C. E., C. W. Chagnon, and J. E. Manson, 1961: Stratospheric aerosols. *J. Meteorol.* **18**, 81-108.
- McCormick, M. P., T. J. Swissler, W. P. Chu, and W. H. Fuller, Jr., 1978: Post-volcanic stratospheric aerosol decay as measured by lidar. *J. Atmos. Sci.*, **35**, 1296-1303.
- Newell, R. E., and B. C. Weare, 1976: Factors governing tropospheric mean temperature. *Science*, **194**, 1413-1414.
- Pepin, T. J., M. P. McCormick, W. P. Chu, F. Simon, T. J. Swissler, R. R. Adams, K. H. Crumbly, and W. H. Fuller, Jr., 1977: Stratospheric aerosol measurements. *NASA SP-421*, pp. 127-136. (Available from NTIS, Springfield, Va.)
- Rosen, J. M., 1969: Stratospheric dust and its relationship to the meteoritic influx. *Space Sci. Rev.*, **9**, 58-89.

- , 1971: The boiling point of stratospheric aerosols. *J. Appl. Meteorol.*, 10, 1044-1045.
- Russell, P. B., 1978: SAGE ground truth plan. *NASA TM 80076*, 157 pp. (Available from NTIS, Springfield, Va.)
- , M. P. McCormick, L. R. McMaster, T. J. Pepin, W. P. Chu, and T. J. Swissler, 1978: SAM II ground-truth plan. *NASA TM 78747*, 113 pp. (Available from NTIS, Springfield, Va.)
- Stief, L. J., J. V. Michael, W. A. Payne, D. F. Nava, D. M. Butler, and R. S. Stolarski, 1978: The reaction $\text{Cl} + \text{H}_2\text{CO} \rightarrow \text{HCl} + \text{HCO}$: decreased sensitivity of stratospheric ozone to chlorine perturbations. *Geophys. Res. Lett.*, 5, 829-831.
- Stommel, H., and E. Stommel, 1979: The year without a summer. *Sci. Am.*, June 1979, 176-202.
- Toon, O. B., and J. B. Pollack, 1976: A global average model of atmospheric aerosols for radiative transfer calculations. *J. Appl. Meteorol.*, 15, 225-246.
- , and —, 1977: Volcanoes and the climate. *Natur. Hist.*, January 1977, 13-26.
- West, S., 1979: The best-read volcano. *Science News*, 115, 314, 318. ●

FIRST EVENT (FILE) HAS NO MET DATA - ZERO FILLED

YEAR	MON	DD	HR:MM:SS.SSS	DAY OF YEAR	DT MET	DT EPH	DILAST	TYPE	EV	EVENT-FILE	EVNT LENGTH	CUM. REC.	TOTAL
79		00	00:29:14.313	60.02030455	0	39	9999			1	56		56
79	MAR	01	01:29:36.314	60.06222586	-2	49	60	SUN SE		2	33		89
79	MAR	01	02:06: 2.314	60.08752678	0	36	36	SUN RI		3	56		145
79	MAR	01	03:06:24.317	60.12944811	-2	46	60	SUN SE		4	33		178
79	MAR	01	03:42:41.323	60.15464494	0	32	36	SUN RI		5	57		235
79	MAR	01	04:43:10.333	60.19664737	-2	43	60	SUN SE		6	36		271
79	MAR	01	05:19:29.338	60.22186734	0	29	36	SUN RI		7	58		329
79	MAR	01	06:20: 2.348	60.26391606	-2	40	60	SUN SE		8	34		363
79	MAR	01	06:56:18.326	60.28910100	0	26	36	SUN RI		9	58		421
79	MAR	01	07:56:50.326	60.33113803	-2	36	60	SUN SE		10	36		457
79	MAR	01	08:33:14.325	60.35641580	0	23	36	SUN RI		11	56		513
79	MAR	01	09:33:38.325	60.39836024	-2	33	60	SUN SE		12	35		548
79	MAR	01	10:09:54.324	60.42354542	0	19	36	SUN RI		13	57		605
79	MAR	01	11:10:26.324	60.46558245	-2	30	60	SUN SE		14	36		641
79	MAR	01	11:46:37.324	60.49070977	0	16	36	SUN RI		15	58		699
79	MAR	01	12:47:15.323	60.53281624	-2	27	60	SUN SE		16	33		732
79	MAR	01	13:23:30.323	60.55798985	0	13	36	SUN RI		17	57		789
79	MAR	01	14:24: 4.322	60.60005002	-2	24	60	SUN SE		18	36		825
79	MAR	01	15:00:14.322	60.62516576	0	10	36	SUN RI		19	58		883
79	MAR	01	16:00:50.321	60.66724909	-2	20	60	SUN SE		20	34		917
79	MAR	01	16:37: 2.321	60.69238797	0	7	36	SUN RI		21	57		974
79	MAR	01	17:37:41.320	60.73450602	-2	17	60	SUN SE		22	36		1010
79	MAR	01	18:13:50.320	60.75961019	0	53	36	SUN RI		23	57		1067
79	MAR	01	19:14:30.320	60.80173981	-2	14	60	SUN SE		24	33		1100
79	MAR	01	19:50:34.319	60.82678610	0	50	36	SUN RI		25	57		1157
79	MAR	01	20:51:18.319	60.86896203	-2	11	60	SUN SE		26	33		1190
79	MAR	01	21:27:22.318	60.89400831	0	47	36	SUN RI		27	57		1247
79	MAR	01	22:28: 6.318	60.93618424	-2	8	60	SUN SE		28	36		1283
79	MAR	01	23:04: 9.322	60.96121900	0	44	36	SUN RI		29	58		1341

YEAR	MON	DD	HR:MM:SS.SSS	DAY OF YEAR	DT	MET	DT	EPH	DTLAST	TYPE	EV	EVENT-FILE	EVNT LENGTH	CUM. REC.	TOTAL
79	MAR	02	00:04:55.329	61.00341816	-2			54	60	SUN	SE	30	36		1377
79	MAR	02	00:40:54.337	61.02840668	0			40	35	SUN	RI	31	58		1435
79	MAR	02	01:41:42.337	61.07062890	-2			51	60	SUN	SE	32	34		1469
79	MAR	02	02:17:46.337	61.09567520	0			37	36	SUN	RI	33	57		1526
79	MAR	02	03:18:33.338	61.13788586	-2			48	60	SUN	SE	34	36		1562
79	MAR	02	03:54:30.338	61.16285113	0			34	35	SUN	RI	35	71		1633
79	MAR	02	05:31:20.339	61.23009652	0			31	96	SUN	RI	36	57		1690
79	MAR	02	06:32: 9.340	61.27233032	-2			42	60	SUN	SE	37	37		1727
79	MAR	02	07:08:10.340	61.29734190	0			28	36	SUN	RI	38	57		1784
79	MAR	02	08:09: 1.340	61.33959884	-2			39	60	SUN	SE	39	33		1817
79	MAR	02	08:44:50.341	61.36447154	0			24	35	SUN	RI	40	58		1875
79	MAR	02	09:45:46.341	61.40678635	-2			35	60	SUN	SE	41	37		1912
79	MAR	02	10:21:38.342	61.43169377	0			21	35	SUN	RI	42	58		1970
79	MAR	02	11:22:38.342	61.47405488	-2			32	61	SUN	SE	43	37		2007
79	MAR	02	11:58:27.342	61.49892757	0			18	35	SUN	RI	44	57		2064
79	MAR	02	12:59:26.343	61.54127712	-2			29	60	SUN	SE	45	36		2100
79	MAR	02	13:35:10.343	61.56609193	0			15	35	SUN	RI	46	58		2158
79	MAR	02	14:36:14.344	61.60849935	-2			26	61	SUN	SE	47	37		2195
79	MAR	02	15:12: 6.344	61.63340676	0			12	35	SUN	RI	48	56		2251
79	MAR	02	16:13: 2.345	61.67572159	-2			23	60	SUN	SE	49	35		2286
79	MAR	02	16:48:46.345	61.70053640	0			8	35	SUN	RI	50	57		2343
79	MAR	02	17:49:54.345	61.74299010	-2			19	61	SUN	SE	51	36		2379
79	MAR	02	18:25:29.346	61.76770076	0			5	35	SUN	RI	52	59		2438
79	MAR	02	19:26:41.346	61.81020076	-2			16	61	SUN	SE	53	37		2475
79	MAR	02	20:02:20.346	61.83495771	0			52	35	SUN	RI	54	58		2533
79	MAR	02	21:03:31.347	61.87744615	-2			13	61	SUN	SE	55	36		2569
79	MAR	02	21:39: 7.347	61.90216837	0			49	35	SUN	RI	56	58		2627
79	MAR	02	22:40:18.348	61.94465681	-2			10	61	SUN	SE	57	37		2664
79	MAR	02	23:15:54.348	61.96937903	0			45	35	SUN	RI	58	56		2720

YEAR	MON	DD	HR:MM:SS.SSS	DAY OF YEAR	DT MET	DT EPH	DTLAST	TYPE	EV	EVENT-FILE	EVNT. LENGTH	CUM. REC.	TOTAL
79	MAR	03	00:17: 7.347	62.01189059	-2	7	61	SUN	SE	59	36		2756
79	MAR	03	00:52:42.349	62.03660126	0	42	35	SUN	RI	60	57		2813
79	MAR	03	01:53:58.353	62.07914760	-2	53	61	SUN	SE	61	37		2850
79	MAR	03	02:29:30.356	62.10382356	0	39	35	SUN	RI	62	56		2906
79	MAR	03	03:30:46.360	62.14636991	-2	50	61	SUN	SE	63	35		2941
79	MAR	03	04:06:18.363	62.17104587	0	36	35	SUN	RI	64	56		2997
79	MAR	03	05:07:38.355	62.21363837	-2	47	61	SUN	SE	65	35		3032
79	MAR	03	05:43:11.355	62.23832587	0	33	35	SUN	RI	66	55		3087
79	MAR	03	06:44:26.356	62.28086060	-2	44	61	SUN	SE	67	37		3124
79	MAR	03	07:19:50.357	62.30544395	0	29	35	SUN	RI	68	57		3181
79	MAR	03	08:21:14.358	62.34808285	-2	41	61	SUN	SE	69	35		3216
79	MAR	03	08:56:34.359	62.37261990	0	26	35	SUN	RI	70	58		3274
79	MAR	03	09:58: 4.360	62.41532824	-2	38	61	SUN	SE	71	37		3311
79	MAR	03	10:33:26.361	62.43988844	0	23	35	SUN	RI	72	57		3368
79	MAR	03	11:34:54.362	62.48257363	-2	34	61	SUN	SE	73	38		3406
79	MAR	03	12:10:14.363	62.50711068	0	20	35	SUN	RI	74	56		3462
79	MAR	03	13:11:41.364	62.54978431	-2	31	61	SUN	SE	75	38		3500
79	MAR	03	13:47: 1.365	62.57432135	0	17	35	SUN	RI	76	56		3556
79	MAR	03	14:48:31.366	62.61702970	-2	28	61	SUN	SE	77	35		3591
79	MAR	03	15:23:50.367	62.64155517	0	13	35	SUN	RI	78	56		3647
79	MAR	03	16:25:21.368	62.68427509	-2	25	61	SUN	SE	79	35		3682
79	MAR	03	17:00:30.369	62.70868483	0	10	35	SUN	RI	80	57		3739
79	MAR	03	18:02: 9.370	62.75149734	-2	22	61	SUN	SE	81	38		3777
79	MAR	03	18:37:18.371	62.77590707	0	7	35	SUN	RI	82	57		3834
79	MAR	03	19:39: 2.477	62.81877867	-2	19	61	SUN	SE	83	37		3871
79	MAR	03	20:14: 6.477	62.84313052	0	54	35	SUN	RI	84	57		3928
79	MAR	03	21:15:50.477	62.88600089	-2	15	61	SUN	SE	85	35		3963
79	MAR	03	21:50:50.477	62.91030645	0	50	35	SUN	RI	86	58		4021
79	MAR	03	22:52:38.395	62.95322216	-2	12	61	SUN	SE	87	36		4057
79	MAR	03	23:27:46.412	62.97762051	0	47	35	SUN	RI	88	56		4113

YEAR	MON	DD	HR:MM:SS.SSS	DAY OF YEAR	DT MET	DT EPH	DTLAST	TYPE	EV	EVENT-FILE	EVNT LENGTH	CUM. REC.	TOTAL
79	MAR	04	01:04:30.459	63.04479698	0	44	96	SUN	RI	89	57	4170	
79	MAR	04	02:06:18.375	63.08771267	-2	6	61	SUN	SE	90	38	4208	
79	MAR	04	02:41:18.376	63.11201824	0	41	35	SUN	RI	91	56	4264	
79	MAR	04	03:43:10.377	63.15498122	-2	53	61	SUN	SE	92	35	4299	
79	MAR	04	04:21: 5.377	63.18131223	3	41	37	SUN	RI	93	12	4311	
79	MAR	04	05:19:59.378	63.22221502	-2	49	58	SUN	SE	94	38	4349	
79	MAR	04	05:54:54.379	63.24646272	0	34	34	SUN	RI	95	57	4406	
79	MAR	04	06:56:46.380	63.28942569	-2	46	61	SUN	SE	96	38	4444	
79	MAR	04	07:31:38.381	63.31363867	0	31	34	SUN	RI	97	57	4501	
79	MAR	04	08:33:38.382	63.35669424	-2	43	62	SUN	SE	98	35	4536	
79	MAR	04	09:08:26.382	63.38086090	0	48	34	SUN	RI	99	57	4593	
79	MAR	04	10:10:27.383	63.42392804	-2	10	62	SUN	SE	100	38	4631	
79	MAR	04	10:45:10.384	63.44803685	0	45	34	SUN	RI	101	58	4689	
79	MAR	04	11:47:18.472	63.49118602	-2	7	62	SUN	SE	102	39	4728	
79	MAR	04	12:22: 2.472	63.51530639	0	42	34	SUN	RI	103	57	4785	
79	MAR	04	13:24: 6.472	63.55840824	-2	54	62	SUN	SE	104	39	4824	
79	MAR	04	13:58:50.472	63.58252861	0	38	34	SUN	RI	105	56	4880	
79	MAR	04	15:00:58.386	63.62567576	-2	50	62	SUN	SE	106	35	4915	
79	MAR	04	15:35:41.387	63.64978457	0	35	34	SUN	RI	107	55	4970	
79	MAR	04	16:37:46.389	63.69289802	-2	47	62	SUN	SE	108	37	5007	
79	MAR	04	17:12:26.390	63.71697211	0	32	34	SUN	RI	109	55	5062	
79	MAR	04	18:14:38.190	63.76016424	-2	44	62	SUN	SE	110	39	5101	
79	MAR	04	18:49: 2.221	63.78405348	0	29	34	SUN	RI	111	58	5159	
79	MAR	04	19:51:26.279	63.82738749	-2	41	62	SUN	SE	112	39	5198	
79	MAR	04	20:25:54.310	63.85132303	0	25	34	SUN	RI	113	57	5255	
79	MAR	04	21:28:18.367	63.89465703	-2	38	62	SUN	SE	114	36	5291	
79	MAR	04	22:02:44.399	63.91856943	0	22	34	SUN	RI	115	57	5348	
79	MAR	04	23:05: 7.456	63.96189185	-2	35	62	SUN	SE	116	37	5385	
79	MAR	04	23:39:30.395	63.98576846	0	19	34	SUN	RI	117	57	5442	

YEAR	MON	DD	HR:MM:SS.SSS	DAY OF YEAR	DT MET	DT EPH	DTLAST	TYPE	EV	EVENT-FILE	EVNT LENGTH	CUM. REC.	TOTAL
79	MAR	05	00:41:57.395	64.02913652	-2	31	9999	SUN SE		1	39		39
79	MAR	05	01:16:18.395	64.05299068	0	16	34	SUN RI		2	56		95
79	MAR	05	02:18:45.396	64.09635875	-2	28	62	SUN SE		3	37		132
79	MAR	05	02:53:10.396	64.12025921	0	13	34	SUN RI		4	55		187
79	MAR	05	03:55:37.397	64.16362728	-2	25	62	SUN SE		5	36		223
79	MAR	05	04:29:54.398	64.18743516	0	9	34	SUN RI		6	56		279
79	MAR	05	05:32:26.398	64.23086109	-2	22	62	SUN SE		7	38		317

MINUTES



EVENT START



TIME FROM MET. TEMPERATURE PROFILE TO EVENT START



TIME FROM 1ST EPHEMERIS DATA TO EVENT START

Time From Last event



OF A SECOND RECORDS/FILE

YEAR	MDN	DD	HR:MM:SS.SSS	DAY OF YEAR	DT MET	DT EPH	DTLAST	TYPE	EV	EVENT-FILE	EVNT LENGTH	CUM. REC.	TOTAL
79	MAR	05	00:00: 0.000	0.	9999	9999	9999	SUN	RI	8	55		372

THIS IS AN EVENT OF DOUBTFUL QUALITY, PROBABLY
DUE TO TELEMETRY LOSS (THE TIME GAP IS ABOUT EQUAL TO 2 ORBI.

YEAR	MON	DD	HR:MM:SS.SSS	DAY OF YEAR	DT	MET	DT	EPH	DTLAST	TYPE	EV	EVENT-FILE	EVNT LENGTH	CUM. REC.	TOTAL
79	MAR	05	08:46:10.401	64.36539816	-2			16	9999	SUN	SE	9	35		407
79	MAR	05	09:20:10.402	64.38900928	0			50	34	SUN	RI	10	57		464
79	MAR	05	10:22:57.402	64.43260882	-2			12	62	SUN	SE	11	36		500
79	MAR	05	10:57:9.403	64.45635883	0			47	34	SUN	RI	12	54		554
79	MAR	05	11:59:49.404	64.49987736	-2			9	62	SUN	SE	13	40		594
79	MAR	05	12:33:54.404	64.52354634	0			43	34	SUN	RI	14	55		649
79	MAR	05	13:36:37.405	64.56709959	-2			6	62	SUN	SE	15	38		687
79	MAR	05	14:10:41.405	64.59075700	0			40	34	SUN	RI	16	56		743
79	MAR	05	15:13:30.406	64.63437970	-2			53	62	SUN	SE	17	36		779
79	MAR	05	15:47:30.407	64.65799082	0			37	34	SUN	RI	18	55		834
79	MAR	05	16:50:22.408	64.70164824	-2			50	62	SUN	SE	19	39		873
79	MAR	05	17:24:14.408	64.72516676	0			34	33	SUN	RI	20	55		928
79	MAR	05	18:27:10.409	64.76887047	-2			47	62	SUN	SE	21	41		969
79	MAR	05	19:00:58.409	64.79234270	0			30	33	SUN	RI	22	56		1025
79	MAR	05	20:04:2.410	64.83613900	-2			44	63	SUN	SE	23	37		1062
79	MAR	05	20:37:50.411	64.85961124	0			27	33	SUN	RI	24	55		1117
79	MAR	05	21:40:54.411	64.90340753	-2			40	63	SUN	SE	25	36		1153
79	MAR	05	22:14:34.412	64.92678718	0			24	33	SUN	RI	26	56		1209
79	MAR	05	23:17:42.413	64.97062978	-2			37	63	SUN	SE	27	37		1246
79	MAR	05	23:51:26.413	64.99405571	0			21	33	SUN	RI	28	56		1302

YEAR	MON	DD	HR:MM:SS.SSS	DAY OF YEAR	DT	MET	DT	EPH	DTLAST	TYPE	EV	EVENT-FILE	EVNT	LENGTH	CUM. REC.	TOTAL
79	MAR	06	00:54:34.415	65.03789832	-2			34	63	SUN	SE	29		41		1343
79	MAR	06	01:28:14.415	65.06127795	0			18	33	SUN	RI	30		53		1396
79	MAR	06	02:31:26.416	65.10516685	-2			31	63	SUN	SE	31		37		1433
79	MAR	06	03:04:54.417	65.12840760	0			14	33	SUN	RI	32		57		1490
79	MAR	06	04:08:14.417	65.17238909	-2			28	63	SUN	SE	33		41		1531
79	MAR	06	04:41:46.418	65.19567613	0			11	33	SUN	RI	34		56		1587
79	MAR	06	05:45:06.418	65.23965762	-2			25	63	SUN	SE	35		40		1627
79	MAR	06	06:18:42.419	65.26299096	0			8	33	SUN	RI	36		54		1681
79	MAR	06	07:21:58.420	65.30692616	-2			21	63	SUN	SE	37		39		1720
79	MAR	06	07:55:18.420	65.33007431	0			5	33	SUN	RI	38		57		1777
79	MAR	06	08:58:48.421	65.37417154	-2			18	63	SUN	SE	39		37		1814
79	MAR	06	09:32:14.421	65.39738913	0			52	33	SUN	RI	40		55		1869
79	MAR	06	10:35:38.422	65.44141692	-2			15	63	SUN	SE	41		37		1906
79	MAR	06	11:09:02.422	65.46461137	0			49	33	SUN	RI	42		55		1961
79	MAR	06	12:12:30.423	65.50868545	-2			12	63	SUN	SE	43		37		1998
79	MAR	06	12:45:46.424	65.53178731	0			45	33	SUN	RI	44		56		2054
79	MAR	06	13:49:22.424	65.57595398	-2			9	63	SUN	SE	45		37		2091
79	MAR	06	14:22:38.425	65.59905584	0			42	33	SUN	RI	46		55		2146
79	MAR	06	15:26:11.425	65.64318779	-2			6	63	SUN	SE	47		38		2184
79	MAR	06	15:59:22.426	65.66623178	0			39	33	SUN	RI	48		55		2239
79	MAR	06	17:03:02.427	65.71044476	-2			53	63	SUN	SE	49		38		2277
79	MAR	06	17:36:06.427	65.73340772	0			36	33	SUN	RI	50		56		2333
79	MAR	06	18:39:53.428	65.77770171	-2			49	63	SUN	SE	51		42		2375
79	MAR	06	19:12:51.428	65.80059523	0			32	32	SUN	RI	52		57		2432
79	MAR	06	20:16:46.429	65.84498182	-2			46	63	SUN	SE	53		41		2473
79	MAR	06	20:49:42.429	65.86785219	0			29	32	SUN	RI	54		55		2528
79	MAR	06	21:53:38.430	65.91225035	-2			43	63	SUN	SE	55		37		2565
79	MAR	06	22:26:34.430	65.93512072	0			26	32	SUN	RI	56		55		2620
79	MAR	06	23:30:30.431	65.97951888	-2			40	63	SUN	SE	57		38		2658

YEAR	MON	DD	HR:MM:SS.SSS	DAY OF YEAR	DT MET	DT EPH	DTLAST	TYPE	EV	EVENT-FILE	EVNT LENGTH	CUM. REC.	TOTAL
79	MAR	07	00:03:22.433	66.00234297	0	23	32	SUN	RI	58	54	2712	
79	MAR	07	01:07:18.433	66.04674112	-3	37	63	SUN	SE	59	39	2751	
79	MAR	07	01:40: 2.433	66.06947260	0	20	32	SUN	RI	60	56	2807	
79	MAR	07	02:44:10.434	66.11400965	-3	34	64	SUN	SE	61	42	2849	
79	MAR	07	03:16:54.434	66.13674113	0	16	32	SUN	RI	62	55	2904	
79	MAR	07	04:21: 1.435	66.18126661	-3	31	64	SUN	SE	63	41	2945	
79	MAR	07	04:53:42.437	66.20396339	0	13	32	SUN	RI	64	56	3001	
79	MAR	07	05:57:53.449	66.24853529	-3	27	64	SUN	SE	65	42	3043	
79	MAR	07	06:30:30.455	66.27118582	0	10	32	SUN	RI	66	56	3099	
79	MAR	07	07:34:45.467	66.31580402	-3	24	64	SUN	SE	67	38	3137	
79	MAR	07	08:07:26.473	66.33850084	0	7	32	SUN	RI	68	54	3191	
79	MAR	07	09:11:37.425	66.38307205	-3	21	64	SUN	SE	69	39	3230	
79	MAR	07	09:44:14.427	66.40572253	0	54	32	SUN	RI	70	54	3284	
79	MAR	07	10:48:30.432	66.45035222	-3	18	64	SUN	SE	71	38	3322	
79	MAR	07	11:20:58.434	66.47289854	0	50	32	SUN	RI	72	55	3377	
79	MAR	07	12:25:22.438	66.51762081	-3	15	64	SUN	SE	73	38	3415	
79	MAR	07	12:57:46.441	66.54012084	0	47	32	SUN	RI	74	55	3470	
79	MAR	07	14:02:14.443	66.58488939	-3	12	64	SUN	SE	75	38	3508	
79	MAR	07	14:34:30.444	66.60729681	0	44	32	SUN	RI	76	56	3564	
79	MAR	07	15:39: 2.445	66.65211163	-3	9	64	SUN	SE	77	42	3606	
79	MAR	07	16:11:15.445	66.67448432	0	41	32	SUN	RI	78	56	3662	
79	MAR	07	17:15:53.446	66.71936859	-3	5	64	SUN	SE	79	41	3703	
79	MAR	07	17:48: 8.446	66.74176442	0	38	32	SUN	RI	80	55	3758	
79	MAR	07	18:52:46.447	66.78664869	-3	52	64	SUN	SE	81	42	3800	
79	MAR	07	19:24:50.448	66.80891722	0	34	32	SUN	RI	82	57	3857	
79	MAR	07	20:29:38.449	66.85391723	-3	49	64	SUN	SE	83	40	3897	
79	MAR	07	21:01:40.449	66.87616260	0	31	32	SUN	RI	84	56	3953	
79	MAR	07	22:06:29.450	66.92117419	-3	46	64	SUN	SE	85	39	3992	
79	MAR	07	22:38:30.451	66.94340800	0	28	32	SUN	RI	86	56	4048	
79	MAR	07	23:43:22.451	66.98845429	-3	43	64	SUN	SE	87	42	4090	

YEAR	MON	DD	HR:MM:SS.SSS	DAY OF YEAR	DT	MET	DT	EPH	DTLAST	TYPE	EV	EVENT-FILE	EVNT	LENGTH	CUM. REC.	TOTAL
79	MAR	08	00:15:22.451	67.01067652		0		25	32	SUN	RI	88		55		4145
79	MAR	08	01:20:14.452	67.05572282		-3		40	64	SUN	SE	89		44		4189
79	MAR	08	01:52:10.452	67.07789875		0		22	31	SUN	RI	90		55		4244
79	MAR	08	02:57: 6.453	67.12299135		-3		37	64	SUN	SE	91		44		4288
79	MAR	08	03:28:54.453	67.14507469		0		18	31	SUN	RI	92		56		4344
79	MAR	08	04:33:58.454	67.19025988		-3		33	65	SUN	SE	93		44		4388
79	MAR	08	05:05:46.454	67.21234322		0		15	31	SUN	RI	94		55		4443
79	MAR	08	06:10:50.455	67.25752841		-3		30	65	SUN	SE	95		40		4483
79	MAR	08	06:42:38.456	67.27961176		0		12	31	SUN	RI	96		55		4538
79	MAR	08	07:47:45.456	67.32483167		-3		27	65	SUN	SE	97		39		4577
79	MAR	08	08:19:30.457	67.34688029		0		9	31	SUN	RI	98		54		4631
79	MAR	08	09:24:37.458	67.39210021		-3		24	65	SUN	SE	99		40		4671
79	MAR	08	09:56:18.458	67.41410252		0		6	31	SUN	RI	100		54		4725
79	MAR	08	11:01:30.459	67.45938031		-3		21	65	SUN	SE	101		39		4764
79	MAR	08	11:32:54.459	67.48118587		0		52	31	SUN	RI	102		57		4821
79	MAR	08	12:38:22.460	67.52664884		-3		18	65	SUN	SE	103		42		4863
79	MAR	08	13:09:54.460	67.54854699		0		49	31	SUN	RI	104		54		4917
79	MAR	08	14:15:14.461	67.59391737		-3		15	65	SUN	SE	105		40		4957
79	MAR	08	14:46:42.462	67.61576924		0		46	31	SUN	RI	106		54		5011
79	MAR	08	15:52: 6.462	67.66118590		-3		12	65	SUN	SE	107		40		5051
79	MAR	08	16:23:30.463	67.68299147		0		43	31	SUN	RI	108		54		5105
79	MAR	08	17:28:58.464	67.72845444		-3		8	65	SUN	SE	109		40		5145
79	MAR	08	18:00:14.464	67.75016741		0		40	31	SUN	RI	110		55		5200
79	MAR	08	19:05:52.465	67.79574612		-3		5	65	SUN	SE	111		40		5240
79	MAR	08	19:37: 6.465	67.81743594		0		37	31	SUN	RI	112		55		5295
79	MAR	08	20:42:42.466	67.86299150		-3		52	65	SUN	SE	113		44		5339
79	MAR	08	21:13:50.466	67.88461188		0		33	31	SUN	RI	114		56		5395
79	MAR	08	22:19:33.467	67.93024846		-3		49	65	SUN	SE	115		42		5437
79	MAR	08	22:50:38.468	67.95183412		0		30	31	SUN	RI	116		56		5493
79	MAR	08	23:56:30.468	67.99757486		-3		46	65	SUN	SE	117		41		5534

(234)	4001600	20118550	41E130E0	50010F05	90730087	940999F5	AEC3344E	71AC4719	2C311F11	1F01149A
(24)	30E4207	20101190	3790A5	11144130	FF5DAAC1	11D530E	9910E901	7AC00341	0E111E05	73003114
(244)	107A2501	0730E89A	7E292616	60307900	1EA37BF0	30EA51AC	10BEFEF3	0EA90209	00212003	32107231
(247)	00670031	09AC3170	24F930ED	FF135190	1F003077	EDF52FA2	FC30E93A	A1A53A75	93CEB132	0002070F
(252)	30005205	0E3114AC	31004790	F0105330	ED54E870	00100003	70444E01	A40E30E1	100E570	E4130E0A
(256)	70E722FB	A930EFA2	A3217E49	003170FB	74903044	30009000	AC00EDC	37A370F	07551E30	00E1A500
(267)	7000930E	D434E15A	E8083003	06A05524	1E9C3073	6110CA73	1030EB07	50021040	003070B1	0100007E
(264)	300070FE	1E30AB93	0EE099AE	02351730	00D13104	4FC59E30	7557F130	000530E0	13702F24	00403070
(263)	09FF0420	F030D911	100414C	D30EE0AE	F3639FFF	30015E71	E071A9AC	31202EFC	02402E70	0A000017
(272)	0079031	00006000	00003000	320B2A60	30A30EF7	707E0A61	00300A4A	04F350E3	30307134	000000F7
(275)	000410A	00E0C920	3106F950	41440130	01350000	0AA5A3CE	009D9252	05003000	2007400E	00000000
(283)	00AC342E	3A30E94F	5F1E005F	40311E3E	E11AAD0E	30ACC054	F20E4753	0E04F000	1E0C4730	00FF5077
(284)	02000030	6F0FE014	0AE1300E	AA0C1300	A1403116	04094150	DF036137	901F0F10	130E0002	400441A0
(287)	300FC307	000FA020	300E0F08	EEF04530	0CA02430	60107031	1FBF0B99	79540342	3F093170	07030F00
(292)	ED40AC04	E630E800	80A0A40E	90310F87	403994A4	300A9152	F09509AC	01290900	0E497103	34100000
(295)	507030F	0EA41F15	04EA30E9	8001E420	00803077	9070FA09	A30017D	00E3F00E	0C3134F0	0A510004
(300)	03279639	07657003	0F00B415	7700F230	EA51EA46	30061030	7251A703	40103000	04CA1137	E2003140
(314)	0341A10	07032525	000EE109	530F9220	13F02109	30000007	E072070	30749AF7	0E0F0730	00015000
(317)	001A0E3	0F4004E3	0E203002	E30E30E3	0D13E30F	42700000	F3301A00	A1AA20CA	73E307E1	00000004
(312)	305F3FFF	FFFFF0B3	0005FFFF	FFFFF430	5EFFFF00	FF0E0031	40702F4F	10F0322	012A040	00300003
(319)	07A003E0	AC30E000	00400010	20307776	E990CF27	30P00001	0460F240	315A032A	140F0003	20000401
(321)	0E0D130F	9340E000	0A013000	5F000553	4030307A	E2790094	A0C31407	20CAE204	003100F7	0A000000
(324)	03101000	002152A3	0F020E93	1503F030	0CF05000	10550003	7EDA1334	0970340	0D000001	90003177
(328)	A9F0200F	F50315F6	01330A30	430F91F9	221340F9	30007090	50503F20	3106033F	F59F9503	30E00033
(332)	5E20E032	0001F000	AA300314	E72AD000	3F030F90	090E400A	0430E0F7	AE0540F0	30311000	040F0500
(335)	03329000	FF0A3000	322050F9	9AE14503	13E35400	1021930F	0E417911	4000300E	03100077	01003115
(340)	0B4A0A7A	00032720	7E9F1E42	6032400E	E771100A	0310E041	0AFA7913	0F000320	05500430	0000010A
(344)	5E032031	27A0E472	33AFC325	144FF014	B500320E	0CA00000	BAC31202	F530F500	030F0031	50700400
(348)	00EE0011	10304130	31348703	30E65403	23007270	50EAD033	2120F200	0AE00311	20055203	F1030F04
(352)	4F0E9700	2A30EFA0	FC9150A9	70314230	E40F330E	03210007	0E00AD00	3365709F	2002AFC3	10000000
(356)	1240030E	F0C300F0	05A6300E	7500B1EA	4F203150	0475A000	20C31700	10F20900	FC045400	00000A55
(360)	03070101	01040443	0EF5090F	200A2030	EF925903	00144031	5F0E0A0A	0A020310	90E3E432	5000307E
(364)	0EE14100	9AC30770	53000815	E30E0A0E	304100FA	300F9073	50070400	31000000	70007203	1000770E
(368)	4E00430A	04020E23	50A00307	31700005	00030E0F	3A2AF49	E3300F9A	00F70037	00020000	00000111
(372)	0314000E	02073103	00F40F32	09009403	00E0300E	9A0EA30E	022F0413	0E00300E	05101400	01203222
(375)	0550403A	F2031400	A7423943	93000F14	03034504	03000000	00000000	00000000	00000000	00000000
(381)	30031032	45000340	30000013	4AFC97A2	CA230001	70000000	EAC30000	00000000	00000000	00000000
(384)	300F29F1	2AF00000	32099A00	F19A1003	1295A593	29025300	A2E30154	40000000	00000000	00000000
(391)	01004040	F0300000	01326421	FC331030	F00F152F	03110001	09A43003	00039024	E1100003	0040A005
(392)	3000530E	90094000	0014300E	0E239524	A2033000	51000000	1FC31155	EA0E0003	13000000	00000000
(395)	03003870	00E05023	0E002000	F0402230	EE20A840	40002034	0242A30F	20000001	00000077	40000000
(400)	4000071A	3E030032	00504700	03000E90	BE200564	30000030	40F21000	39170503	00000003	10300A42
(414)	0000930E	90323730	0A070300	3770204A	E0630000	A0100072	43300030	00000000	00000000	00000000
(418)	03070504	F1000923	0E900A10	10003703	0640A709	81090000	A200052F	40F03000	90000000	30000000
(412)	E40F4602	D103070A	39700400	4300A030	4A00300F	03000030	E2901273	00000145	40000000	00000000
(416)	77000300	00001720	EF410307	A750007F	04230000	20001393	0FC00004	20000000	20000000	20000000
(42)	30005279	F2014100	00930003	09100003	07007340	0CA0730E	05500002	09A50000	00001703	5000000A
(424)	00000000	A730E000	740E7FA0	63000009	04553109	05070000	00A00000	00000000	20000000	00000000
(428)	05700300	00400000	AA053000	D405A000	0D630000	A9004705	29030774	02000000	00000000	00000000
(432)	03072033	30070000	30300040	45F17230	E9003A03	97000000	FE000000	0E100007	70000000	40000000
(436)	FF000000	00000000	947F0000	70340000	00E21000	30000000	4FC00000	00000000	40000000	00000000
(440)	30000000	00000000	51010000	00000000	FE000000	AP000000	50300000	00000000	00000000	00000000
(444)	03079510	09400000	0EF40000	4A440000	10000000	10040000	76290400	3F513000	00402000	07000000
(448)	FC200000	30000000	3A000000	00000000	00000000	00000000	00000000	00000000	00000000	00000000
(452)	40000000	00000000	04220000	00000000	E0000000	70000000	0A000000	10000000	00000000	70000000
(456)	30000000	12072000	0E000000	2E002103	10000000	2E000000	12A00000	E1010012	00000000	07100000
(460)	00000000	00000000	00000000	00000000	00000000	00000000	00000000	00000000	00000000	00000000

FILE	1	0	5	LEN	402	BYTES
()	92	00	3	32	5E	70420001
(40)	00305000	1A012140	00300000	02003003	00205000	01020000
()	00000000	02003003	00205000	30020030	70700000	02003003
(12)	00000000	00000000	00000000	00000000	00000000	00000000
(16)	7F20CA00	02003003	00305000	00000014	00000000	00000000

D-35363
3/5/79-3/8/79

INPUT TAPE X-399 UNIT 1
DATA INPUT 09 OF 117 FL 1 2 2 SR 117 1 2 SK 117 LAST 2

FILE	RECORD	LENGTH	BYTES	1979	3
(3)	010515460255	555555552321	170555555555	5555 00000000	000000003673
(4)	000000000000	000000000000	000000000000	000000540000	000000000000
(75)	555555555523	25165523 7555	5555 00000000	000000000000	000000000000
(144)	000000000000	173043200000	000000001730	413000000000	000017227776
(192)	720000000000	000017276720	000000000000	172764200000	000000001727
(24)	173547036000	000000001735	470360000000	000017354703	600000000000
(26)	000017354703	650000000000	173547036000	000000001727	614000000000
(336)	000000001722	500000000000	000017225000	000000000000	172250000000
(364)	000000000000	172250000000	000000001722	000000000000	000000001722
(434)	7634 00000000	000017317634	000000000000	173176340000	000000000000
(4)	173176340000	000000001731	763400000000	000017340000	000000001731
(52)	000017330136	000000000000	173450014000	000000001734	733440000000
(57)	000000001735	614660000000	000017356755	600000000000	173547436000
(624)	760000000000	174000047600	000000001740	600000000000	000017400000
(672)	606476000000	000017406064	760000000000	173577504000	000000001732
(72)	173160031463	146314621731	506146031463	463517314211	777777777777
(76)	1462173 4732	314631463145	172770377777	777777777127	541463146314
(816)	400000021755	734624154000	000217557346	241540000002	175573462415
(864)	241540000002	175573462415	400000021727	570463146314	631417214000
(912)	400000000000	000017214000	000000000000	172140000000	000000001721
(960)	172140000000	000000001721	400000000000	000000000000	000017214000
(1008)	000017317634	000000000000	173176340000	000000001731	763400000000
(1056)	000000001731	763400000000	000017436017	103777777764	172540377777
(1104)	777777777753	17155313 6003	263414626060	247436411112	1135171463 5
(1152)	560406666423	4477606 33630	575073637534	171561714060	534233136060
(1200)	171007557577	312155061714	401511234552	534260673604	465224674750
(1248)	655317126553	612342417454	171656 64367	342 745431714	646231371006
(1296)	510432660000	26 317352 113	21406 662354	265533126717	171654234177
(1344)	506721371133	171642265532	775747706060	266137547433	007160641753
(1392)	9651 6 6341	72656 6 3576	724704534306	171645161312	140246146060
(1440)	17165 116576	32722431715	7 407 047667	36116 653617	276273126647
(1488)	134660630202	443060623031	171645641725	366041741716	410510555461
(1536)	460563566060	317557565534	467600622764	644000456714	171643242002
(1584)	462 37062562	171654651471	732522316160	332600171433	642760621663
(1632)	52235375375	5742606 33767	1211 4 5264	171657 1607	160576546 61
(1680)	171573574304	635425031716	565277236614	371560610126	753261740321
(1728)	37 66 613655	144 05737 35	171565713424	601551261716	626600453541
(1776)	622335736 61	0674167516	23136 0613243	751361532577	171557642271
(1824)	574107417661	171664227141	125741226 61	046272132156	522660612644
(1872)	724245557161	043460610765	463550000430	171665500122	550522026061
(1920)	171543 33437	131613551716	76 175335 50	71306 611237	426743632641
(1968)	377 6 611711	471924365605	17147 652733	4237214 1717	475 272142 14
(2016)	752263776061	220250377025	072660611357	346713446547	171453253727
(2064)	753141361 57	17167 1156347	343513016061	266767301631	262260611043
(2112)	433431630543	031660612362	655573 55231	17167 5 231	335 24326 61
(2160)	171277057426	111410541717	445017721654	625260612723	002440140572
(2208)	505160510272	04265740269	170772750301	046323151717	455212755730
(2256)	001321546 62	14525 0743163	60046 61 135	741311576237	6065174413 7
(2304)	07 034154255	17167 267366	2250111776 62	27361 172325	66 46 6 3711
(2352)	471705344741	412260620547	006664365763	171667622560	374213676063
(2400)	6 655 126775	2752 72 1717	476146626067	403760621565	556201741504
(2448)	326676 3532	2 225641 41	6 6312412 22	07 215451717	5 1121 66251
(2496)	73320746065	657031766716	465560603460	540464031 17	606236426554
(2544)	201102172655	17104517117	400550421711	771370355644	737060603420
(2592)	5 2763441131	4 778 031732	577712122 63	17165 3116170	647542611713
(2640)	5 0221436151	52370 201717	5 161172 475	34156 64 262	023622576251
(2688)	3412606 3350	47265 0463654	606213261011	653561051717	477153573456

(2832)	465776666335	134517135614	537355541711	171653017575	64234012115	23327708575	606137655116	311767711717
(2833)	666135145436	146114601717	457303347546	344617145075	735407027357	171655407401	3175664151716	424656312770
(2928)	457161613441	636124252234	626132372221	574213631717	447354012444	442017147254	455716145441	171645646137
(2975)	14715161716	47521437114	562560615517	221657166763	606131041111	356277121717	4362111746171	441117154615
(3024)	133054115430	171642761340	726175171716	544233046171	332560603566	276757363563	606125637463	015524651717
(3172)	423661322144	452517155551	525031327575	171577740431	630466661715	611644741162	533460613656	701333130363
(3121)	616123572554	533074371717	411171417427	746717156711	266365574231	171571521152	317215001716	655514441233
(3156)	723460603760	433774072230	606121667105	351411101716	766770363137	775217157711	717162722466	171563112623
(3216)	450022231716	717503100100	613260610166	173571605501	606120131042	521121171716	733253071334	566117164340
(3264)	407165155475	171554314520	122772651716	757475737571	221667610434	434512534260	606116544217	727153201716
(3312)	675512149131	621517164722	276334424232	171545343524	735341541717	436573311217	125161611223	142672427531
(3363)	606115334605	655044761716	636027550620	630217165271	107526122766	171474541736	642554571717	424426677712
(3413)	114561611231	401633611337	606114303060	711524361716	574533122056	273617165624	107353201425	171456167102
(3456)	101713151717	441120774731	061161611556	452114007634	616113433626	337227131716	531537520715	62617166142
(3504)	236616613607	171377115354	600102661717	454420404675	235360612121	433165545524	606112747717	733145431716
(3552)	465164213307	412417166442	600156470516	171341441752	560073741717	466473767350	701060612501	226313603133
(3577)	606112457466	773446871716	417353165071	214017166724	535477362577	171775314173	011456031717	477275505225
(3646)	203160613074	72141761725	676112336526	731456131715	72163417055	434417167167	14647535256	60614136174
(3693)	401423021717	506602541214	445660613503	203254357222	606112412156	265043211715	601257207472	575017167411
(3744)	501755711641	606410352201	501331441717	514573351254	472760620243	326467254430	606112652733	205674751715
(3792)	457775222146	663417167613	531333236700	616325417415	666711311717	521233317214	717161621327	135541655125
(3840)	606113277723	044005131714	672650735546	762117167774	330031432200	606307006650	211234371717	524331111612
(3888)	224560622426	305611475075	606114107614	727150331714	423734253017	175117174055	610065671142	606234275273
(3936)	616122761717	526156465777	751460623541	432474727762	606115111446	171761141712	667151334146	271217174124
(3984)	237677717021	606225305105	174613051717	526230717507	520460631554	237672642254	606116247712	156217266066
(4032)	030511455517	172217174161	546474476514	606216451676	666053641717	525030333022	201560640116	434253472314
(4080)	616117572625	634763156064	176134415443	244017174205	645747224360	174357660713	170716731714	434343434343
(4128)	432117435766	717777777763	172155217552	625177371743	601711377777	776417264037	777777777764	17337177777
(4176)	777777561725	737777777777	775360620777	222563065526	171752226062	163331416065	161325203635	356360612126
(4224)	572564164355	616313541534	536444741717	422047364523	648460620150	446777306461	171751615063	352760721711
(4272)	645622365724	415160612312	532515251626	616235033234	213231661717	422203471660	236260616561	317111545127
(4320)	171751051234	302142751713	631570636346	217060612512	504113771661	606222731761	655473321717	421212147752
(4368)	604060613267	635256771445	171750154262	754407711714	544110465526	026560612726	011767634552	606210777412
(4416)	333466521717	417177200477	152150613110	211345164266	171747131714	434231771714	771716652145	755661613154
(4464)	152666313277	616137522256	721272511717	413651112467	352160612543	407553454137	171745757272	45732131715
(4512)	506605503261	153360613414	414140411466	606132756434	703056671717	407320732676	435460612312	163530064646
(4560)	171744464343	456255241715	617137715370	211760613666	203664355543	606126336317	516103411717	401701722425
(4608)	462161612175	117111353167	171743152434	034527671715	725732456573	667461623321	244623141714	616122153351
(4656)	643334401716	766423610521	576260611674	400165621211	171741325056	363156631716	415257117727	415661621135
(4704)	722412212746	606113736631	701643341716	747161571727	156560611511	121446241700	171677157405	410626021716
(4752)	456454136622	032260621710	523471161043	606112101035	033115031716	725702173612	072260611343	361072710377
(4800)	171673255052	5175551111716	516435560602	544161622527	724315236215	616116232240	134353551716	712455632462
(4848)	164360611213	652762343547	171667153333	107662371716	555100036672	006760623361	754503305366	606102662064
(4896)	463456241716	655341624774	727460611102	462532733506	171662663447	473763051716	612122525637	472366636452
(4944)	10552420153	616137647546	307531451716	626413214377	134160611111	73151115174	171656217116	115111311716
(4992)	645430420412	431260632176	737714303762	606036274223	261337721716	575741566751	27261611734	316542527322
(5040)	171651407544	400645471716	677130220730	264760633736	610421020145	606035031547	276666551716	543627566521
(5088)	524561616977	646757131317	171644447702	443160371715	726734350272	023261643214	14432173745	650033702403
(5136)	73571521716	51151655322	122160610662	323466311373	171576764326	515206361716	754563525711	73261662611
(5184)	164423424116	606032670746	446576761716	453223120517	250660610664	146667035367	171564423154	500525321717
(5232)	41171316211	644317124162	606071352501	606031776755	173252521716	415122223577	037260610705	123071670503
(5280)	171651712361	132661621717	411025452516	651217135411	131155325675	616031226112	117734261715	733717316532
(5328)	564360610745	153173647716	171476061665	251705461717	420577227775	711517144345	633564642471	616131577612
(5376)	670102631715	633453305452	660760611024	142663433734	171450133172	746127271717	427245651065	664617146174
(5424)	544722713124	616131274616	2424468241715	531511064436	041661611121	716651171241	171344137161	374663371717
(5472)	434573564264	454417147515	64414442566	616130115623	411141111715	426232317577	113561611236	045612516715
(5520)	606637355672	516235361717	440766111245	443317154536	723406525104	616130063063	726113561714	643610147310
(5568)	31266161137	31174271137	606413450707	023245531717	444014440535	032217155360	541733277622	606030154536
(5616)	25247751714	41231450116	634160611541	333737063372	616317602364	716714331717	445671767465	46317156166
(5664)	526650773257	61633372132	756257761713	433411320737	332260611725	627474571175	616234753111	02421761717
(5712)	445567711012	757417151757	22430755631	616030732725	450335171704	666136557522	134660612127	770745755502
(5760)	616226136727	551112521717	445711216577	326517157531	040745352727	616131415724	64661666364	353337451403
(5808)	61461612346	35345347566	61627463204	4617161717	44453514524	533317164131	213355173616	616132221716
(5856)	25146416363	352256417107	323660612600	500047311277	606136477156	401721711717	441045747220	431417162775

(6030)	606124347742	757336431717	427373515265	43 617165747	735257753657	63601655574	77366 615325	54526164 720
(6040)	551563513515	547615763353	606117777771	402473531717	423753215320	472217165255	447335764164	25 5566742511
(6090)	216366326 62	147124443536	67606 62 241	55 222 331234	606113375131	667736 71717	411232151447	606136647121
(6144)	1 27331 3167	1 27331 3167	1 27331 3167	1 27331 3167	1 27331 3167	1 27331 3167	1 27331 3167	706317165450

FILE	1 RECORD	2 LENGTH	6160BYTES					
------	----------	----------	-----------	--	--	--	--	--

(3)	42233233000	140014001400	100564000001	140007074027	472300020003	000200020135	000000047320	137777600000
(40)	006 706 1147	006 706 1147	0026 5130010	01700001470	100010001475	77 3000271400	00001237116	000200020003
(96)	0 31136 157	641735130355	442755000040	0 40706 17160	274207565 46	251036454 31	67 10001420	14 100564 6
(144)	556775072210	721130410002	000200030002	013600000073	105170001440	004636231400	000002720000	000000000000
(192)	776 032533 5	140014001400	100564000021	140007120400	504000030002	000200030136	000000047320	126054000000
(240)	004 004 0 65	0 4 274 00334	00635133000	010070001000	14 014 001005	74 000201400	00001237117	0 27002 103
(288)	000301360007	644436506000	777223600040	004000400060	274003476771	522737254000	0000100 1 000	14 011 1574 0
(336)	626001121470	737767100003	000300030002	013700000073	105170001440	004636330000	000002730000	000000000000
(384)	01003326 000	140014001400	100564000041	140007112164	515200331002	000200030137	000000047320	100002000000
(432)	006 006 1561	006 30100334	006635130000	0 3000010000	14 014 001400	77 3000271400	00001237117	0 27002 103
(480)	000301370007	644545031000	441141600060	004000600060	275003505130	444637254567	54 0100 1000	140010057400
(528)	016524002250	721104020003	000300030002	013700000073	105170001440	004636426400	000002740000	000000000000
(576)	336 0326 0 00	1 3 14 0 14 0	100604 00061	14 0071111752	527 00020003	103 0 03 141	000000047320	1 10 2 0 000
(624)	006000600060	006030000226	004605130000	013700000073	105170001440	004636525000	000002750000	000000000000
(672)	000201410007	300051724000	001132200060	004000600060	302000054030	051637054360	200010001000	140014060400
(720)	225724 0 1630	70000373 003	0002 0003 002	0142 00000073	135170000040	004636525000	000002750000	000000000000
(768)	422 0326 0 0 0	140 14 001400	100614 000101	140007111157	54 3200030003	1002 0000144	000002760000	13 0 00000000
(816)	006000600060	006030600377	010605137760	200000001400	100014001406	140000201400	000001237117	0030003 003
(864)	000201445014	117563100000	337134000060	006000600060	310001753600	722137254502	340014001400	140010062400
(912)	316150001250	714330410003	0003 0000003	014500000273	105170000040	004636623400	000002760000	000000000000
(960)	427777260000	14 014 001400	100634 000121	14 0071113175	55160 030003	1003 0 30150	00000147320	1 06 04 00000
(1008)	006000600060	006032200006	000605130000	000000001400	140014001406	500000201400	000001237117	000300030003
(1056)	013015400007	357241673 00	2 51516 0060	006 00600060	336003733631	265237054600	740014001400	140014070400
(1104)	0 344 01 5	714067100003	00 3000 30003	016300000073	105170000040	004636722000	0000 277 000	000000000000
(1152)	424003260000	140014001400	140734000141	140007076724	563300040004	000300030174	00000147320	1142374 0
(1200)	010001000100	010040200077	010605130000	000000002400	200020002010	440000201400	000001237117	000600050005
(1248)	00 40 2230 007	56 2 0124 000	56477 0000160	014 0012 00121	51 0000000010	111737654331	74 0144 034	3 0 3 1414
(1296)	00020000131	725304 2 0 17	013 0100010	0411 0 000073	105170000040	004637 20400	00003 000	000000000000
(1344)	424003260007	746314452045	5777764 00161	140007031326	575052645 16	403237767777	562000047320	100401067414
(1392)	61377522232	267777742612	0046 5130000	0 0103141320	327056774377	771200201400	000001237117	541566126066
(1440)	622777776332	565153723400	471314751675	657446750437	777472742001	077737454734	4324 736 312	332113777715
(1488)	04040001650	721503736466	671162026411	777762467473	105170000040	004637117000	00003 1 000	000000000000
(1536)	4240032600317	732653002307	437777050001	140007276102	606362336312	547155647777	566000047340	137777600013
(1584)	731354316651	65377723432	0022 5130000	0 0136464626	516261566377	7433 02014 0	0000 1237117	4710376 261
(1632)	2467777 0 47	641735 00000	443 00000740	05404200361	702 00605 46	211026454574	210050003400	34 0 5 1454 0
(1680)	556775072210	721130410012	000700070006	030600000073	105170001440	004637215400	000003020000	000000000000
(1728)	776 0326 0 00	5 0054 034 0	301430000021	140007300455	613300120006	000700060307	000000047340	126054100140
(1776)	24 0160 14 0	14 026 00334	00 275130010	0 014 0005400	34 034 03014	6 0 0 2 14 0	00001237117	0 13 0 7 007
(1824)	100603170007	647437306000	777022200260	016001600140	646003476771	562637254056	67 00 0034 0	34 034153 0
(1872)	626001131470	737767100014	061000070006	033100100073	105170001440	004637314000	000003030000	000000000000
(1920)	1 0 326 0 0 0	6 0 40003400	3 1574 00041	14 0073 00455	61270 015010	0007 0000342	0000 0047340	1 0002100000
(1968)	02 0 0 0 0	014 714 03344	0062 5130000	0 000 000073	4 0 4 0 3416	500 002 014 0	0000 1237117	0 16 0 0 007
(2016)	000703600007	644545032000	441017600360	022002000160	752003506010	344636654455	700074000400	400034175001
(2064)	016524 0 2250	7211070200020	001100110007	040000300073	105170001440	004637412400	000003040000	000000000000
(2112)	03 0 326 0 0 1	0 0 00 0044 0	402 034 010061	14 007276741	612100210013	0011001 0415	002 0047340	1 10 21 000
(2160)	046002601220	022106000604	004205130000	0000000114 0	54 0 50 004421	74 1 0 2014 0	0000 1237117	0 25 014 012
(2208)	001104510027	300051724400	000773400540	032002600221	150004054030	111737454443	04 1400064 00	540050241401
(2256)	22573 0 1630	7 0 00374 032	0016 013 012	0521 0 3 0073	105170001440	004637511 00	000003050000	000000000000
(2304)	422 0326 0 0 1	6 0 004 00000	54261 0 1 1 1	14 0 0 2274 032	6112 036 0020	0 15 0 14 570	0 20 004734	13 0 61 0 000
(2352)	1 2004400340	030142401377	010205137760	2004700023001	2000740007033	140200201400	000001237117	005300270020
(2400)	0 17 731 0073	117563100000	336755001460	006004400422	036015753600	722136454042	000374020001	240114462405
(2448)	31615 0 125	71433 550132	0 054 033 030	14 1 25 00073	105170001440	0046376 74	00003 000	000000000000
(2496)	431777260013	200614030003	25454437 121	14 0 0 7276175	61 411370671	0350 4167777	2 00 0 04734	1 0 0 41 0 4
(2544)	456347400702	221777600000	000205130000	001471635537	247520756377	760100201400	000001237117	417134272313
(2592)	225477774067	357341473400	26477371 407	53 525651337	777113733631	265237454601	022756025535	353213777520
(2640)	0 0 0 1 0	7140571 4674	41773 552764	7777465 0 73	105170001440	0046377 0	0000 03 7 0	000000000000
(2688)	426003260257	6215155 3344	67776350141	140007305175	607450534425	331732257777	500000047340	1142375 0 12
(2736)	27312 007540	707777721777	010205133000	002472500230	556511617377	7645002014 0	000001237117	524747633622

1 37 41 462 3 3 3 3

FILE	RECORD	LENGTH	BYTES	1979	3
()	151544255	555555523	1755555555	5555555555	00000003673
(40)	151544255	555555523	1755555555	5555555555	00000003673
(96)	25555555523	25165523555	5555000000	00000000036	00000000000
(144)	00000000000	17334340000	00000001730	41400000000	000017304000
(192)	72727272727	17272727272	17272727272	17272727272	61400000000
(240)	17272727272	17272727272	66272727272	17272727272	17272727272
(288)	000017304100	00000000000	173041100000	000000001727	613000000000
(336)	17272727272	41727272727	17272727272	17272727272	17272727272
(384)	17272727272	17272727272	17272727272	17272727272	17272727272
(432)	40000000000	000017224000	00000000000	172240000000	000000001722
(480)	172344000000	000000001723	00000000000	000017234000	00000000000
(528)	173344000000	000000001733	00000000000	000017334000	00000000000
(576)	000000001735	604700000000	000017356755	40000000000	173567550000
(624)	00000000000	173656401000	000000001736	74605000000	000017374323
(672)	572750000000	000017376635	540000000000	173641724000	000000001732
(720)	173165526314	631463131731	504777777777	777717314201	146314631462
(768)	146217314732	314631463145	172776377777	777777771727	537631463146
(816)	631463121725	631217270243	655617237405	075341217265	172270702436
(864)	72724365576	171741520541	711735431727	53631463146	314517214000
(912)	40000000000	17214000000	00000000000	172140000000	00000000000
(960)	17214000000	000000001721	400000000000	000017214000	00000000000
(1008)	17214000000	000000001721	400000000000	000017214000	00000000000
(1056)	17214000000	000000001721	400000000000	000017214000	00000000000
(1104)	777777777753	606213311314	066475356060	327217045113	047717165345
(1152)	21353467537	241260611107	225403227210	606221167443	227266266060
(1200)	171652623613	277731146161	257113671327	671361613650	164631552141
(1248)	024717164347	356044141743	171654057203	167417166761	3245174536
(1296)	743365226369	266133355723	227017157663	662175574552	171555155734
(1344)	75241632137	6637507542	331146766666	25564362466	745317156611
(1392)	164572534	02226061147	7511372773	606324442533	636674216160
(1440)	171656713034	122327106062	230217536703	714260603744	257753170405
(1488)	46111715447	57766431515	171657345444	637623046062	353432747371
(1536)	2623517660	23521275716	173317146557	661425515732	171657633341
(1584)	15463004770	606703340316	016243026060	232534004410	464317144311
(1632)	125741251537	677560603611	527054756225	171246111275	265604776760
(1680)	171657723463	112463166066	267112135677	51167633575	256101334204
(1728)	6446672354	627155751343	171657531105	322207501713	406311566661
(1776)	536665616360	233664537062	063060642447	556000225756	171657166434
(1824)	1176430541	171461023331	132767546060	237164331365	425760632736
(1872)	7325144213	66576163617	137331574731	171475674672	11127776676
(1920)	171655602166	447233331715	501471317232	425760603647	14434533363
(1968)	672561623115	055554077723	171654563112	720147651715	624741526347
(2016)	4535353266	266112251473	77046622712	31716213217	171653413215
(2064)	3117676516	171561227577	766433136060	273214376153	15516162724
(2112)	433166041556	616360610112	275325557325	171567022443	745254556160
(2160)	1716541325	33713631716	501766573701	731360610361	030507652336
(2208)	65466613314	45575117722	171646611556	63142501716	54733552715
(2256)	726232626360	336564602335	126260612714	072374573146	171644661444
(2304)	91634324366	171643333552	415471356060	355335612671	413360612326
(2352)	655371151523	20226061126	54157111113	171645562672	721565666
(2400)	17164142521	27616361716	71623273356	46566611474	331423153016
(2448)	311660611421	142194003417	171574261223	027743171715	754745460041
(2496)	8274174661	1541121357	2406661113	3771171324	171567262645
(2544)	6516233754	1716535745	415156426061	14252514415	5427661163
(2592)	421762624371	730560612656	652251777634	171655307241	407337156061
(2640)	171594517736	265321411717	436016677775	143160613227	643310107617
(2688)	166611666	52167744325	17154712344	2116461717	457253542

(2830)	4724174173	32715521433	30644571427	171651767743	226702518662	146553130112	365027673941	430697424764
(2831)	171452172615	232273261717	5157665536	5525622464	621726337741	171652477415	41122777777	31711337722
(2924)	46366563466	227656432105	171373565626	776474571717	507262034541	217460623532	375075370212	17166312355
(2973)	56677755763	57572543014	460765633424	565111643445	171342550431	311633241717	513433645766	516767631424
(3024)	343217712454	171463154673	712234376163	36122626435	56456763374	724471572262	171146122756	36171431717
(3072)	516261432301	47046633612	61766243115	171663136714	6633127665	26345473576	45446763557	7642414365
(3120)	506601010130	375557731717	517553740511	475660643766	630317717317	171662740672	543500531712	632521036342
(3168)	263361603353	45827177176	666427730162	243477631717	517506634034	475617077451	622154334166	171662363070
(3216)	464737311714	44615723104	6416663361	37515774635	676336777543	403306551717	51611226776	636717134756
(3264)	753716667662	171661626452	406173351714	731515603676	134760603401	134246533114	606302467465	66126721717
(3312)	513135615460	426617144560	727707020350	171660714552	741774501715	510176557764	633360603433	332405644652
(3360)	616356317446	13134271717	516641727632	114617146741	500126452371	171657627311	144112521715	642215044416
(3408)	770261633476	611344126106	616235161314	163734221717	51126501244	535417134441	642355564161	171656371104
(3456)	536643271715	772364351614	655660603554	104702501105	606227306026	4276134441717	471710032455	261517155567
(3504)	41151677511	171654764376	616325131716	450204670043	053060603642	752714303171	606221562646	575237561717
(3552)	461375441764	417617156541	777667221536	171653214641	71524161716	52213355712	13315767743	14241274271
(3600)	626214204362	426726751717	447441533570	705017157555	711162760762	17165136104	414344111716	572232546342
(3648)	521568610130	012243626111	606207637220	547144031717	434361762105	070417164264	344615414477	171647244364
(3696)	66532421716	64760771174	6462661373	232467545432	6562200732	614377111717	42111717521	667717164650
(3744)	315322564244	171645153512	777611221716	71561243731	37126161657	122214317463	09613657437	71654451717
(3792)	402524251433	217517165221	537406174270	171642541426	157402511716	750612353635	415560611162	644571355666
(3840)	616134324733	673152611716	750077622711	570517165557	2464366661743	171640113012	113221461717	434627614073
(3888)	31766611575	341653111733	616132260634	117345131715	711645414271	12101716617	247327577271	171577733414
(3936)	536044741717	424054163546	143050612046	067613505377	616130337505	256220201716	64744123263	74417166413
(3984)	614576676272	171565237240	653613221717	442141033632	544360612423	665203441661	606126545641	566225641716
(4032)	614373213734	515617166675	64766563427	171557355634	353357501717	45727321721	41476061315	513614017551
(4080)	616125177116	313140571716	537615653112	274417167136	521436055362	174357675211	34343421714	434343434343
(4128)	432117435766	767777777763	172155217552	625177371743	601711377777	776417264237	777777777764	000000000000
(4176)	77500661725	737777777777	775317155132	371633431173	171747246321	125002126061	342232201337	113460612360
(4224)	705125655477	171647142313	707231361716	736445372274	121517154313	67523144375	171751463343	337501216662
(4272)	010201475437	326560612245	046114627510	171642177174	104037001716	757175121130	332017147147	13222044566
(4320)	171751547226	053036766062	116044412562	450660612145	617571101662	171572244726	757711401716	775614616215
(4368)	615217145446	632140255655	171752477440	764647636162	225602610541	211667612763	207271464351	171557717111
(4416)	316704541717	405032442712	677617137664	304337655564	171753272253	425615726162	336775773445	47766161215
(4464)	564240313037	171545224514	462067601717	412056100673	245517134411	746762156651	171753726035	433527066063
(4512)	122750372543	251561611765	237251366771	171465032660	655731621717	415766575354	776117114526	364213742343
(4560)	171754221467	312361356063	351603271355	551661611752	662256224153	17137650657	23426211717	42554641245
(4608)	236750553475	355423243657	171754354222	204670036065	007002306225	107560611754	070301344457	171245715642
(4656)	254527231717	422213356343	261761642354	511542147131	171754345640	17612350171	644447333600	763060611773
(4704)	235544754627	676516363126	55457611717	422520442455	45436635443	2347617356	171754176253	733175621713
(4752)	545325552110	471760612027	460092546105	606335655541	050517051717	421674566242	777760631731	747635446373
(4800)	171753666327	034222321714	512274455557	013760612107	63705130417	606310170445	343632161717	417725213671
(4848)	32466663235	64471566141	171753217030	057545731714	74047524734	62761612166	576211172771	61231346662
(4896)	77213471717	414632125516	072460623271	150617327537	171752411466	567303421715	47232321762	2146612271
(4944)	17312474166	606216753454	754610331717	410431774702	435260622455	441733704255	171751447707	326035601715
(4992)	613133537112	743461612477	511262423171	61624543377	63140241717	413135662777	11576621655	514556352174
(5040)	171753354045	764011731715	712232641141	311060612541	72205453313	606135261757	11575741716	771366412277
(5088)	261660621573	646661124046	171747130557	553740551716	407573664477	344460612707	404146361046	606130401113
(5136)	336473421716	752324227551	457161620327	263017447034	171745561574	11244141716	451157133247	31446161567
(5184)	772126373373	616123651424	532341231716	731251063165	63576061371	77321632421	171744167325	15207461716
(5232)	511537427364	325560613262	626304427207	606117264761	434621471716	706215302032	114360613441	13341655552
(5280)	171742267256	553511151716	552116641716	71536613467	327252635602	616113054572	557322311716	601255465424
(5328)	226361613211	715245173527	171741337336	515463641716	6154514467	32661613715	2113114635	61617131536
(5376)	662417151716	632471731755	737360612774	615166264076	171674621644	314306571716	641265752155	63346662667
(5424)	325121067220	606103274035	264320041716	602145703415	163060612572	301316134363	17175342467	657506071716
(5472)	673135571167	6677621764	14142447666	616137671313	101421721716	557157333327	5776616243	1717426621
(5520)	171663672344	726773441716	723211047273	50346621477	3712142274	616136167471	42756211716	514573366664
(5568)	525360512227	647342243726	171657043451	222074621715	751273353244	003760622227	710330022126	606034576622
(5616)	114564411716	457733425111	776661612171	453232534737	171652150235	454414021716	775337166140	351260622773
(5664)	753463512154	616033322156	747766261716	421707312146	25726611745	715651644411	171644723316	12222211717
(5712)	407541401453	250160623652	142405323141	606032164372	172754771715	745410323371	653360611640	336176661530
(5760)	171577137753	137253721717	417440776366	530460630702	103713574077	606031147673	551501741715	645221473156
(5808)	2466611547	312254622	171564222672	61742261717	426236136166	223061632276	23372736142	61613256215
(5856)	624753451715	543313731167	371163611474	03434021334	171651126652	320425331717	43371312777	2316663174

DUMP OF TAPE DIN1

INPUT TAPE DIN1 ON MT4
 DATA INPUT H9 NF 114 FL 1 1 1 SR 114 1 1 SR 114 LAST 1

D-42917
 SAGE
 03/29/79
 -04/01/79

FILE	1	RECCRC	1	LENGTH	4620BYTES						
(0)	0453660A	DB6D86D4	C11C5B6D	B6DB6D00	00000000	007BB000	00000000	00030000	00000000	01D00000	
(40)	00000000	00000000	00000003	20000000	0000000A	B608EF80	EB6DB6DB	5D85EBE2	16DB6DB5	354EB531	
(80)	6DB6D000	00000000	001E0000	00000000	0013D881	80000000	003D8800	00000000	03D7F800	00000000	
(120)	3D7EC000	00000003	D7E30000	0000003D	7DB00000	000003D7	D9000000	00003D7D	B0000000	0003D7DE	
(160)	00000000	003D7E00	00000000	03D7DF00	00000000	3D7DD000	00000003	D7D90000	0000003D	7DC00000	
(200)	000003D7	E7000000	00003D7F	20000000	0003D7FC	00000000	003D8800	00000000	03D7D800	00000000	
(240)	3D1C0000	00000003	D1C00000	0000003D	1C000000	000003D1	C0000000	00003D1C	00000000	0003D1C0	
(280)	00000000	003D1C00	00000000	03D1C000	00000000	3D1C0000	00000003	D1C00000	0000003D	18000000	
(320)	000003D1	80000000	00003D1C	00000000	0003D1C0	00000000	003D2C00	00000000	03D38000	00000000	
(360)	3D390000	00000003	D3C00000	0000003D	2C000000	000003D6	9E000000	00003DAA	32000000	0003DBAB	
(400)	30000000	003DCA02	80000000	03DCCF50	00000000	3CD84E00	00000003	DD971000	0000003D	DAD54000	
(440)	000003CD	CA700000	00003DDF	3F000000	0003DE8C	10000000	003DE9D3	20000000	03DEB6F8	00000000	
(480)	3DEEE340	00000003	DF895400	0000003D	FA259000	000003DF	B67A0000	00003DFD	13F00000	0003DD8A	
(520)	00000000	003DAA82	00000000	03DA90A0	00000000	3D9F5D33	33333323	D9B88666	6666653D	99979999	
(560)	999993D8	EE999999	99983D8C	8B333333	3323D89F	19999999	983D7EB6	66666666	53D79B7F	FFFFFFFF	
(600)	3D6DACC0	CCCCC0B3	D69DA3D7	0A3D6E3D	5C0A3D70	A3D6E3D3	FD70A3D7	0A3A3D2F	14FDF3B6	4513D1B8	
(640)	4189374B	BF3D0B0E	56041893	03CF8B57	3EAB3677	3D8E5D99	99999983	D0800000	0000003D	08000000	
(680)	000003C0	80000000	00003D08	00000000	0003D080	00000000	003D0800	00000000	03D08000	00000000	
(720)	3D080000	00000003	D0800000	0000003D	08000000	000003D0	80000000	00003D08	00000000	0003D080	
(760)	00000000	003D0800	00000000	03D1C000	00000000	3D1C0000	00000003	D2800000	0000003D	2A000000	
(800)	000003D1	C0000000	00003E3C	0F38FFFF	FF43D6AF	FFFFFFFF	F03DAE0F	FFFFFFFFE	E3D5EFFF	FFFFFFFFEB	
(840)	3CEE8C8B	9D04F4C3	CEC0FCB9	A7BD9A3C	EBB599E2	85384C31	0C069FEF	A4C03CDB	93108F17	3753CED3	
(880)	7FCD4EFE	203CED75	B2C929ED	E3CEC700	24694739	3CEC9A02	A32E228C	307F1DA9	0920153C	DA10F535	
(920)	ECBFB3CE	C77E537D	3D0B3CEC	502457D7	18F3CECC	2A155AEA	733CED70	9C4E7C39	CC3078C7	68B0B532	
(960)	3CD88470	7D522023	CEBAA70F	A0AF773C	EB1D265F	0BCD73CE	D0753F98	F6403CEE	38818E31	DA0C3073	
(1000)	071E30BF	0E3CCDDE	82B4B4CB	13CEAD08	E7983A54	3CE9DE0C	BF4C9983	CED3DD4F	C5DAAC3C	EEF0DDFC	
(1040)	C7B95C30	6DE2A3C1	F1343CCA	A65777E1	6CE3CE9E	B378382B	E73CE894	37909BB0	63CED65E	EF950DE8	
(1080)	3CEF98EE	FC712D6C	30695F1C	22A27F3C	BEC7E521	859803CE	8FB7197B	04233CDE	8222EDBE	E003CED7	
(1120)	F7C6BD1F	343CF818	02330E48	9C306580	E53BB1FE	3CB835CE	04ED77C3	CE8024B2	4E4FA63C	DBCC1C26	
(1160)	332383CE	D8A67CF8	52F33CF8	5AC09B85	BADC3062	4BAF2F55	D63C8CED	042097D5	93CDE01B	86172DA5	
(1200)	3CD90950	9B0F4C13	CED86AB8	CEC3843C	F8946E09	9701FC30	5FC25FEA	679BC356	0D054B75	2193CDBF	
(1240)	08632335	803CCC79	82F68AE2	B3CED745	1F561CFC	3CF8C4CF	DF65757C	305DE729	3D9B93C3	447798AE	
(1280)	0896C3C0	9D3492FA	BFE03CBD	A5DF6137	7693CED5	37506A81	CE3CF8EB	B5BA34CD	3C305CBB	6E30BA6C	
(1320)	C336FBF0	88507EE3	CCF58A54	D44CCF3C	99281732	97D733CE	D243E416	3C9A3CF9	08F99604	4D6C305C	
(1360)	3PDF0EC7	E0C333C7	242BB90A	B3CCAFBF	58C49E76	C346EBB5	AB9A1993	CECE6E64	BAFD713C	F91C7FDC	
(1400)	A6C97C30	5C746CD5	DB02C330	A0C496E0	B483CBD2	A6CAFFE9	A2C335CB	920CBFE7	03CEC9BB	4B1BAA5B	
(1440)	3CF92637	780685CC	305DE851	B0D32AC3	26C6119B	D0D8A3CA	8A48DC31	445AC330	2C390A51	8913CEC4	
(1480)	2FF6FFC7	143CF926	19CBDC43	DC305EEA	11DA3252	C3254639	83DB051C	356F1C78	AF1BB3C3	254EE808	
(1520)	C05FD3CE	BDD2A9C9	AC143CF9	1C2AB961	75EC3061	278221C5	C5C323D2	6A76F3CE	FC342A7B	2103F19C	
(1560)	C3229320	8AE09213	CEB6AA7C	BD62973C	F9087879	401DBC30	640DCA04	CCAAC322	6C20430F	3D2C334F	
(1600)	3F71880B	51C317F2	D676020D	53CEAEBF	59F3BDE8	3CF8EB1B	8AF1A61C	30679969	ABA59FC3	2114CB2E	
(1640)	49DE8C33	0A164C7B	AFF0C316	A4B17D3C	D853CEA6	19F1C91F	FB3CF8C4	368060CD	1C306BC6	35F50954	
(1680)	C317E6E3	5192139C	326304F2	0BBE73C3	15608266	1C2653CE	9CC3B2DD	9C443CF8	93F5DE7E	E03C3070	
(1720)	8F7396E5	72C3174C	309ACE08	0C3241B0	A431A3DB	C314279E	F96F0633	CE92C6BE	9C7D1F3C	F85A8FDA	
(1760)	48D78C30	75EFC4EE	68CEC316	BAE95C16	041C3221	30A662F4	F6C312FB	50805E25	13CE882D	DEEDE182	
(1800)	3CF81844	1CDB7A5C	307BE143	A5D067C3	1633A03E	C2F91C32	01A684D4	7F51C311	DCD27234	8503CDFA	
(1840)	08F495F6	4A3CEF9A	E6EE5E86	AC3104BA	DD41B533	C315B6DC	B32CD78C	31719951	E823E4C3	10CD514F	
(1880)	EDD943CD	E2AD1024	9E9C3CEE	F44F25D2	01FC3112	BA92145A	F2C31545	1BA9A55A	DC3162FA	211CADE3	
(1920)	C307E6F4	C0844FE3	CDCA6108	80E9EF3C	EE3E0534	CC4D0AC31	21B2AC11	8050C314	DECEDE6B	540C3155	
(1960)	04AAE012	5DC3076F	D32082DF	63CDB13E	C46FDACE	3CED789D	AB98FE2C	31319340	8426B8C3	14845BBE	
(2000)	B17FAC31	47C72E45	571EC307	01C050B5	FA23CD97	60FF912F	7C3CECA4	EC8A5FF8	BC31424B	88C8878D	
(2040)	C314361C	142B8A7C	313B4F2F	8D12FFC3	069D2F4A	ECCB83CC	F9C65ECD	F28E3CEB	C3D467AE	BF8C3153	
(2080)	C9E871B5	51C313F4	5D663C31	7C312FA9	6A72AFA5	C3064289	11064513	CCC3C2CE	D41BB43C	EAD64582	
(2120)	99822C31	65FC1430	AE51C313	BF60708D	A2DC3124	E18BACEE	10C305F2	2C455BD0	13CC8CF0	7A32A741	
(2160)	3CE9DD3C	D20AD93C	3178CF09	E00827C3	1397594A	E9578C31	1B032487	E5D5C305	AC6CCDB5	6A63CBAB	
(2200)	12A8BC3B	E13CE8D9	C2FF4018	5C32185E	4E9749C7	C3137C6E	54BDC7CC	311217B3	B65FC6C3	05719385	
(2240)	D516B3C9	EE3F1566	CA053CDF	99D6C784	682C3240	109A9D98	47C3136E	BA20488E	4C310A28	90012EDE	

1979

3

29

INPUT TAPE DIN637 ON TUI
DATA INPUT H9 NF 27 SR 1 1 1 SR 27 1 1

17

11/17/81 - 11/18/81

FILE	1	RECORD	1	LENGTH	4620BYTES	1981	REV.			
(0)	0453660A	DR6DB6D4	C11C5B6D	B6DB6D00	00000000	007BD000	00000000	00000000	00000000	01100000
(40)	00000000	00000000	00000000	80000000	0000002E	B5F82F74	E66DB6DB	5D7DEBE3	16DB6D4D	53AD4C55
(80)	2D56D000	00000000	001E0000	00000000	0013D88F	80000000	003D88C0	00000000	03D88800	00000000
(120)	3D880800	00000003	D7F50000	0000003D	7E400000	000003D7	DC000000	00003373	70000000	0003D7D8
(160)	00000000	003D7D70	00000000	03D7D400	00000000	3D7D7000	00000003	D7D90000	0000003D	7E100000
(200)	000003D7	E6000000	00003D7F	00000000	0003D7F5	00000000	003D7FE0	00000000	03D7D800	00000000
(240)	3D1C0000	00000003	D1C00000	0000003D	1C000000	000003D1	C0000000	00003D1C	00000000	0003D1C0
(280)	00000000	003D1C00	00000000	0000003D	00000000	3D1C0000	00000003	D1C00000	0000003D	18000000
(320)	0C0003C1	80000000	00003D1C	00000000	0003D1C0	00000000	003D2C00	00000000	03D38000	00000000
(360)	3D390000	00000003	D3C00000	0000003D	2C000000	000003D6	B4000000	00003DAB	46000000	0003DB8C
(400)	A0000000	003DCB00	00000000	03DCE370	00000000	3DD90FC0	00000003	DDA3B800	0000003D	DB9E8000
(440)	000003D0	D6600000	00003DDF	EA400000	0003DE90	C8000000	003DEA13	C0000000	03DEBAB4	00000000
(480)	3DEF34E0	00000003	DF8B8900	0000003D	FA470000	000003DF	B7F80000	00003DFD	24800000	0003DDB7
(520)	94000000	003DA97C	00000000	03DA8440	00000000	3D9E0266	66666653	D9A97333	3333323D	98E33333
(560)	333323D8	E6333333	33323D8C	5F333333	3323D8A2	0CCCCCCC	CC3D7F1E	66666666	53D7A1FF	FFFFFFFF
(600)	3D6E5FFF	FFFFFFFF3	D6A20A3D	70A3D53D	5C0A3D70	A3D6E3D3	F7AE147A	E1443D2F	25604189	36B3D1B9
(640)	CAC08312	673D0060	4189374B	53CF8C71	0CB295E6	3D8A54CC	CCCCCCC3	D0800000	0000003D	08000000
(680)	000003D0	80000000	00003D08	00000000	0003D080	00000000	003D0800	00000000	03D08000	00000000
(720)	3D080000	00000003	D0800000	0000003D	08000000	000003D0	80000000	00003D08	00000000	0003D080
(760)	00000000	003D0800	00000000	03D1C000	00000000	3C1C0000	00000003	D2800000	0000003D	2A000000
(800)	000003D1	C0000000	00003E3C	606BFFFF	FF43D89F	FFFFFFFF	F33E0A40	FFFFFFFF	63D5EFFF	FFFFFFFFEB
(840)	C31324CC	4BCFE283	CDC10662	4931E8C3	07611F7E	4FCC6C34	14146715	BA47C306	0802541D	7C7C3248
(880)	68C83604	2AC3130A	F94F12C0	53CD9458	449267D0	C30732D0	51EC4D1C	347829EE	3CBFD5C3	05DEA666
(920)	71F7EC32	6A465A55	D037C312	FF16419A	9453CCCE	151E81DD	E3C3070D	FF5464FD	9C3672D6	A4C0E5C3
(960)	C305C038	94F950DC	33197826	C5B06FC3	13012C56	DD9393CB	E5388508	9C03C306	F2D13C3A	31F3CA82
(1000)	9D00243B	13C305AC	D4CF526F	EC335F4A	EB379650	C3131136	044E8E33	C9B542AF	ADA634C3	06E1628D
(1040)	CA7233CB	A58B371C	03D8C305	A489C24E	2FFC344B	76D2391F	B0C3132F	1F5BF9B8	AC347538	4327586C
(1080)	C306D9C2	96F1C753	CC848204	387082C3	05A75C74	54F48C36	63FE9E27	07DDC313	5AC5BF12	CD8C335E
(1120)	DA4AC0D8	58C306DB	F84D178F	73CCB5A8	50132545	C305B544	AE7C2A33	CACD377D	E98027C3	1393F87A
(1160)	7BF8AC33	03C51A52	15A1C306	E7FFEA2A	4553CCE6	05A313B5	30C305CE	31327142	83CBF3B7	6C1196C5
(1200)	C313DA78	9FAF445C	3254DF00	899EFDC3	06FDCB60	0CC503CD	8AB3C8EE	1331C305	F20524B8	F613CCBF
(1240)	DFB49986	BCC3142D	F9BA8567	7C322892	A89727CD	C3071D42	843F5693	CDA1CEC3	8FA607C3	06209A19
(1280)	9D33F3CD	828899F4	9636C314	8E21B08D	2FEC317E	9671DB71	2BC30746	4311B8AA	63CDB83B	BDA566A1
(1320)	C30659BE	6B0D3A23	CDA4940E	3652CFC3	14FA8969	BB749C31	696E10FE	D245C307	78A0D8C0	2E23CDCD
(1360)	E388C95F	43C3069D	36A4A0BD	63CDC6EE	C2DEACDF	C31572BC	EF7E323C	3154E6D7	D0978FC3	07B425E7
(1400)	08EC63CD	E2AF7A98	704CC306	EABC836C	0243CDE6	75EC3D1C	48C315F6	3C1A4FE1	8C314116	C74E9583
(1440)	C307F892	BAF37033	CDFF889E7	18E1A6C3	07420048	AA1913CE	8303C291	4D3AC316	847ADEF3	D6DC312E
(1480)	13225E80	01C3108B	3CFD9267	93CE84AE	F7437E3E	C307A2A8	0045EA03	CE924136	05E883C3	171CE1F7
(1520)	AAD9AC31	1BF05D5E	2429C311	35EE95FB	CEA3CERD	8BE3DBE6	F1C31018	A2C979A6	93CEA0E3	3FD14B09
(1560)	C317BECF	526576FC	310AC204	6B2C2EC3	11F084E8	18AB83CE	95D24FA6	D7DAC310	FD2036F8	EAC3CEAE
(1600)	DA6315DD	4CC320D3	2D936072	CC307D4D	558E2F51	C312BA39	C831B933	CE9D7969	7A1D64C3	11F1DED8
(1640)	AD07A3CE	BC17C6F9	A85EC322	39053C45	CF2C3075	C5EA85DC	BDC31392	36CD33A2	A3CEA478	E4A45C13
(1680)	C312F5E2	64FBCC33	CEC88D2F	859015C3	23ADA89D	E427CC30	6ED2F3A2	1E5BC314	77963FAB	5F43CEAA
(1720)	C9245B25	FCC31408	1FE30A09	B3CED42D	2A73FF46	C3252F8A	5D5BF3DC	30687C0A	6AEDE4C3	156963D3
(1760)	9590F3CE	806328C0	903CC315	277C9378	BC93CEDE	EB07BD4C	45C3268D	0E9D9953	7C3062C8	26ED63F4
(1800)	C316669D	BB86C513	CEB540C2	E8CB09C3	1652CED0	953853CE	E8BB0360	0CDAC330	A9188155	338C305D
(1840)	BC9852C2	DBC3176E	35784825	93CEB95C	5B885D08	C31788DF	A05A6A93	CEF1922F	865631C3	33E89D75
(1880)	8CFE3C30	5961FD1A	406AC320	FE21E870	DA43CERC	B12D5966	CCC32190	D65E1E49	F3CEF966	95AF68FE
(1920)	C337352F	661F2D6C	3055BA3D	7A3D06C3	2330172F	FD3283CE	BF3B349B	FB86C324	20466066	BC33CF80
(1960)	17A03A9D	A1C34516	833D48DF	9C3052CA	842F1FBB	C3256FEE	CF711CD3	CEC0F73C	9ECD82C3	26BD5BF7
(2000)	020133CF	82F2219B	8DA6C357	9CEBE987	DB4C3050	9639400A	FDC327BB	3C6A15AF	13CEC1E2	E30CA890
(2040)	C332CAA2	DC76DC53	CF853F64	0519A3C3	9A2BCCAA	9E87EC30	4F1FFE52	ECE0C334	1F0B53E2	FFB3CEC1
(2080)	FC9DE9E5	50C34055	4F483B2D	83CF86FC	8C3B288C	3CB944AD	5AD5DF7C	304E69A9	85FF66C3	41A91378
(2120)	066B83CE	C143C60E	1156C356	540FA883	3823CF88	27584864	433CBFF4	559262DF	6C304E74	43ACB107
(2160)	C356475E	261C4EB3	CEBFB89D	5876943C	AC0F9457	464A83CF	88BE24E9	36983CCB	4950DD4B	CCDC304F
(2200)	4003583E	2F3CA947	2E4537C3	13CEBD5C	2F7808D4	3CC87162	A4327EA3	CF88BFD3	52FF783C	CE8C2B1C
(2240)	AB010C70	50CC4FBF	61523CBE	1E6D2C61	62D3CERA	307DC678	453CCDD7	95269C1F	93CF882C	18D57A26